INFORMATION TO USERS

This manuscript has been reproduced from the microfilm master. UMI films the text directly from the original or copy submitted. Thus, some thesis and dissertation copies are in typewriter face, while others may be from any type of computer printer.

The quality of this reproduction is dependent upon the quality of the copy submitted. Broken or indistinct print, colored or poor quality illustrations and photographs, print bleedthrough, substandard margins, and improper alignment can adversely affect reproduction.

In the unlikely event that the author did not send UMI a complete manuscript and there are missing pages, these will be noted. Also, if unauthorized copyright material had to be removed, a note will indicate the deletion.

Oversize materials (e.g., maps, drawings, charts) are reproduced by sectioning the original, beginning at the upper left-hand corner and continuing from left to right in equal sections with small overlaps.

Photographs included in the original manuscript have been reproduced xerographically in this copy. Higher quality 6" x 9" black and white photographic prints are available for any photographs or illustrations appearing in this copy for an additional charge. Contact UMI directly to order.

Bell & Howell Information and Learning
300 North Zeeb Road, Ann Arbor, MI 48106-1346 USA
800-521-0600

Static and Dynamic Strain Aging in "Interstitial-Free" Steels

by

Kamran Dehghani

A Thesis submitted to the Faculty of Graduate Studies and Research in
Partial Fulfillment of the Requirements for the Degree of
Doctor of Philosophy

Department of Mining and Metallurgical Engineering
McGill University
Montreal, Canada

March 1999

To my parents, to whom I owe everything.

To my wife who believed in me; also for her patience and understanding.

To my sisters and brothers for their continual support and encouragement.

ABSTRACT

The effect of chemical composition and cooling rate on the static strain aging (SSA) and dynamic strain aging (DSA) behaviors of four IF steels was investigated after reheating to different temperatures and cooling to room temperature at various rates. In the case of DSA, tensile tests were carried out over the range from room temperature to 450 °C and at strain rates of 10^{-4} to 10^{-1} s^{-1}. The DSA behavior was also studied in torsion in the austenite and ferrite regions. Aging index (AI) tests were carried out to evaluate the response to SSA and to estimate the amount of carbon in solution after employing various cooling rates. In all cases, although the atomic Ti/C ratio was greater than one, even still air cooling (3 °C/s) led to a supersaturated/unstabilized material and to the occurrence of both DSA and SSA. By contrast, there were no signs of SSA and DSA after furnace cooling (0.05 °C/s).

The three Ti and the Ti-Nb IF grades studied displayed serrated flow behavior at all strain rates in the blue brittleness temperature range (100 to 300 °C). A simple model is described that predicts whether or not DSA will occur at the strain rates and temperatures involved in the processing of IF steels. It was found that the higher the Ti/S ratio, the higher the solute C. Steels with different chemistries but equal Ti/S ratios displayed the same aging behavior. Internal friction measurements were executed to establish a calibration between the AI values and solute C levels. Two novel techniques for the strengthening of IF steels by *dynamic* bake hardening (BH) are presented. These techniques lead to much higher BH values compared to those produced by conventional BH methods. The observations also show that when C supersaturation results from cooling after coiling, lower annealing temperatures after cold rolling lead to higher solute C levels.

Resume

L'influence de la composition chimique (trois aciers au titane et un acier au titane-niobium) et de la vitesse de refroidissement sur le vieillissement statique par écrouissage et sur le vieillissement dynamique par écrouissage des aciers sans interstitiels a été étudiée après réchauffage à différentes températures et refroidissement à différentes vitesses jusqu'à la température ambiante. Le vieillissement dynamique par écrouissage a été caractérisé par des essais de traction dans un domaine de température compris entre la température ambiante et 450°C pour des vitesses de déformation comprises entre 10^{-4} et 10^{-1} s^{-1}. Le vieillissement dynamique par écrouissage a aussi été étudié en torsion dans les domaines austénitique et ferritique. Des mesures de l'indice de vieillissement ont été effectuées pour évaluer la réponse au vieillissement statique par écrouissage et pour estimer la quantité de carbone en solution solide après refroidissement à différentes vitesses. Dans tous les cas, si le rapport Ti/C est supérieur à 1, des vitesses de refroidissement plus rapide qu'un refroidissement à l'air (3°C/s) conduisent à une solution solide sursaturée et instable et à l'apparition de vieillissement statique et dynamique par écrouissage. Par opposition, aucun signe de vieillissement n'a été observé après refroidissement au four (0.05 °C/s).

Quelque soit la vitesse de déformation, les courbes de déformation des quatre nuances d'acier sans interstitiels présentent un aspect dentelé dans le domaine de température de fragilité au bleu (100 à 300°C). On présente un modèle simple prédisant l'apparition ou non du vieillissement dynamique par écrouissage en fonction des vitesses de déformation et des températures utilisées lors de la mise en forme des aciers sans interstitiels.

On constate que plus le rapport Ti/S est élevé, plus la concentration de carbone en solution est élevée. Pour un rapport Ti/S donné, le comportement au vieillissement des aciers ne dépend pas de leur composition chimique. Une corrélation entre l'indice de vieillissement et la teneur en carbone en solution a été obtenue par des mesures de frottement intérieur. Deux nouvelles techniques pour durcir les aciers sans interstitiels par durcissement *dynamique* sont présentées. Ces techniques permettent d'obtenir des durcissements supérieurs à ceux obtenus par les méthodes conventionnelles de durcissement sous recuit. Les observations montrent aussi que quand la sursaturation en carbone résulte du refroidissement après bobinage, des températures de recuit inférieures après le laminage à froid conduisent à des niveaux plus élevés de carbone en solution.

ACKNOWLEDGMENTS

I would like to express my sincere gratitude and appreciation to my thesis supervisor, Professor J.J. Jonas, for his guidance, encouragement and support throughout the whole course of this study, which made the completion of this work successful. His unique scientific approach and habits of hard work make everybody wish to take a leaf out of his book.

I am also grateful to Professors S. Yue and T. Maccagno for their very useful discussions and help during the courses taken and the performance of the mechanical tests, respectively. I would also like to express my gratitude to Professor M. Wuttig and Dr. Y. Zheng (both from the University of Maryland, USA) for their help in carrying out the internal friction tests.

The author would like as well to thank the Ministry of Culture and Higher Education of Iran for granting him a postgraduate scholarship. Also, the financial support of the Canadian Steel Industry Research Association (CSIRA) is acknowledged with gratitude.

The help of Mr. E. Fernandez with specimen preparation and of Mrs. L. Mello with administrative affairs is warmly appreciated.

I am also grateful to my fellow graduate students and friends, who created a friendly working environment throughout this work. Of particular note is Dr. Philippe Bocher, my former understanding roommate.

Last, but not least, I am also greatly indebted to all those who taught me in various ways, in particular: my parents, my wife, and my sisters and brothers.

TABLE OF CONTENTS

ABSTRACT.....i
RESUME.....ii
ACKNOWLEDGMENTS.....iv
TABLE OF CONTENTS.....v
LIST OF FIGURES.....ix
LIST OF TABLES.....xvi

CHAPTER 1
INTRODUCTION.....1

CHAPTER 2
LITERATURE REVIEW.....5

2.1. Introduction.....5
2.2. Carbon and Nitrogen Aging Effects.....5
2.3. Static Strain Aging (SSA).....7
2.4. Dynamic Strain Aging (DSA).....10
2.4.1. The Characteristics of Dynamic Strain Aging.....11
2.4.2. Effect of Dynamic Strain Aging on the Subsequent Mechanical Properties at Room Temperature.....13
2.5. Bake-Hardenable (BH) Steels.....14
2.5.1. Effect of the Amount of Carbon in Solution.....16
2.5.1.1 Batch Annealing.....16
2.5.1.2. Continuous Annealing.....17
2.6. Stabilization of IF Steels.....18
2.6.1.. Effect of Chemical Composition.....18
2.6.2. IF Steel Grades.....19
2.6.3. Effect of Cooling Rate.....20
2.7. A Critical Review of the Use of Ti in Steels.....22
2.7.1. Effect of Ti on Aging Behaviour and Mechanical Properties.....22
2.7.2. Using Ti to Produce High Formability Sheet Steels.....28
2.7.3. Using Ti to Prevent Aging in the Wire Rod Industry.....28
2.8. Measurement and Estimation of the Amount of Carbon in Solution.....29
2.8.1. Measurements by Internal Friction.....29
2.8.2. Estimation Using the Established Correlation.....31
2.8.2.1. Aging Index Test.....32

CHAPTER 3
EXPERIMENTAL TECHNIQUES....33

3.1. Experimental Materials....33
3.2. Specimen Preparation....34
3.2.1. Tension Tests....35
3.2.2. Torsion Tests....35
3.2.3. Internal Friction Tests....35
3.3. Experimental Equipment
3.3.1. Tension Machine....37
3.3.2. Torsion Machine....39
3.3.3 Internal Friction Apparatus....40
3.3.4. Cooling System....40
3.4. Experimental Methods....42
3.4.1. Tension....42
3.4.1.1. Dynamic Strain Aging Tests....42
3.4.1.1.1. Effects of Chemical Composition, Reheat Temperature and Cooling Rate....42
3.4.1.1.2. Effects of Chemical Composition, Tensile Strain Rate and Test Temperature....44
3.4.1.2. Static Strain Aging Tests....45
3.4.1.2.1. Aging Index (AI) Test....45
3.4.1.2.2. Effects of Chemical Composition, Reheat Temperature and Cooling Rate....45
3.4.1.3. Quench Aging Tests....47
3.4.1.4. Bake Hardening Tests....47
3.4.1.4.1. Dynamic Bake Hardening (DBH) Method....47
3.4.1.4.2. Static (Conventional) Bake Hardening (SBH) Method....48
3.4.1.4.3. Dynamic-Static Bake Hardening (DSBH) Method....48
3.4.2. Solute Carbon Measurement....49
3.4.2.1. Solute Carbon Estimation....50
3.4.3. Torsion....51
3.4.3.1. Hot Rolling Simulation....52
3.4.3.2. Warm Rolling Simulation....52
3.4.4. Coiling Simulation....52
3.4.5. Continuous Annealing Simulation....54
3.4.6. Flattening Simulation....56

CHAPTER 4
RESULTS....57

4.1. Dynamic Strain Aging....57

4.1.1. Effects of Chemical Composition, Reheat Temperature and Cooling Rate....57
4.1.2. Effects of Chemical Composition, Tensile Strain Rate and Test Temperature....63
4.2. Static Strain Aging....71
4.2.1. Effect of Reheat Temperature and Cooling Rate....71
4.2.2. Effect of Chemical Composition and Cooling Rate....76
4.3. Quench Aging at Room Temperature....79
4.4. Bake Hardening....79
4.4.1. Dynamic Bake Hardening (DBH) Method....81
4.4.2. Static (Conventional) Bake Hardening (SBH) Method....81
4.4.3. Dynamic-Static Bake Hardening (DSBH) Method....84
4.4.4. Comparison of the DBH, SBH, and DSBH Methods....86
4.5. Torsion....92
4.5.1. Hot Rolling....92
4.5.2. Warm Rolling....93
4.6. Coiling....93
4.7. Continuous Annealing....98
4.8. Internal Friction/Solute Carbon Measurements....101
4.9. Calibration between the Aging Index and Solute C Level....106
4.10. Flattening....106

CHAPTER 5
DISCUSSION....109

5.1. Effect of Cooling Rate....109
5.2. Effect of Chemical Composition....113
5.3. Work Hardening Rate, Strain Rate, and Temperature....115
5.4. Aging Index Tests....117
5.5. Activation Energies....120
5.6. Application to Mill Processing....126
5.7. Implications with Regard to Flattening....129
5.8. Stabilization of Interstitials in IF Steels....132
5.8.1. Stabilization by Chemical Composition....132
5.8.2. Stabilization by Control of Cooling Rate....136
5.9. Bake Hardening....139
5.9.1. Effect of Prestrain and Temperature....139
5.9.2. Industrial Applications of the DBH and DSBH Methods....142
5.10. Continuous Annealing Techniques....146

CHAPTER 6
CONCLUSIONS....149

STATEMENT OF ORIGINALITY AND CONTRIBUTION TO KNOWLEDGE.....155

REFERENCES.....157

LIST OF FIGURES

Chapter 2

Fig. 2.1 (a) Fe-C , and (b) Fe-N equilibrium diagram in the near-Fe region.....6

Fig. 2.2 Stress-strain curve of a low carbon steel strained to point A, unloaded, and then restrained immediately (curve a) and after aging (curve b).....8

Fig. 2.3 Changes in tensile properties due to strain aging in low carbon steel prestrained 4% then aged at 60 °C; grain size (grains/mm^2): (a) 50; (b) 195; (c) 1850.....9

Fig. 2.4 Stretcher strains on a steel sheet.....10

Fig. 2.5 Stress-strain curves of a low carbon steel showing the range of blue-brittleness effects.....12

Fig. 2.6 Temperature and strain rate range for the presence of serrations in a 0.03%C steel.....12

Fig. 2.7 Force-velocity diagram for a mobile dislocation.....13

Fig. 2.8 (a) DSA vs. (b) SSA at 200 °C in a 0.03%C steel.....14

Fig. 2.9 Measuring method for assessment of bake hardenability in a tensile test.....15

Fig. 2.10 An outer panel after press forming.....16

Fig. 2.11 The principles for producing bake hardening steels by a) batch annealing b) continuous annealing.....17

Fig. 2.12 Precipitation sequence under *equilibrium* conditions in a Ti IF steel.....21

Fig. 2.13 Precipitation sequence under *non-equilibrium* conditions in a Ti IF steel.....21

Fig. 2.14 Changes in δ_o in the Hall-Petch equation as a function of Ti concentration.....24

Fig. 2.15 Internal friction measurement in a sample containing about 2 ppm solute C.....30

Fig. 2.16 The correlation between aging index and amount of solute carbon....31

Fig. 2.17 Measurement of aging index....32

Chapter 3

Fig. 3.1 Geometries of a) tension, b) torsion, and c) internal friction samples....36

Fig. 3.2 The workstation of the TestStar tensile testing equipment and its components....38

Fig. 3.3 Schematic diagram of the torsion machine....39

Fig. 3.4 Schematic diagram of the forced torsion pendulum....41

Fig. 3.5 Geometry of the cooling system and specimen....41

Fig. 3.6 The heat treatment cycle applied to the samples....43

Fig. 3.7 The steps employed to compare the SSA behaviours of 4 IF steels....46

Fig. 3.8 The treatments employed to study the effects of reheat temperature and cooling rate on the SSA behaviour of steel A....46

Fig. 3.9 Schematic diagram of the DBH method....48

Fig. 3.10 The steps of the SBH method....49

Fig. 3.11 The steps employed in the DSBH method....50

Fig. 3.12 Schematic diagram of the simulation of the coiling process....54

Fig. 3.13 Schematic diagram of the simulation of the continuous annealing process....55

Chapter 4

Fig. 4.1 Stress vs. strain curves of specimens cooled from a) 900, b) 1050, c) 1150, and d) 1200 °C at different rates and then tensile tested at 300 °C and 10^{-3} s^{-1}....58

Fig. 4.2 UTS vs. cooling time to room temperature for various

reheat temperatures and cooling rates....60

Fig. 4.3 Stress/strain curves of specimens cooled from 1100 °C at different rates and tested at 300 °C and 10^{-3} s^{-1}: a) steel B, b) steel C, and c) steel D....61

Fig. 4.4 Stress vs. strain curves of specimens cooled from different reheat temperatures in still air (3 °C/s), then tensile tested at 300 °C and 10^{-3} s^{-1}....62

Fig. 4.5 Stress/strain curves of specimens tensile tested at different temperatures and strain rates of: a) 10^{-1}, b) 10^{-2} and, c) 10^{-3} s^{-1} (steel A)....64

Fig. 4.6 Stress/strain curves of specimens tensile tested at different temperatures and strain rates of: a) 10^{-1}, b) 10^{-2} and, c) 10^{-3} s^{-1} (steel B)....65

Fig. 4.7 Stress/strain curves of specimens tensile tested at different temperatures and strain rates of: a) 10^{-1}, b) 10^{-2} and, c) 10^{-3} s^{-1} (steel C)....66

Fig. 4.8 Temperature dependence of the yield, flow, and ultimate stresses at strain rates of: a) 10^{-1}, b) 10^{-2}, c) 10^{-3}, and d) 10^{-4} s^{-1} (steel A)....67

Fig. 4.9 Temperature dependence of the UTS at various strain rates (steel A)....69

Fig. 4.10 Temperature dependence of the fracture strain at various strain rates (steel A)....69

Fig. 4.11 Strain rate dependence of the flow stress and UTS at 25 and 65 °C....70

Fig. 4.12 Strain rate dependence of the flow stress and UTS at 150 and 200 °C....70

Fig. 4.13 Stress vs. strain curves of specimens tensile tested at various temperatures and strain rates of: a) 10^{-1}, b) 10^{-3} and, c) 10^{-4} s^{-1} (steel D)....72

Fig. 4. 14 Temperature dependence of the UTS for steels A, B, and C (cooled in still air), and steel D cooled in the furnace from 1100 °C, then tensile tested at 10^{-4} s^{-1}....73

Fig. 4.15 Stress vs. strain curves for specimens tensile tested at various temperatures and strain rates of: a) 10^{-2}, b) 10^{-3} and, c) 10^{-4} s^{-1} (steel D)....74

Fig. 4.16 Aging index tests on specimens cooled from different reheat temperatures at different rates: a) 0.05 °C/s, b) 3 °C/s, and c) 400 °C/s (steelA)....75

Fig. 4.17 AI vs. cooling time to room temperature for various reheat temperatures and cooling rates....76

Fig. 4.18 Aging index tests on specimens cooled from 1100 °C at different rates: a) steel B, b) steel C, and c) steel D (W=400, S.A.=3, and F=0.05 °C/s)....77

Fig. 4.19 Stress vs. strain curves of specimens of steel A tensile tested at 300 °C and 10^{-3} s^{-1}: immediately after quenching (left) and after storing at room temperature for three weeks (right)....80

Fig. 4.20 Effects of temperature and prestrain on the DBH values....82

Fig. 4.21 Dependence of the yield strength before DBH on temperature....82

Fig. 4.22 Dependence of the yield strength after DBH on temperature....82

Fig. 4.23 Effect of temperature and prestrain on SBH....83

Fig. 4.24 Dependence of the yield strength before SBH on prestrain....83

Fig. 4.25 Dependence of the yield strength after SBH on temperature....83

Fig. 4.26 Effects of temperature and prestrain on the DSBH values....85

Fig. 4.27 Dependence of the yield strength before DSBH on temperature....85

Fig. 4.28 Dependence of the yield strength after DSBH on temperature....85

Fig. 4.29 Comparison of DBH, SBH, and DSBH values after an an 8% prestrain at: a) 150, b) 200, and c) 250 °C (Steel B)....87

Fig. 4.30 Comparison of DBH, SBH, and DSBH values after a 6% prestrain at: a) 150, b) 200, and c) 250 °C (Steel B)....88

Fig. 4.31 Comparison of DBH, SBH, and DSBH values after a 4% prestrain at: a) 150, b) 200, and c) 250 °C (Steel B)....89

Fig. 4.32 Comparison of DBH, SBH, and DSBH values after a 2% prestrain at: a) 150, b) 200, and c) 250 °C (Steel B)....90

Fig. 4.33 Comparison of DBH, SBH, and DSBH values after prestraining at 100 °C: a) 4%, b) 6%, and c) 8% (Steel B)....91

Fig. 4.34 Stress-strain curves determined in torsion when both finishing and roughing were carried out in the γ phase....94

Fig. 4.35 Torsion stress-strain curves when the first finishing pass was carried out in the γ and the rest in the α....94

Fig. 4.36 Torsion stress-strain curves for cases where all the finishing passes were carried out in the α region with different finishing temperatures, T(f): 500 °C (above), 750 °C (below)....95

Fig. 4.37 Torsion stress-strain curves for cases where both the roughing and finishing passes were carried out in the α range with different finishing temperatures, T(f): 650, 700, and 750 °C....96

Fig. 4.38 Aging index tests on specimens cooled at 0.01 °C/s (coiling simulation)....97

Fig. 4.39 Aging index tests on specimens cooled at 0.03 °C/s (coiling simulation)....97

Fig. 4.40 Aging index tests carried out on specimens cooled from different annealing temperatures at different rates (continuous annealing simulation)....99

Fig. 4.41 Aging index tests carried out on specimens cooled from different annealing temperatures at different rates (continuous annealing simulation)....100

Fig. 4.42 Internal friction tests carried out on specimens cooled from 1100 °C in still air (steel B)....102

Fig. 4.43 Internal friction tests carried out on specimens water quenched from 1100 °C (steel B)....102

Fig. 4.44 Internal friction tests carried out on specimens cooled from 1100 °C in still air (steel C)....103

Fig. 4.45 Internal friction tests carried out on specimens water quenched from 1100 °C (steel C)....103

Fig. 4.46 Internal friction tests carried out on specimens cooled from 750 °C in still air (steel B)....104

Fig. 4.47 Internal friction tests carried out on specimens cooled from 850 °C in the furnace (steel B)....104

Fig. 4.48 Internal friction tests carried out on specimens cooled from 650 °C in still air (steel C)....105

Fig. 4.49 Internal friction tests carried out on specimens water quenched from 850 °C (steel C)....105

Fig. 4.50 Calibration between the measured aging indices and amounts of solute C in the present steels....107

Fig. 4.51 Stress/strain curves determined on specimens tensile tested at different temperatures and a strain rate of 10^{-4} s^{-1}: a) steel A, b) steel B, and c) steel C....108

Chapter 5

Fig. 5.1 Temperature and strain rate range over which serrations are observed....121

Fig. 5.2 Cooling times associated with a UTS of 260 MPa vs. inverse reheat temperature....123

Fig. 5.3 Cooling times pertaining to an AI value of 25 MPa vs. inverse reheat temperature....123

Fig. 5.4 Stability and precipitation temperatures of Ti compounds in IF steels....134

Fig. 5.5 Comparison between work hardening behaviors of two steels....143

Fig. 5.6 An apparatus for warm press forming....145

LIST OF TABLES

Chapter 3

Table 3 .1 Chemical compositions of the experimental steels, wt%.....33

Table 3.2 An industrial rolling schedule employed on one of the present materials.....34

Table 3.3 Schedule for the simulation of hot and warm rolling.....53

Chapter 4

Table 4.1 Aging index values and estimated amounts of carbon in solution for different reheat temperatures and cooling rates (steel A).....73

Table 4.2 Aging indices and the corresponding estimated amounts of carbon in solution (cooled from 1100 °C at different rates).....78

Table 4.3 Aging indices and estimated amounts of solute carbon resulting the coiling simulation.....93

Table 4.4 Aging indices and estimated amounts of solute carbon resulting from the continuous annealing simulation carried out on steel B.....98

Table 4.5 Aging indices and estimated amounts of solute carbon resulting from the continuous annealing simulation carried out on steel C.....98

Table 4.6 Measured and estimated amounts of solute carbon in in samples cooled from 1100 °C at different rates.....101

Table 4.7 Measured and estimated amounts of solute carbon remaining in steel B after the continuous annealing simulation.....106

Chapter 5

Table 5.1 Relation between type of particle and nucleation site.....114

Table 5.2 Aging times required to give rise to the same amount of aging as observed after 60 min at 100 °C.....118

CHAPTER 1

Introduction

Producing steels with high formability is the main objective of steel companies providing sheet for the automotive industry. To realize this requirement, resistance to aging is of major concern, particularly for products with high ductility. Aging is a well known phenomenon in low carbon steels and is caused by the presence of interstitial elements such as C and N in solution. The ductility and/or formability of these steels is much deteriorated when aging occurs.

The elimination of interstitial elements in solution is therefore a vital key to the production of interstitial-free (IF) steels with deep drawability. In IF steels, the C and N are tied up by strong carbide and nitride formers such as Ti and/or Nb. This yields a steel with high formability provided it is stabilized and there is no solute C or N in the steel. The stabilization of IF steels depends on the conditions involved in their processing, e.g. the cooling rate after hot rolling.

Since TiN has a low solubility product in austenite and its precipitation temperature is relatively high, the N content is generally of subordinate importance in these steels. Thus, the concentration of C is one of the most important concerns during and after the processing of IF steels. The amount of Ti required to fix the C also increases as the C content is increased, as does the cost of alloying.

It is actually easier to suppress strain aging in plain carbon than in IF steels, because the higher C levels permit cementite precipitation to take place, which can

then remove the carbon from solution during continuous annealing. As a result of the much lower C levels, this route is not available in the processing of IF steels. An alternative is therefore to suppress strain aging by controlling the cooling rate during processing. For this approach to succeed, the Ti concentration must be much greater than the stoichiometric amount necessary to tie up the C, and even at these levels, the complete removal of carbon may not be possible in practice.

Since the first Ti IF steel was produced around 1970 and the first Ti-Nb IF steel around 1973, many investigations have been carried out on the steelmaking, rolling, and annealing technologies as well as on the formability of these steels. In all cases, the aim has been to produce a real IF steel (i.e. one that is resistant to aging) with the least Ti/C or Nb/C (atomic) ratio. This, along with the steelmaking techniques required to reduce the C level as much as possible, make these steels very expensive in terms of production cost.

In order to produce a real IF steel, it is necessary to study the effects of the two most important parameters mentioned above: cooling rate and chemical composition. This is because these two factors determine the concentrations of C available in solution and available to cause aging phenomena such as SSA (static strain aging) and DSA (dynamic strain aging). Carbon can be in solution when there is insufficient Ti to fix this interstitial, or when the cooling rate through the precipitation temperature range is too rapid for full carbide precipitation to occur (even though there is excess Ti).

The cooling rate influences the amount of C in solution by determining the amount of carbonitride that can precipitate. For example, the cooling rate after hot rolling will determine whether or not interstitial effects can be expected to arise during warm rolling. This, in turn, affects the solute C level present during coiling

and process annealing, which are further modified by the cooling history after annealing.

The chemical composition is also important because the solubility products of the various precipitates are modified by the presence of alloying elements. In IF steels, for example, elements such as S, P, and Mn can affect the amount of C in solution, regardless of the cooling rate.

In addition to studying the effects of reheat temperature, cooling rate and chemical composition on the aging behaviour of IF steels, the other aims of this work were:

i) to find a link between dynamic strain aging and the bake hardenability of IF steels. Based on this link, two novel methods, referred to as *dynamic* bake hardening (DBH) and *dynamic*-static bake hardening (DSBH), are introduced here. These have significant advantages compared to conventional bake hardening.

ii) to establish a calibration between aging indices and the amount of solute carbon in the case of IF steels. Because this calibration can be used to predict the aging behaviour of these steels, it can be of interest to steelmakers.

iii) to suggest a simple model that predicts whether or not dynamic strain aging will occur at the strain rates and temperatures involved in the processing of IF steels.

In *chapter two*, the mechanisms of dynamic and static strain aging are reviewed briefly. Bake hardenable steels and their characteristics are pointed out. Then, the kinds of IF steel and their methods of stabilization are described, followed by a critical review of the use of Ti in steels, including its role to prevent

aging. This chapter closes by addressing the methods used to measure and/or estimate the amount of solute C.

Chapter three deals with the experimental materials and techniques used to carry out the present work. After applying various reheating temperatures and cooling rates to different IF steels, mechanical tests (tension, torsion, and internal friction) were carried out to study the aging behaviour of these steels. Dynamic strain aging tests were conducted at high temperatures using tension and torsion machines, while aging index tests were performed to investigate the static strain aging phenomena. Then, two new techniques for studying bake hardening are introduced followed by the methods used to simulate coiling, continuous annealing, and flattening.

Because of the link between the phenomena (static and dynamic strain aging and bake hardening), all the results of these tests are presented in *chapter four*. This chapter also includes the results of the internal friction measurements and the above mentioned simulations.

In *chapter five*, the effects of cooling rate and chemical composition are discussed, as well as the stabilization that can result. Then, some possible applications of DSA to mill processing, e.g. warm/ferrite rolling and flattening, are pointed out. This chapter then discusses the potential industrial applications of the novel techniques introduced here for bake hardening.

The general conclusions of this research are collected in *chapter 6*. Finally, following this chapter, there is a statement of originality and contribution to knowledge.

CHAPTER 2

Literature Review

2.1. Introduction

Interstitial-free steels are generally considered to be non-aging because they not only contain low levels of the interstitial elements C and N but the compositions also include strong carbide and nitride formers [1-3]. Most applications of IF steels are based on this property. Nevertheless, significant strain aging can take place at interstitial levels as low as 1 ppm [4, 5]; this increases the strength and decreases the ductility. The term "interstitial-free" steel is therefore a misnomer because even ultra high purity iron contains at least a few atomic parts per million of carbon and nitrogen in solution. Consequently, the presence of interstitial carbon and/or nitrogen atoms in solution in the so-called IF steels is deleterious to the formability of deep-drawing sheets through the mechanism of strain aging [4, 6, 7]. This will be the case when there is insufficient Nb or Ti present in the steel to "fix" the C and N or, in the presence of sufficient Nb and Ti, when the cooling rate through the precipitation temperature range is too rapid to permit full precipitation of the particles.

2.2. Carbon and Nitrogen Aging Effects

The main differences between the strain aging effects of carbon and nitrogen arise from their widely differing solubilities in iron [8]. The equilibrium solubilities of carbon and nitrogen in iron decrease sharply between about 730 °C (for carbon) and 585 °C (for nitrogen) and room

temperature. The solubility of C decreases from approximately 200 ppm at 720 °C to less than 0.001 ppm at room temperature, while that of nitrogen drops from 1000 ppm at 585 °C to about 0.1 ppm at room temperature [9]. The solubility limits for nitrogen and carbon in iron are shown in Fig. 2.1.

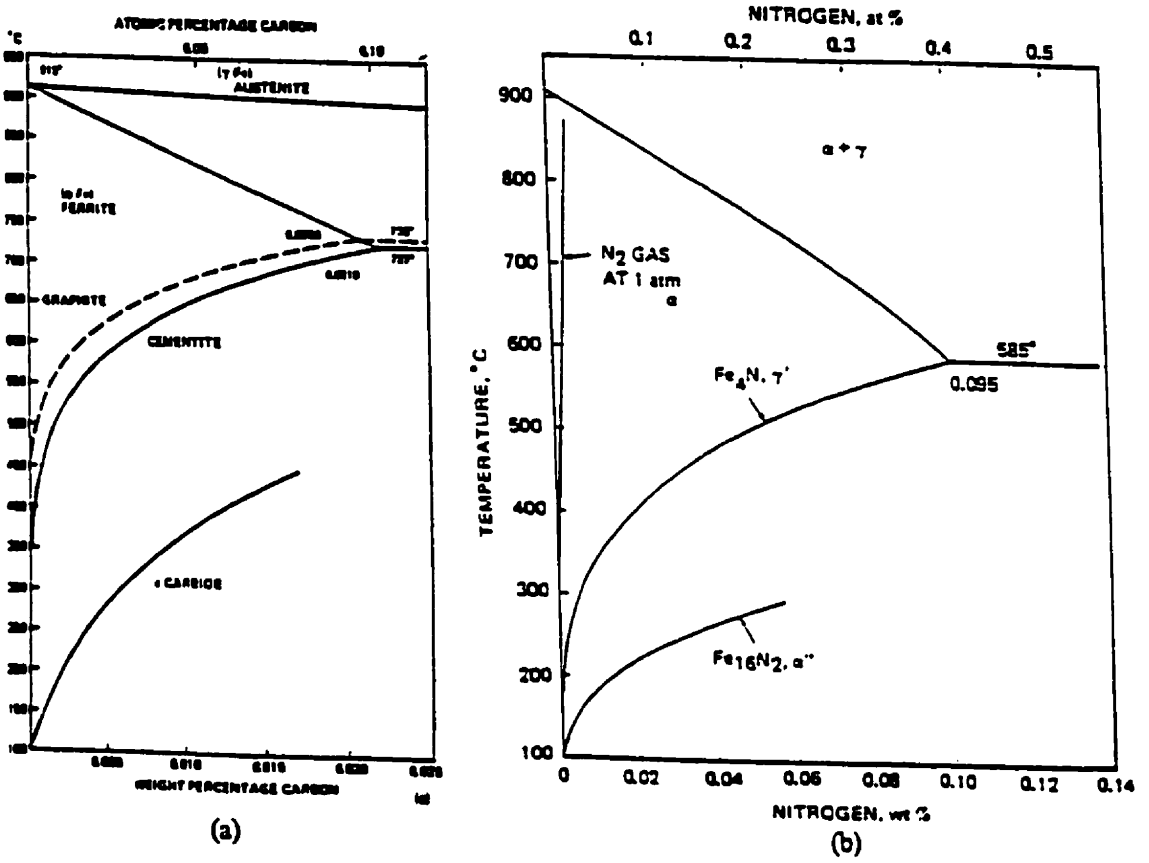

Figure 2.1. (a) Fe-C, and (b) Fe-N equilibrium diagram in the near-Fe region [9].

Low temperature aging, at temperatures below 100 °C, in slowly cooled steels is believed to be largely due to nitrogen [5, 9]. Therefore, if the nitrogen is removed from solution, the steel will show negligible aging below 100 °C [8] and a " non-strain aging" steel can be made provided that the aging temperature is not much above ambient [9].

As little as 1 ppm carbon/nitrogen produces detectable aging at room temperature, while quickly cooled iron-carbon alloys show appreciable strain aging below 100 °C [5].

As for dynamic strain aging, less than 10 ppm of interstitial solutes are required in order to permit this mechanism to take place [9, 10].

2.3. Static Strain Aging (SSA)

Static strain aging is defined as the change in properties of a metal that occurs as a result of interactions between interstitial atoms and dislocations after plastic deformation [8, 9, 11-15]. The stress-strain curve of a mild steel takes the form of curve (a) in Fig. 2.2. If the specimen is strained to point A, unloaded and then immediately restrained, the stress-strain curve follows the same curve (a). If the specimens is unloaded at A and then allowed to age at room temperature or above, the discontinuous yielding behavior returns and the stress-strain curve follows a curve such as (b) [5, 8].

The effects indicated on the figure are [9]:

1. an increase in yield strength, ΔY
2. a return of the yield drop,
3. an increase in the ultimate tensile stress, ΔU, and
4. a decrease in total elongation, ΔE.

It is well known that the aging phenomenon in iron is produced by the migration of interstitial carbon and nitrogen to the dislocations created by prior plastic deformation [4, 8, 16-19]. This leads to the locking of dislocations and to the return of the yield point. Therefore, if solute carbon and nitrogen are removed from the steel, both strain aging and the initial discontinuous yielding are eliminated [5, 8].

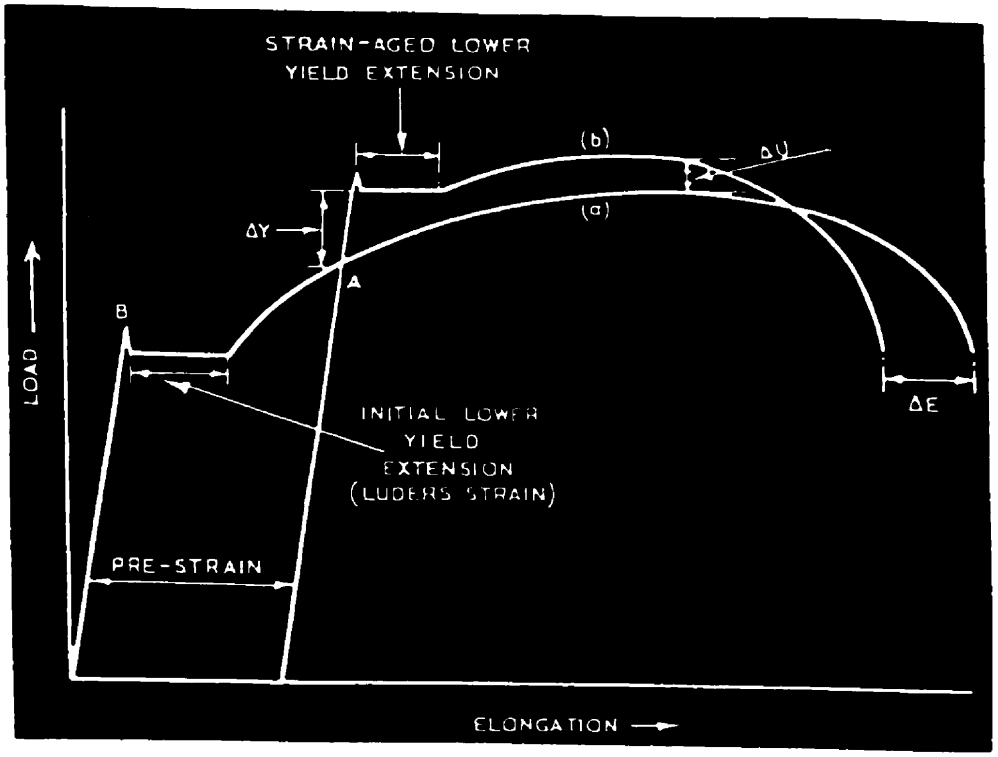

Figure 2.2. Stress-strain curve of a low carbon steel strained to point A, unloaded, and then restrained immediately (curve a) and after aging (curve b) [8].

In general, three distinct mechanisms, (a) atmosphere formation, (b) precipitation hardening, and (c) overaging contribute to changes in the tensile properties [5, 8]. These changes are summarized in Fig. 2.3 for a low carbon steel subjected to tensile prestraining, aging at 60 °C and re-straining. Strain aging under these conditions occurs in four stages. In stage I, the yield stress and the Luders strain increase but the other properties remain constant. In stage

II, the yield stress continues to rise, and the Luders strain remains roughly constant. Stage III is similar to stage II except that the UTS increases and the elongation decreases. A fall in the yield stress in stage IV gives rise to the observed increase in elongation to fracture [5, 8].

The second and third stages are attributed to the formation of precipitates on the dislocations. Since the dislocations are fully locked at the end of the atmosphere stage, the locking contribution is not increased, and the Luders strain does not increase sharply.

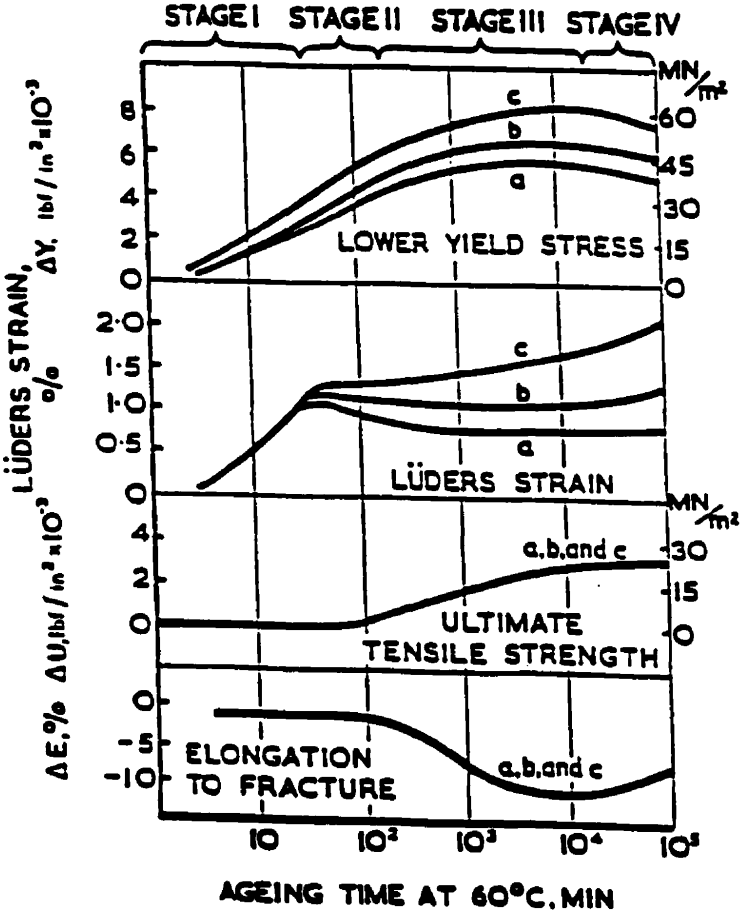

Figure 2.3. Changes in tensile properties due to strain aging in low carbon steel prestrained 4% then aged at 60 °C; grain size (grains/mm^2): (a) 50; (b) 195; (c) 1850 [8].

However, precipitation raises the general level of the basic curve, and so raises the lower yield stress and the UTS. In the last stage, there are signs of slight overaging, probably due to coarsening of the precipitates on the dislocations [8, 13].

Figure 2.4 shows one of the worst defects, stretcher strains, which occur during press forming. They result from static strain aging, which causes the return of the yield point and the Luders strain [20].

Figure. 2.4. Stretcher strains on a steel sheet [20].

2.4. Dynamic Strain Aging (DSA)

At slightly elevated temperatures, the stress vs. strain curves of low carbon steels display serrations in the work hardening region when tensile

tested [21-26]. Since this phenomenon occurs *during* deformation, it is known as dynamic strain aging. This serrated behavior is accompanied by increased rates of work hardening, negative strain rate dependence of the flow stress, and a reduction in ductility known as "blue brittleness". This phenomenon is due to interactions between dislocations and solute nitrogen and/or carbon during deformation and is referred to as the Portevin-Le Chatelier effect [27-31]. The significant increase in flow stress, which is displayed in the blue brittleness temperature range, is the most important practical phenomenon produced by dynamic strain aging, as it leads to a considerable decrease in ductility [21, 22, 28, 32-34].

Dynamic strain aging has four distinct characteristics [9]:

1. high rates of work hardening
2. negative strain rate dependences of the flow stress
3. serrated stress-strain curves
4. the ultimate tensile stress goes through a maximum as a function of temperature.

Figure 2.5 illustrates a typical range of dynamic strain aging behaviors [8], and the temperature-strain rate regime in which the serrations appear is shown in Fig. 2.6 [9]. The most important variables affecting dynamic strain aging are the temperature and strain rate [35].

2.4.1. The Characteristics of Dynamic Strain Aging

In the absence of interstitials, the motion of dislocations is retarded by lattice friction. This retarding force increases with the velocity of the dislocations, line 1 in Fig. 2.7. When this velocity is approximately equal to

that of solute diffusivity, solute atmospheres will be formed around the dislocations. The force required to drag the atmospheres increases very quickly

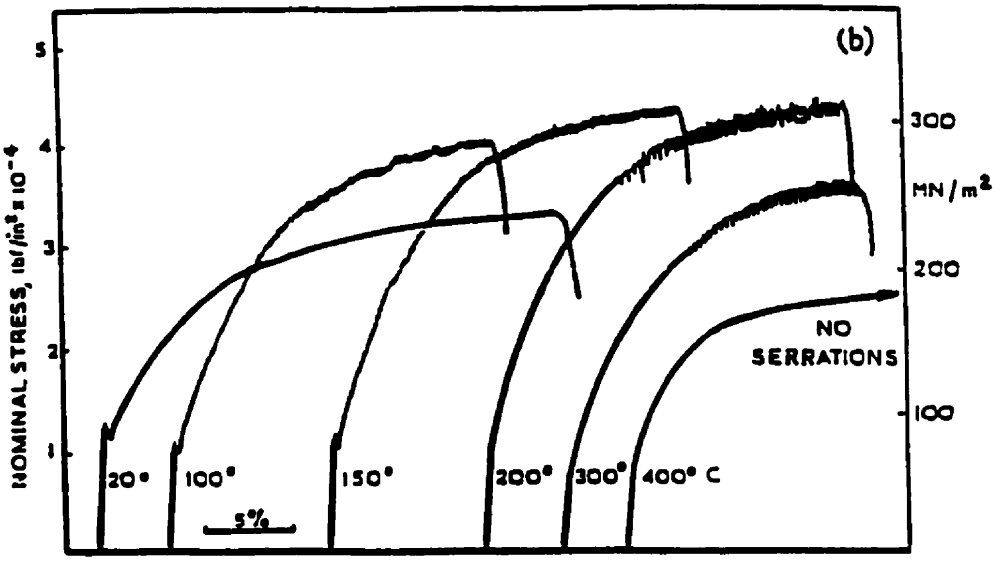

Figure 2.5. Stress-strain curves of a low carbon steel showing the range of blue-brittleness effects [8].

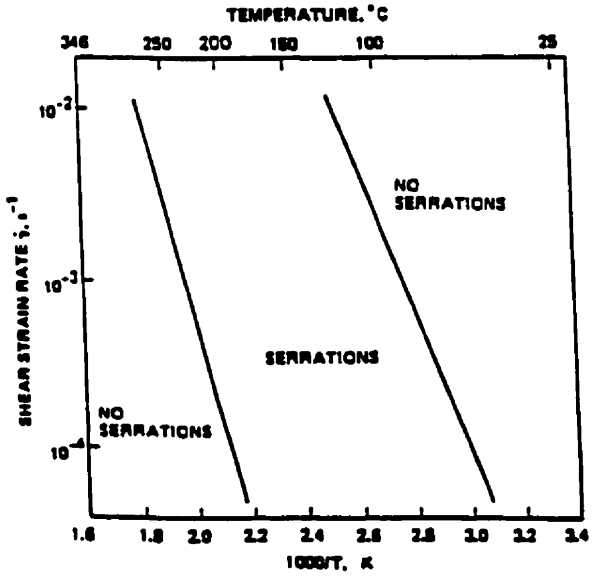

Figure 2.6. Temperature and strain rate range for the presence of serrations in a 0.03%C steel [9].

with the dislocation velocity, as represented by curve 2 in Fig. 2.7. Beyond a critical velocity, V_m, the atmosphere can no longer keep pace with the moving dislocations. The drag force then decreases with velocity; this is accompanied by a drop in solute concentration, as shown by curve 3 in Fig. 2.7. When a dislocation is suddenly freed from its atmosphere, it will encounter obstacles which will slow its speed so that the solute atmosphere can once again keep up with the dislocation. This cycle continues [36-38], as shown by curve 4 in Fig. 2.7.

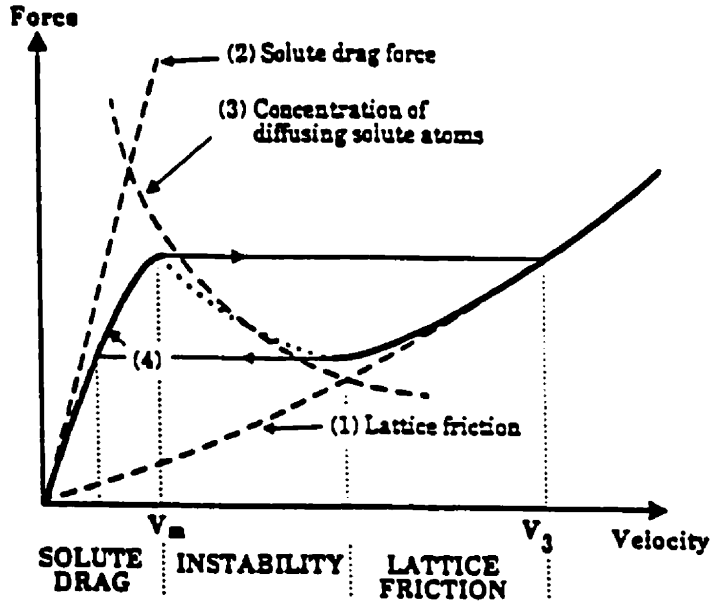

Fig. 2.7. Force-velocity diagram for a mobile dislocation [37].

2.4.2. Effect of Dynamic Strain Aging on the Subsequent Mechanical Properties at Room Temperature

One of the most important applications of dynamic strain aging is strengthening the material [22, 39]. It has been reported [9, 22, 39, 40] that the strengthening obtained from dynamic strain aging is much more effective than the one produced by static strain aging; furthermore, the amount of straining required at elevated temperatures is less than at room temperature. The

amounts of strengthening obtained at room temperature after applying these two methods are compared in Fig. 2.8. The former technique can be of interest because it does not depend on the presence of alloying elements and their high costs [22]. This strengthening has two sources: dynamic strain aging, which involves straining at elevated temperatures, and static strain aging during cooling to room temperature [22, 39].

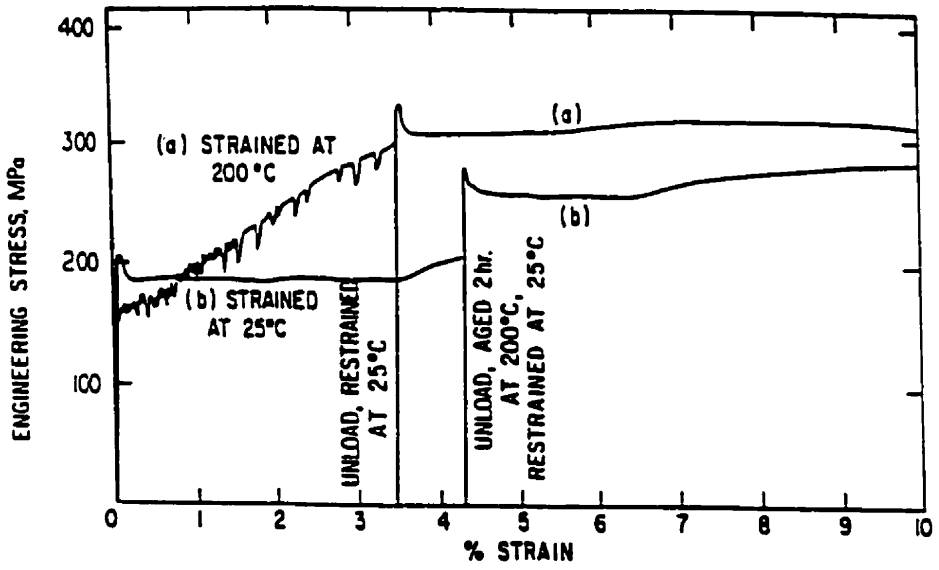

Figure 2.8. (a) DSA vs. (b) SSA at 200 °C in a 0.03%C steel [40].

2.5. Bake Hardenable (BH) Steels

Two important objectives being pursued by the automobile industry are a decrease in car weight and improvements in safety. To realize these requirements, reductions in sheet thickness, higher strength, and improvements in press formability are generally demanded for automobile body panels [41-46]. Bake hardenable high strength steels are an interesting solution that can satisfy all these requirements. This property provides a capacity for a yield strength increase of approximately 20% [47] to 30% [48] of the initial yield strength, i.e. 30-60 MPa [49]. Figure 2.9 shows the measuring method for bake

hardening by means of tensile testing. The target bake hardening value of about 40 to 60 MPa requires solute carbon levels between about 10 and 20 ppm [50].

The procedure is as follows:

- the specimen is prestrained 2%
- the sample is aged at 170 °C for 20 minutes
- the specimen is tensile tested at room temperature

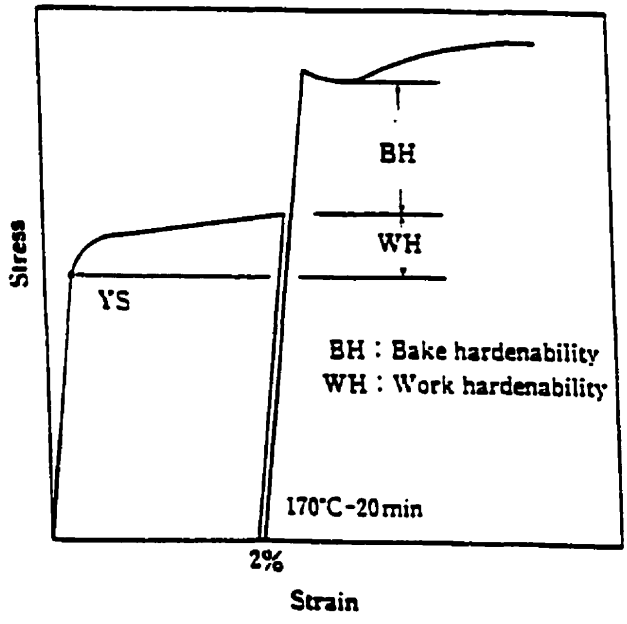

Figure 2.9. Measuring method for assessment of bake hardenability in a tensile test [41].

The amount of bake-hardening is determined by subtracting the flow stress after the 2% initial strain from the lower yield strength after baking. Although a 2% prestrain and aging at 170 °C for 20 min are typical values employed to cause bake hardenability in steels, some workers have investigated the effects of prestrain, temperature, and time on this process [51, 52].

A typical outer panel after press forming is illustrated in Fig. 2.10.

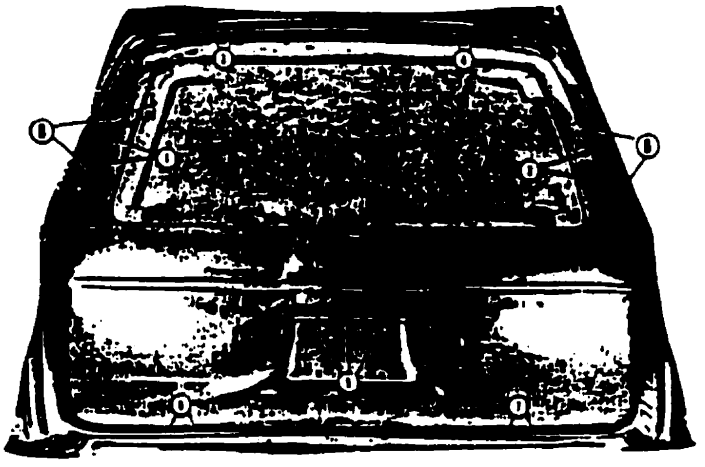

Fig. 2.10. An outer panel after press forming [53].

2.5.1. Effect of the Amount of Carbon in Solution

Bake hardenable steels must contain significant amounts of solute carbon. These interstitial elements are responsible for the strength increment [49], as bake hardening occurs by static strain aging as a result of interstitial atom segregation to dislocations. In the initial stages of strain aging, strengthening is accomplished solely by the formation of solute atmospheres [49, 52, 54]. During atmosphere formation, carbon segregates to dislocations and strengthening arises from the additional force needed to separate the dislocations from their atmospheres [49, 50, 52].

2.5.1.1 Batch Annealing

Bake hardenable steels can be produced by both conventional batch annealing and continuous annealing processes, as shown in Fig. 2.11. In the case of batch annealing, in which very low carbon, <0.01%, steel is normally used, the precipitation of Fe_3C is suppressed because of the sparseness of

nucleation sites. This results in some amount of carbon remaining in solution, even after the use of relatively slow cooling rates [49, 50, 52, 54].

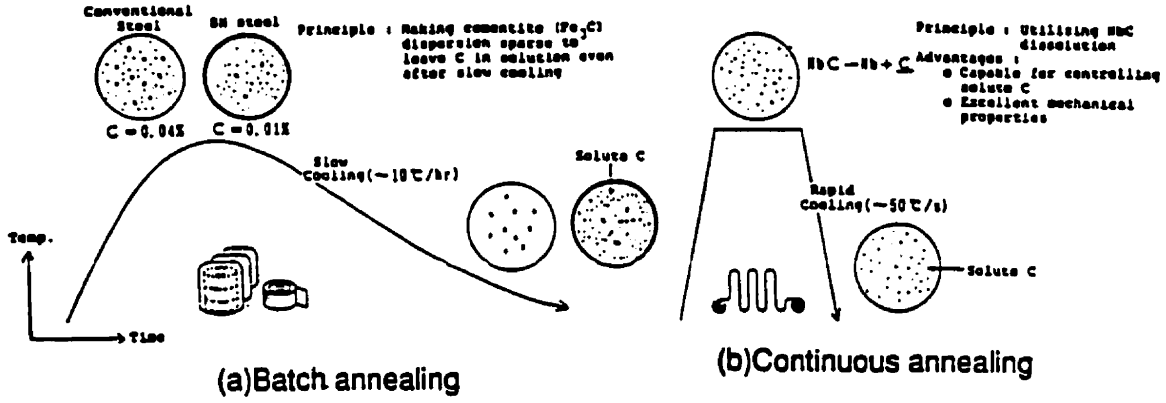

Figure 2.11. The principles for producing bake hardening steels by a) batch annealing b) continuous annealing [54].

As for N, most bake hardenable steels contain sufficient aluminum to remove the dissolved nitrogen and rely on carbon to provide the bake hardenability [49, 54].

2.5.1.2. Continuous Annealing

With regard to continuous annealing, a high annealing temperature, about 900 °C [51, 52, 54, 55], is required in order to produce bake hardenability. The cooling rate from the soaking temperature should also be high so as to provide enough carbon in solution at room temperature. This cooling rate normally ranges from 20-30 [54], through 70 [49], to 100 °C/s [56].

The higher the Ti*/C or Nb/C atomic ratio, the higher the annealing temperature during continuous annealing. By contrast, the lower the Ti*/C or Nb/C atomic ratio, the higher the bake hardenability [54].

When the solute carbon level is too low, bake hardening values are also low. On the other hand, excessive amounts of carbon in solution lead to room temperature aging. In order to have sufficient susceptibility for bake hardening, different required amounts of solute carbon have been reported: 5 ppm [49], 10 ppm [41], 5-15 ppm [45]. These amounts of solute carbon at room temperature can be produced by employing a suitable cooling rate after the annealing of low or ultra low carbon steel.

2.6. Stabilization of IF Steels

2.6.1. Effect of Chemical Composition

The elimination of alloying elements in solution, both substitutional as well as interstitial, is a vital key to the production of interstitial-free (IF) steels with deep drawability [57, 59]. Because of the deterioration of the mechanical properties due to carbon in solution, the concentration of this element is one of the most important concerns during and after the processing of IF steels [59, 60]. The amount of Ti required to fix the C also increases as the C content is increased [57], as does the cost of alloying.

Previous work has suggested that solute carbon is deleterious to the formability and ductility of IF steels through the mechanism of static or dynamic strain aging [4, 61]. It is actually easier to suppress strain aging in plain carbon than in IF steels, because the higher C levels permit cementite precipitation to take place, which can then remove the carbon from solution during continuous annealing [57, 58, 61]. This route is not available in the processing of IF steels [61].

The chemical composition is important because the solubility products of the various precipitates are modified by the presence of alloying elements

[62, 63]. In IF steels, for example, elements such as S, P, and Mn can affect the amount of C in solution, regardless of the cooling rate.

Alloying elements can influence the precipitation process by a) changing the activity and subsequently the solubility of carbon, b) affecting the density of nucleation sites, and c) changing the composition of the final precipitate. In addition to its effect on the amount of C in solution, chemical composition can also change the mechanical properties by affecting the extent of grain refinement, the precipitate size distribution, etc. Formability increases as the carbon content is decreased and the anisotropy is also improved more by lowering the C content than the N level [64]. Furthermore, the amount of Ti and therefore the cost of alloying increase with the C level. For these reasons, the N content is usually of subordinate importance in IF steels [59]. Compared to Nb IF steels, the precipitates are dispersed more coarsely in Ti IF steels [59, 65]. Finally, finer grains can be produced in Ti-Nb IF steels than in Ti IF steels [66].

2.6.2. IF Steel Grades

There are three kinds of IF steel. In Ti-IF steels, the Ti combines with the N and S prior to scavenging the C. Thus, theoretically, the titanium level necessary to stabilize a Ti-IF steel is given by the following relationship (in wt. %) [58, 67]:

$$Ti \geq 3.42N + 1.5S + 4C \qquad (2.1)$$

In the case of Ti-Nb IF steels, sufficient Ti is added to combine with the N and S, leaving Nb to scavenge the C [58, 68]. Regarding the Nb IF

steels, the C is tied up by the Nb, whereas Al and Mn combine with the N and S, respectively [58, 69].

In a Ti IF steel, the typical precipitation sequence is considered to be TiN, TiS, $Ti_4C_2S_2$ and TiC [70-74]. This is the case when equilibrium conditions predominate, as shown in Fig. 2.12. In practice, it is almost impossible to reach equilibrium under normal mill processing conditions. Therefore, Subramanian et al. [74] reported that, under such non-equilibrium conditions, the precipitation sequence is the one illustrated in Fig. 2.13.

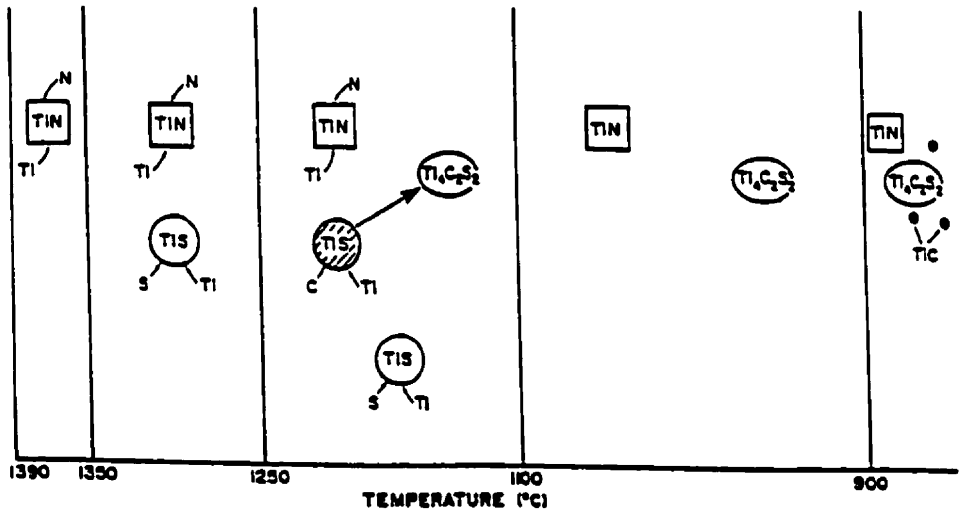

Figure 2.12. Precipitation sequence under *equilibrium* conditions in a Ti IF steel [74].

2.6.3. Effect of Cooling Rate

Another alternative for the stabilization of IF steels is to remove the carbon from solution by controlling the cooling rate during processing. For this approach to succeed, it is suggested that the Ti concentration must be at least three times the stoichiometric amount necessary to tie up the C [75], and even at these levels, the complete removal of carbon is not possible in practice [57].

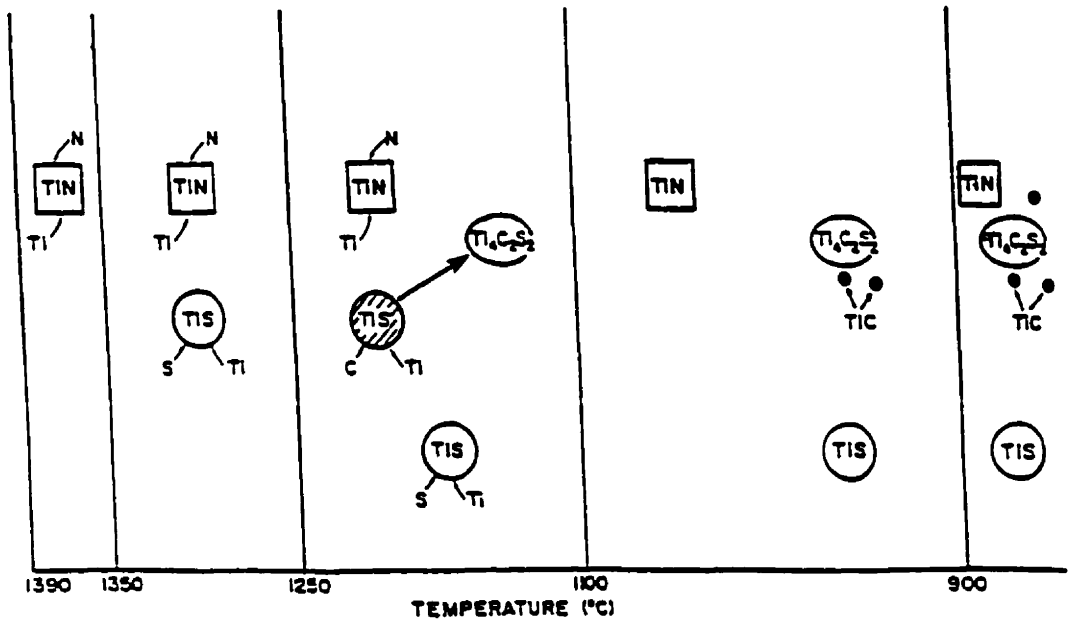

Figure 2.13. Precipitation sequence under *non-equilibrium* conditions in a Ti IF steel [74].

The cooling rate influences the amount of C in solution by determining the amount of carbide that can precipitate. This effect on the amount of carbon that remains in solution at room temperature depends on several parameters. The foremost of these are the reheating temperature and total amount of carbon, which determine the maximum available amount of carbon. Also of importance are the type of particle that will act as a nucleation site for TiC and the size distribution and spacing of these nuclei. The latter determines the length of the carbon atom diffusion path. Here it is important to recall that the nucleation rate is more important than the diffusion rate with respect to precipitation [40, 76], and that higher dislocation densities promote nucleation [76].

As mentioned before, the solubility of C in iron decreases sharply as the temperature decreases to room temperature. Therefore, the cooling rate

down to temperatures as low as 50 to 100 °C can affect the amounts of C in solution, by influencing the formation of carbides. By contrast, to produce a bake-hardenable steel, the cooling rate must be rapid enough not to allow full precipitation of the particles.

2.7. A Critical Review of the Use of Ti in Steels

Since the present work focuses mostly on the aging behaviour of Ti IF steels, a critical review of the use of Ti in steels is of interest.

2.7.1. Effect of Ti on Aging Behaviour and Mechanical Properties

The idea of using Ti to produce a non-strain aging steel was first put forward by Hayes and Griffis [77] in 1934. They suggested that, in addition to the importance of composition, a very slow cooling rate is necessary to reduce the aging tendency of low carbon steels. The aging tendency was eliminated in this work by the addition of 0.058 and 0.067% Ti to 0.042 and 0.05% C steels, respectively. They were then cooled very slowly from high reheating temperatures. Later, Edwards et al. [78] found that 0.21% Ti was necessary to eliminate the yield point and strain aging in a 0.025% C steel. When the C level was raised to 0.085%, for the same amount of Ti, the aging behaviour returned. For this level of C, even with 1.08% Ti (i.e. a Ti/C ratio » 4), they reported slight aging.

Comstock [79] studied the response of more than 40 Ti added low carbon steels to aging after processing under different conditions. He found that steels containing 0.1 to 0.12% carbon with less than 4.5 times as much as Ti displayed a yield point when aged at 200 °C. Steels with Ti>4.5 C (wt. ratio) did not exhibit a yield point, even when they were strained and aged. To determine the influence of different carbide formers on the typical yield curves,

Dies [80] investigated the effect of titanium levels from 0.11 to 2.53% on the yield behaviors of a series of mild steels with 0.03-0.36% C. All samples with Ti/C (wt. ratio) < 4, even when furnace cooled from 930 °C, showed a well-defined yield point. By contrast, those with Ti/C > 4 exhibited continuous annealing. However, steels with 3 < Ti/C < 4, which did not display a yield point after furnace cooling, developed a definite yield point after cooling in still air from 930 °C.

When he increased the Ti/C (wt. ratio) from 0 to 5.2 for a series of steels (%C = 0.124 - 0.135, %Ti = 0 - 0.705), Comstock [81] reported that a stabilized steel was obtained and the yield point disappeared when the Ti/C (wt. ratio) exceeded the critical value of 4. Steijn and Brick [82] used 0.1 or 0.3% Ti to fix the C, N, and O (0.0014% C, 0.0001 - 0.0005% N, and 0.0002 - 0.0006% O) in a high purity iron in order to investigate the flow and fracture behaviour of ferrite. They found no yield point at room temperature, while appreciable ductile behavior was reported at liquid air temperatures.

Glen [83] studied the effect of individual alloying elements on the high-temperature tensile strength of low carbon steels. In the case of Ti added steels, hot-rolled specimens were reheated to 950 °C, then cooled in air in order to tie up the C and N with Ti. He observed a minimum in ductility and a maximum in flow stress at around 200-350 °C during tensile testing and attributed this to the effect of solute C. The minimum in ductility occurred at 200 °C for lower Ti (Ti = 0.22, C = 0.075 wt%) and shifted to higher temperatures as the Ti (Ti = 1.44, C = 0.06 wt%) level was increased. Referring to the ternary phase diagram for Fe-C-Ti, he mentioned that the reason for still having carbon in solution at such high Ti/C ratios could be

that Ti probably increases the solubility of C at room temperature, especially at high Ti levels.

Morgan and Shyne [84] added 0.049% Ti to a base iron (0.06% C, 0.05% N, and 0.008% O) to suppress aging in α-iron. They found several alloying elements (Ti, Al, V, and B) effective for the control of strain aging. For economic reasons, it was suggested that B offers the most promising practical solution to the problem of nitrogen aging. Castagna et al. [85] studied the mechanical properties of a series of pure irons using 0.0421-0.5450% Ti to precipitate the C and N (C+N < 0.01%) as carbides and nitrides. It was concluded that the value of δ_o, the friction stress in the Hall-Petch equation, increased linearly with the amount of Ti, as shown in Fig. 2.14.

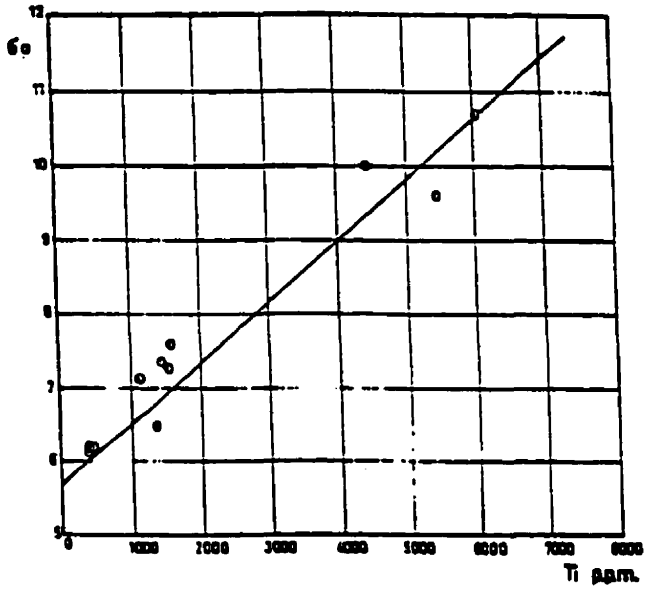

Fig. 2.14. Changes in δ_o in the Hall-Petch equation as a function of Ti concentration [85].

Beresnev et al. [86] made an interstitial-free iron by adding 0.33% Ti to α iron (0.025% C, 0.005% N). The aim was to investigate the

temperature dependence of the dislocation density and the deformation resistance of a bcc iron free of any interstitial impurities. They observed a rise in the deformation resistance of the base iron, without Ti, after 5% deformation and aging for 1 hr at 250 °C. By contrast, the Ti-modified iron displayed no increase. They attributed the former to the trapping of free dislocations by interstitial atmospheres. It was concluded that interstitial atmospheres reduced the mobile dislocation density and their speed by trapping them. This led to an increase in the deformation resistance.

In order to study the tensile properties from room temperature to -195 °C of a polycrystalline bcc iron containing no interstitials, Leslie and Sober [87, 88] added 0.15% Ti to an iron with low concentrations of C, N, O, and S (0.0073% C, 0.0009% N, 0.005% S, 0.006% O). To make sure that the C, N, O, and S were fully tied up by the Ti, the Ti level was set at at least 2 1/2 times the Ti required to scavenge all these interstitials. To promote completion of the desired reactions between the Ti and the C, N, S, and O, the steel was also reheated to 815 °C and then cooled in a furnace to room temperature. With this technique, the weight percent of C or N remaining in solid solution was less than 0.5 ppm. Rosinger et al. [89] produced a Ti interstitial-free steel using the same technique (adding 0.15% Ti to a 0.01% C and 0.0002 % N steel, annealing at 870 °C then cooling at a very slow rate of 75 °C per hr). The purpose was to investigate how the interstitial solute atoms affect the mechanical properties of a bcc metal in the temperature range from -20 to 200 °C. They did not observe serrated flow and attributed this to the almost complete absence of interstitials in solution.

Leslie et al. [90] alloyed an iron base material (0.0037% C, 0.0006% N, 0.005% S, and 0.003% O) with 0.16% Ti to eliminate the

interstitial solutes. Then, they determined the effects of different substitutional alloying elements on the yielding and plastic flow behavior of Fe. They showed that the presence of interstitials complicated the interpretation of the results. Solomon et al. [91] studied the low temperature plastic behavior of an iron (0.0017% C, 0.0011% N, 0.0011% O) by making a Ti (0.15%) interstitial-free iron. After hot rolling, the specimens were reheated again to 810 °C, then furnace cooled. This treatment was done to make sure that all the interstitials were tied up. They reported that the temperature dependence of yielding and of the flow stress in interstitial-free iron is as large as that in impure iron and steel.

In a new attempt, Ti (0.15%) was used by Rellick and McMahon [92] as an oxygen scavenger in a high purity iron, 0.0017% C, 0.0011% N, 0.0011% S. They observed that oxygen-induced brittleness could occur even in a zone-refined iron with 3 ppm O. Compared to Al, they suggested that Ti was not as effective in deoxidizing the ferrite grain boundaries and preventing intergranular fracture.

To study the aging behaviour of dilute substitutional solutions of iron, Leslie [93] produced an interstitial-free iron, containing 0.15% Ti, as a base, to make binary alloys. Then, he studied the effect of different substitutional elements. Most of these alloys contained 3% of only one substitutional element in solution in addition to the Ti. For the original interstitial-free iron without any alloying element, he observed upper and lower yield points at temperatures below ambient, indicating that the presence of interstitial solutes is not essential for discontinuous yielding to occur in iron. Meanwhile, no discontinuous yielding was observed at room temperature or

above. This can be explained by the occurrence of twinning below room temperature.

As for the binary alloys, he found that the presence of substitutional solutes in interstitial-free bcc iron leads to abrupt yielding at temperatures up to 500 °C. Serrated flow in the temperature range 230 to 500 °C was another phenomenon, except for the binary alloys of cobalt and chromium. This was attributed to complex interactions between iron, the various substitutional solutes, the titanium added for gettering, and probably the interstitial solutes at above 200 °C. With respect to the Ti level, no serrated yielding was observed in the 0.15% Ti interstitial-free iron (0.005% C, 0.0022% N, 0.005% S, 0.0039% O), but when the Ti content was increased to 0.6% (0.011% C, 0.003% N, 0.005% S, 0.0055% O) and 1.4% Ti (0.027% C, 0.003% N, 0.006% S, 0.0027% O) in the interstitial-free steels, they reported the occurrence of serrated flow. In this case, serrated flow can be attributed to the presence of Ti in solution, i.e. to DSA caused by a *substitutional* element.

To study the serrated flow behavior of substitutional solid solutions of iron, Cuddy and Leslie [94] prepared a 0.15 % Ti interstitial free steel as described above. They reported serrated flow in this Ti-IF base steel when Si, Mn, Ni, Ru, Rh, Re, Ir, or Pt were present as additional substitutional solutes. When the interstitials C and N were again added to these "binary" alloys, various effects were observed. They attributed this variety of behaviors to the pinning of dislocations by some complex or by clusters of solutes, probably containing both substitutional and interstitial atoms and not only individual substitutionals.

2.7.2. Using Ti to Produce High Formability Sheet Steels

In order to attain the high ductility and extra-deep drawability required by the automobile industry, it is necessary to tie up carbon and nitrogen by strong carbide and nitride formers in extra-low-C steels. This requirement led to the first production of IF steels as cold-rolled sheet steels [95-98].

Comparing rimmed, aluminum-killed, and IF steels, Elias and Hook [95] found that IF steels had much better properties for deep drawability. They said that 0.08-0.31% Ti should be high enough to scavenge 0.002-0.012% C, 0.004-0.008% N, 0.008-0.02% S, and 0.002-0.01% O. Fukuda and Shimizu [96] observed that the mechanical properties of Ti-IF steels as cold rolled and annealed sheets improved when Ti was added in amounts of 10 to 20 times the carbon content.

Since then, commercial Ti-IF steels are being produced with deep and extra-deep drawing qualities. This requires high resistance to aging in order to get high ductilities, good drawabilities, and desirable formabilities. However, aging problems can arise even in IF steels, which has led to recent investigations on this subject.

2.7.3. Using Ti to Prevent Aging in the Wire Rod Industry

Recently, in addition to the automobile industry, Ti has also been used to suppress strain aging in the rod and wire drawing industries. These applications require the low work hardening rates and flow stresses provided in the absence of aging phenomena. For example, the occurrence of dynamic strain aging in commercial wire drawing steels not only results in shear cracking and increasing wear of the tools [99] but, most importantly, also

promotes flow localization, leading to wire breaks during drawing [35, 37, 100, 101].

McIvor [102] studied the effect of adding 0.02-0.11% Ti to a low-carbon wire-rod steel (0.02 - 0.06% C, 0.002 - 0.01% N). He suggested that, in order to have a non-aging, highly drawable, and low strength steel, the Ti level should not exceed:

$$\%Ti \leq 0.07+3.4\%N \qquad (2.2)$$

Boratto et al. [103] found that the addition of 0.029% Ti to a low-carbon wire steel (0.02% C, 0.0076% N, 0.009% S) could not prevent aging because of the C and N that remained in solution. Ochiai et al. [75, 104] used a wide range of Ti levels, $0 < Ti_{eff.}/C < 3$ atomic ratio, to suppress strain aging during the rolling of wire rod. They concluded that, during the conventional processing of wire rod, the minimum amount of Ti needed to prevent aging had to be at least 3 times as much as the Ti required stoichiometrically to fix the 0.005% C in their steels. By controlling the cooling rate during processing, these amounts of Ti were reduced significantly. Also, for 0.02% C, this amount was reduced to about twice.

2.8. Measurement and Estimation of the Amount of Carbon in Solution

2.8.1. Measurements by Internal Friction

Internal friction measurement is commonly used to detect the dissolved interstitials in steels [105-107]. Such measurements can be done either as a function of temperature at constant frequency or as a function of frequency at constant temperature. In the conventional method, an apparatus with an inverted torsion pendulum is used to determine the amount of an interstitial in

solution [105]. Such experiments are usually carried out at approximately constant frequency as a function of temperature. There is a temperature at which the diffusion jump frequency of the interstitials is about the same as the frequency of the applied stress. This indicates the position of the Snoek peak. The conventional internal friction technique has a number of disadvantages: i) at elevated temperatures, metallurgical reactions occur in the steel during a test, and ii) at low frequencies, the procedure is very time consuming. It has therefore been claimed that this conventional method is neither fast nor accurate enough for ultra low carbon steels [61, 75, 104, 108].

Recently, Wen et al. [109] and Ritchie and Pan [4] have invented two new techniques that overcome these shortcomings. Although both methods can be used at high frequencies, the advantage remains with the first one, which measures solute interstitial levels at room temperature. In this case, the internal friction is measured as a function of frequency at constant temperature. Fig. 2.15 shows a Snoek peak in a sample containing about 2 ppm carbon measured by this technique.

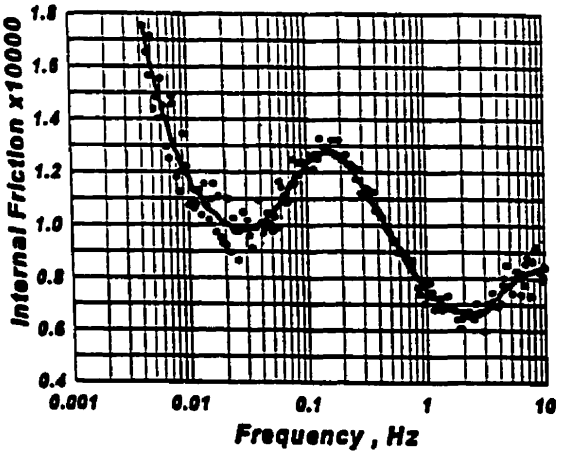

Fig. 2.15. Internal friction measurement in a sample containing about 2 ppm solute C [109].

The amount of solute is given by [109]:

$$Q^{-1} = 2\times10^{-5}\, C_i(ppm) \qquad (2.3)$$

where Q^{-1} is the internal friction value.

2.8.2. Estimation Using the Established Correlation Method

In the case of very low carbon steels, another approach can be used to estimate the amount of carbon in solution at room temperature. As mentioned above, because of some disadvantages associated with the conventional internal friction method, some workers have established a correlation between the amount of carbon in solution and aging indices [61, 75, 104, 108]. This correlation is shown in Fig. 2.16.

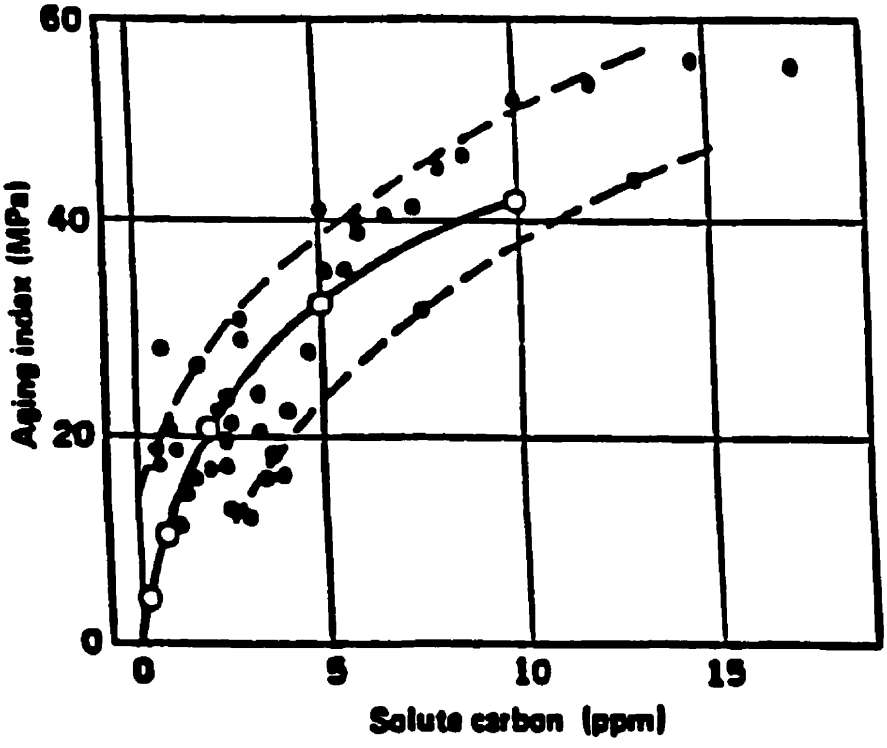

Figure 2.16. The correlation between aging index and amount of solute carbon [61, 75, 104, 108].

2.8.2.1. Aging Index Test

The aging index test is commonly used to assess the aging behaviour of steels [3, 102, 110-114]. It is also possible to estimate the amount of carbon that corresponds to each value. As illustrated in Fig. 2.17, the aging index is the difference between the flow stress after an 8% prestrain and the lower yield stress after aging at 100 °C for 1 hr.

The aging-index approach characterizes the return of the upper and lower yield points, any upward shift of the flow curve, and any reduction in the elongation to fracture. The changes in mechanical properties attributable to this treatment are then used to judge the likelihood of a return of the yield point after storing for longer times at room temperature [3, 102, 112].

Although an 8% prestrain may seem high, investigations have shown that heavy temper rolling only leads to a moderate increase in the yield strength, while maintaining the ductility and formability at acceptable levels. This is especially true for IF steels, which have excellent formabilities prior to temper rolling [115]. It is also of interest that Bailey et al. [49], who investigated the effects of amount of prestrain and strain path on the aging response of bake hardenable sheet steels, found that an 8% prestrain in uniaxial tension gives rise to aligned cell structures that are comparable to those produced by biaxial straining and plane strain rolling.

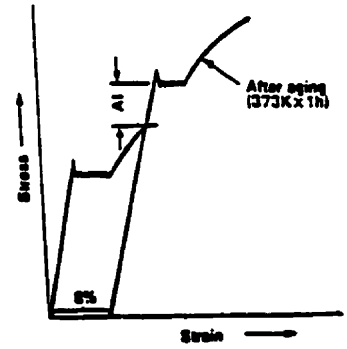

Figure 2.17. Measurement of aging index.

CHAPTER 3

Experimental Techniques

3.1. Experimental Materials

In order to investigate a variety of aging behaviors in IF steels, four IF grades were selected for this study.

The materials were supplied by Stelco Steel and by Dofasco Inc., Hamilton, Canada. Samples for laboratory testing were taken from strip mill transfer bars that had been rolled down to thicknesses of approximately 26 to 28 mm. The original 245 or 268 mm thick slabs were reheated to about 1260 to 1280 °C before rolling and the last roughing pass was carried out at about 1140 or 1120 °C. Tables 3.1 and 3.2 show the compositions of the four IF grades studied and an example of an industrial rolling schedule employed to process one of these materials, respectively.

Table 3.1. Chemical compositions of the experimental steels, wt%.

	C	N	Ti	Nb	S	P	Mn	Ti_{exc}	$(Ti^*_C+Nb)/C$	Ti^*_S/S
steel A	0.0019	0.0030	0.044	0.007	0.015	0.008	0.13	0.004	1.48	1.50
steel B	0.0023	0.0032	0.06	0.005	0.023	0.011	0.16	0.005	1.58	1.43
steel C	0.0022	0.0025	0.055	0.007	0.009	0.005	0.18	0.033	3.75	3.50
steel D	0.0030	0.0018	0.018	0.02	0.005	0.003	0.18	___	1.22	1.58

Ti^*_S is the amount of Ti available to combine with S after all the N is tied up as TiN.

Ti^*_C is the amount of Ti available to tie up the C after the formation of TiN and TiS.

Ti_{exc} is the amount of Ti remaining in solution after the precipitation of TiN, TiS, and TiC.

Table 3.2. An industrial rolling schedule employed on one of the present materials.

Pass No.	Exit thickness	Temp. (°C)	Interpass time (s)
1	215	1260	10.9
2	195	1255	10.5
3	175	1250	12.0
4	155	1245	12.1
5	130	1239	14.8
6	100	1231	15.8
7	70	1219	22.0
8	45	1195	22.1
9	26	1139	

Among the three Ti IF steels, steels A and B had approximately the same Ti_{exc}, Ti^*_C/C, and Ti^*_S/S values, even though the Ti and S levels of steel B were about 1.5 times those of steel A. (See Table I for definitions of Ti_{exc}, Ti^*_C, and Ti^*_S.) Steel C had the highest Ti^*_S/S ratio and the lowest S content, with almost the same Ti concentration as steel B. A Nb IF steel was chosen with a $(Ti^*_C+Nb)/C$ ratio $\cong$ 1.2; this is theoretically more than enough to tie up all the C, so that its aging behavior should be comparable with that of the Ti IF steels. Note also that the Ti^*_S/S ratio for this steel is almost the same as that of Ti IF steels A and B; nevertheless, the mechanism of C stabilization in this material is based on the formation of NbC not on that of $Ti_4C_2S_2$ and TiC.

3.2. Specimen Preparation

Three types of mechanical tests were performed in the present study: tension, mostly at elevated temperatures, torsion, and internal friction. It is well

known that tension testing is the most common technique employed to investigate the aging behaviour of steels. Therefore, the major part of the present investigation was carried out using this technique. However, for the first time, DSA was investigated on IF steels in torsion. Internal friction tests were also carried out to measure the amount of carbon in solution after employing different reheating temperatures and cooling rates.

3.2.1. Tension Tests

For the tensile testing at elevated temperature, standard ASTM specimens with threaded ends were prepared [116], with their longitudinal axes parallel to the rolling direction. Their dimensions are shown in Fig. 3.1.a. The use of threaded shoulders for gripping the specimens enables aging phenomena, such as the propagation of Luders bands, serrated flow, increases in flow stress, and decreases in ductility, to be observed clearly [35].

All samples were cleaned with alcohol before carrying out the tests, in order to remove stains that could possibly lead to stress concentration at elevated temperatures.

3.2.2. Torsion Tests

Torsion specimens with gage lengths of 22.2 mm and diameters of 6.3 mm were used, as shown in Fig. 3.1.b. They were prepared from the as-received material with the longitudinal axes parallel to their rolling direction.

3.2.3. Internal Friction Tests

To prepare the 0.7 mm thick specimens for the internal friction measurements, a cold reduction of about 75% was applied using a laboratory

mill. Then, specimens were machined from the sheets aligned along the rolling direction with the dimensions shown in Fig. 3.1.c.

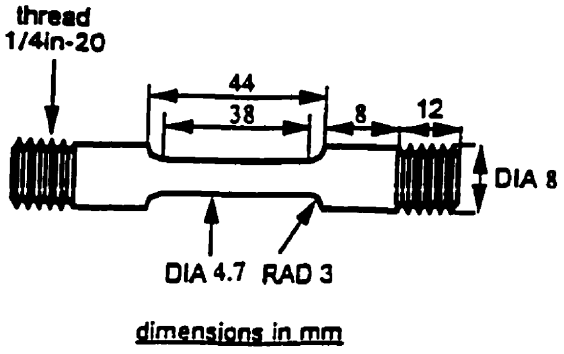

(a)

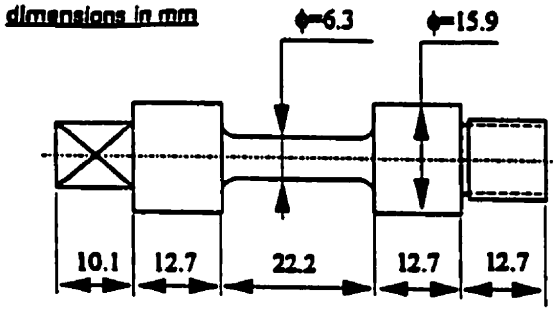

(b)

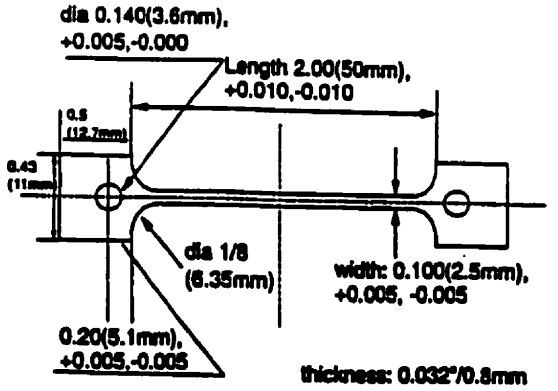

(c)

Figure 3.1. Geometries of a) tension, b) torsion, and c) internal friction samples.

3.3. Experimental Equipment

3.3.1. Tension Machine

The tensile tests were carried out using a computer-controlled MTS machine. This closed-loop servo-hydraulic device has a capacity of 100 kN. Displacement of the actuator was measured from the output of a linear variable differential transformer (LVDT) with a total linear range of ±50 mm. A personal computer connected to the MTS TestStar workstation interface was used for data acquisition and to control the process. This workstation runs the TestStar software and includes a load unit control panel, and a digital controller, Fig. 3.2.

A microprocessor-controlled tungsten lamp radiant furnace mounted on the machine frame was used to heat the specimen to the desired elevated temperature. The heat generated by the four tungsten filament lamps is reflected to the centre of the furnace, where the specimen is located, by four mirror finished elliptical reflectors of aluminum. The specimen was heated at 1 °C/s and held at the testing temperature for 5 min prior to testing. A type-K (chromel-alumel) thermocouple fixed against the centre of the specimen gage length was used to measure the temperature and its deviations were found not to exceed ±1 °C. To make sure that the distribution of temperature was uniform along the gage length, another type-K (chromel-alumel) thermocouple was placed against the shoulder of the specimen for some of the tests. Temperature variations between the two thermocouple measurements were found to be within ±2 °C. The specimen and grips were enclosed in a quartz tube and argon gas was passed through it to minimize oxidation. The gripping bars were water-cooled to prevent oxidation.

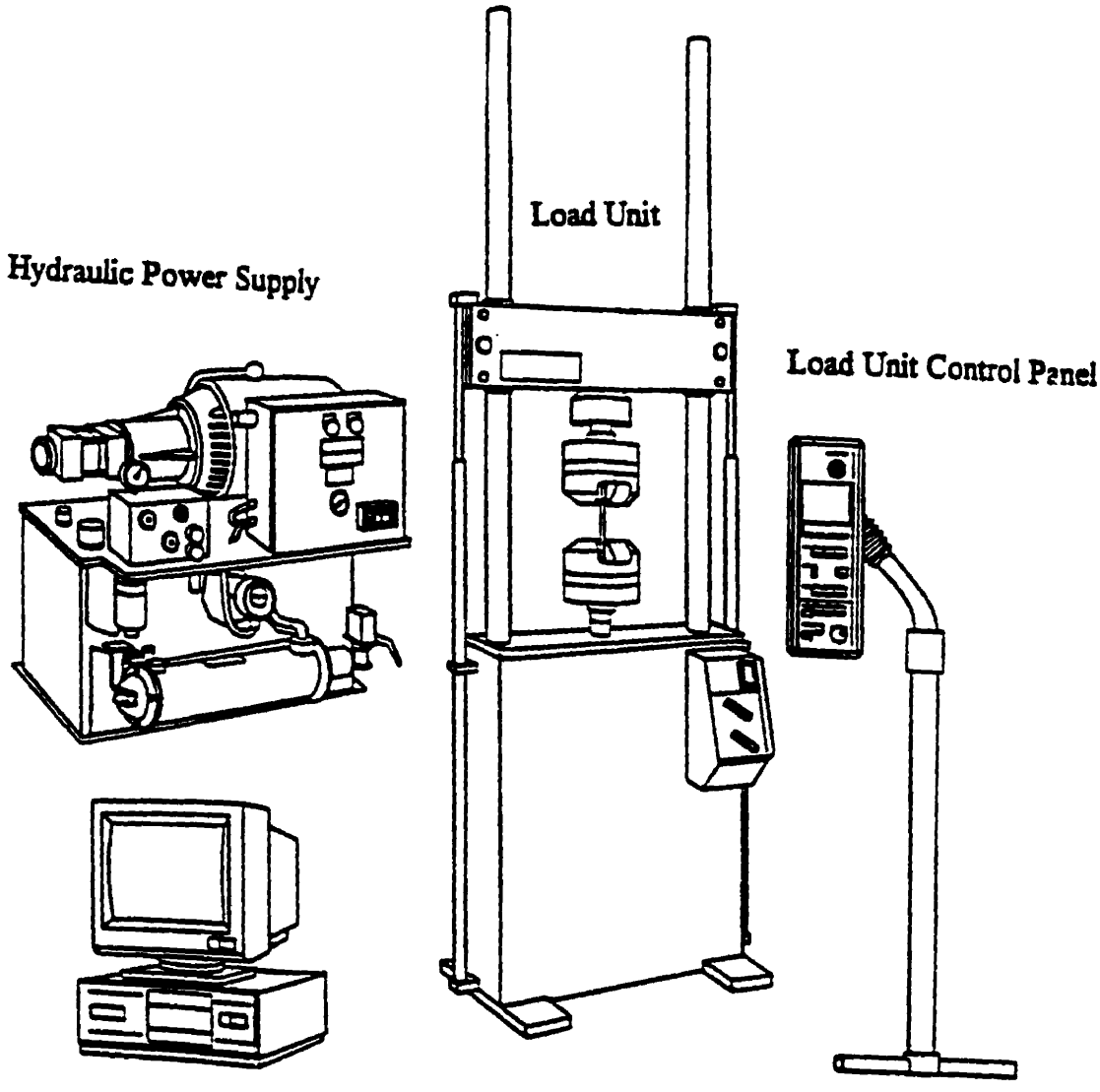

Figure 3.2. The workstation of the TestStar tensile testing equipment and its components.

3.3.2. Torsion Machine

The torsion tests were carried out on a servo-hydraulic computer controlled MTS torsion machine, which is mounted on a lathe base and is used for the simulation of hot rolling [117]. The specimen is connected to the rotating hydraulic actuator at one end and is fixed into a grip at the other end. A torque cell is connected to the end of the right-side loading bar to record the load. The displacements are measured by the transducer connected to the rotating bar on the left hand side, Fig. 3.3.

The specimen was located along the central line of a radiant furnace, where it was heated by four tungsten filament lamps. An Elecromax process controller was used to control the temperature. The temperature was detected by a K-type chromel-alumel thermocouple, which was in contact with the specimen on the gauge length. To prevent oxidation, the specimen was located in a quartz tube, while a constant flow of high purity argon passed through the tube.

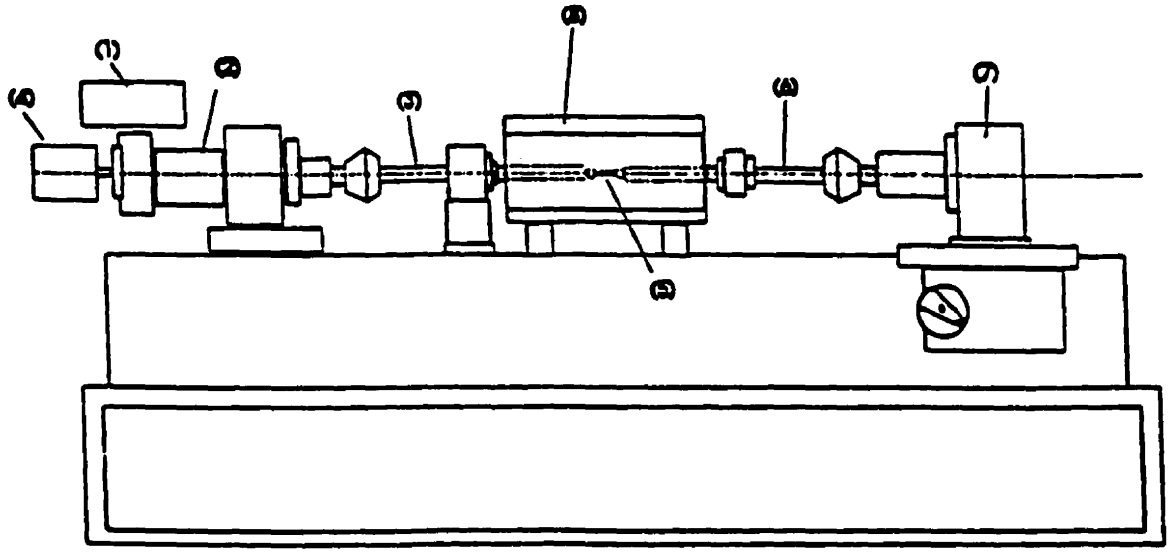

(1) hydraulic servovalve, (2) hydraulic motor, (3) rotating torsion bar, (4) potentiometer, (5) specimen, (6) stationary grip, (7) torque cell, (8) furnace.

Figure 3.3. Schematic diagram of the torsion machine.

A TestStar workstation was used to record the twist and torque as well as the temperature. The data were acquired by a microcomputer connected to the digital controller of the TestStar.

3.3.3 Internal Friction Apparatus

A forced torsion pendulum was used to measure the amount of carbon in solution. The components of the pendulum were selected and dimensioned such that the measured internal friction equals the internal friction of the sample. The torque is applied by a coil which provides a field perpendicular to a magnet; that torque is proportional to the current flowing through the coil. A digital frequency generator and associated electronics provide the required excitation. The angular displacement is of the order of 3×10^{-5} and is measured by a photocell detector. Then, the damping due to the reorientation of the carbon interstitials at ambient temperature is approximately given by equation 2.3. The different peaks represent different carbon concentrations, i.e. C_i in equation 2.3 [109].

A schematic illustration of the forced torsion pendulum used to measure the solute carbon is given in Figure 3.4.

3.3.4. Cooling System

Accelerated cooling was simulated by cooling with water, helium gas and compressed air. For this purpose, a cooling device was used, as illustrated in Fig. 3.5. The internal wall was pierced with three rows of four holes set at 90 deg from one another, which served as coolant outlets. The coolant was introduced into the cooling device under pressure through inlets on the external wall. The pressure of coolant was controlled by means of a two-stage pressure regulator in order to obtain different cooling rates.

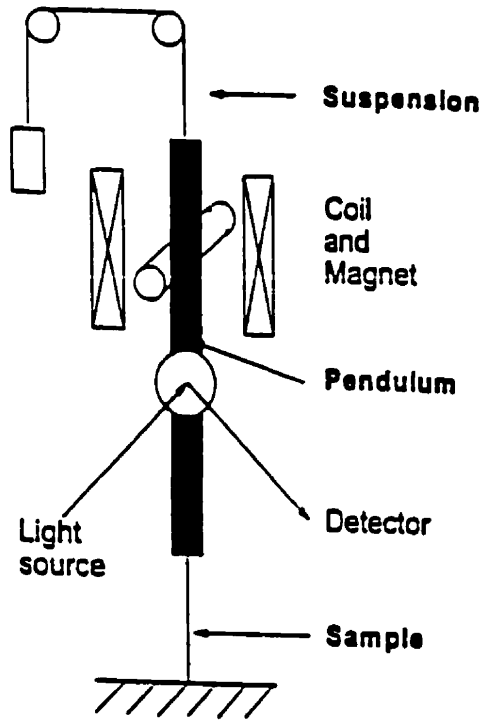

Figure 3.4. Schematic diagram of the forced torsion pendulum.

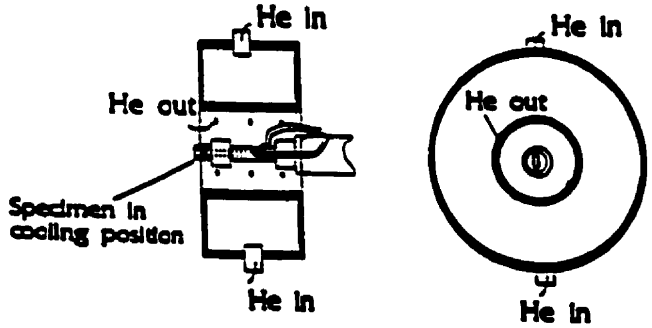

Figure 3.5. Geometry of the cooling system and specimen.

3.4. Experimental Methods

3.4.1. Tension

To investigate the aging and bake hardening behaviors of IF steels, engineering stress-strain curves were plotted from the load-displacement data, as was done by previous workers [9, 35, 40, 49, 100, 101, 118]. The mechanical properties of the material were then derived. In the cases where a well-defined yield point was not observed, the 0.2% offset method was used as a measure of the yield strength.

3.4.1.1. Dynamic Strain Aging Tests

3.4.1.1.1. Effects of Chemical Composition, Reheat Temperature and Cooling Rate

The effects of reheat temperature and cooling rate were studied on samples of steel A. These treatments consisted of reheating to five temperatures (900, 950, 1050, 1150, and 1200 °C) and then cooling at six rates to room temperature.

The different cooling rates were produced by: (a) water quenching, W, (b) cooling with helium gas, He, (c) with compressed air at a high flow rate, H.F.R., (d) compressed air at a low flow rate, L.F.R., (e) in still air, S.A., and (f) furnace cooling, F. The cooling rate for water quenching was about 400 °C/s. For the gas cooling procedures, the rates were about 50, 25, 12, 3 and 0.05 °C/s, respectively. This heat treatment cycle is shown in Fig. 3.6.

For steels B, C, and D, the samples were reheated to 900, 1000, and 1100 °C, then cooled at three rates of 400, 3, and 0.05 °C/s to room temperature.

All the samples prepared in this way were tensile tested at 300 °C and 10^{-3} s^{-1}.

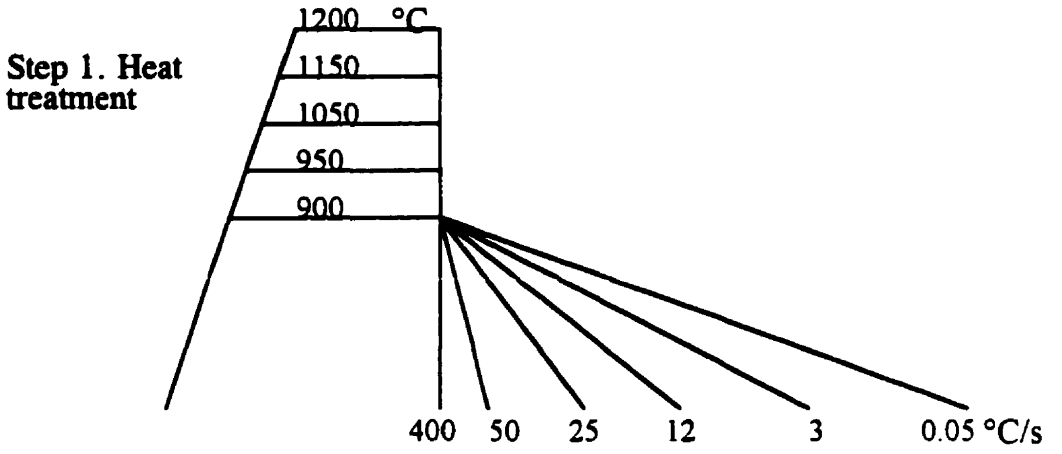

Figure 3.6. The heat treatment cycle applied to the samples.

The reheat temperatures were chosen considering the solubility products of $Ti_4C_2S_2$, TiC and NbC as follows [119, 120]:

$$\log[Ti][C]^{0.5}[S]^{0.5} = -17045/T + 7.9 \quad (3.1)$$

$$\log[Ti][C] = -10800/T + 5.02 \quad (3.2)$$

$$\log[Nb][C] = -8970/T + 3.46 \quad (3.3)$$

For example, the TiC dissolution temperatures obtained for steels A, B, and C are about 841, 864, and 903 °C, respectively. In the case of steel D, the dissolution temperature for NbC is about 866 °C.

In some cases, the reheat temperature was 1100 °C in order to simulate the last finishing temperature of the as-received materials and the cooling rates

on the run-out table. Holding for 10 min at the reheat temperature has been reported to approximate satisfactorily the condition of the material at the beginning of cooling on the run-out table [35]. This enables the precipitates to be identified [121].

As for C and N, their solubilities in α-iron can be calculated using the following equations [122-124]:

$$\log [C]_{ppm} = 6.38 - (4040/T) \quad (3.4)$$

$$C\ (wt\%) = 2.55 \exp(-4850/T) \quad (3.5)$$

$$N\ (wt\%) = 12.3 \exp(-4177/T) \quad (3.6)$$

3.4.1.1.2. Effects of Chemical Composition, Tensile Strain Rate and Test Temperature

For this purpose, samples of steels A, B, and C were reheated to 1100 °C and then cooled in still air at the rate of 3 °C/s. Then, tensile tests were carried out on samples of these three grades at four different strain rates of 10^{-4}, 10^{-3}, 10^{-2}, and 10^{-1} s^{-1}. At each strain rate, up to 13 temperatures (depending on the strain rate) were employed: 25, 65, 100, 125, 150, 175, 200, 225, 250, 300, 350, 400, and 450 °C.

The aim was to extrapolate these results and to predict the occurrence of DSA at higher temperatures and higher/lower strain rates, such as those involved in the processing of IF steels, i.e. ferrite rolling and flattening.

In the case of steel D, tensile tests were carried out on two sets of samples (cooled from 900 °C in still air and from 1100 °C in the furnace) at the four strain rates and at the elevated temperatures mentioned above.

3.4.1.2. Static Strain Aging Tests

3.4.1.2.1. Aging Index (AI) Test

Static strain aging tests were carried out on all four IF steels using different reheat temperatures and cooling rates. Then, the specimens were prestrained 8% in tension and at room temperature. Following this, artificial aging at 100 °C for 1 hr was carried out on the prestrained samples. After cooling in still air from 100 °C, they were pulled to fracture at room temperature. This method, known as the aging index test, is a common technique [3, 102, 110-114] used to study the static strain aging behaviour of steels.

By carrying out repeated tests under the same conditions, the deviations associated with the aging indices and the amounts of carbon in solution were determined to be about 3 MPa and 1 ppm, respectively.

3.4.1.2.2. Effects of Chemical Composition, Reheat Temperature and Cooling Rate

Samples of all four IF steels were reheated to 1100 °C and then cooled at three rates to room temperature. The different cooling rates were produced by: (a) water quenching (W), (b) still air cooling (S.A.), and (c) furnace cooling (F), with values of 400, 3, and 0.05 °C/s, respectively. To compare the SSA behaviors of the present IF steels, aging index tests were then carried out on all the samples prepared in this way. These steps are represented in Fig. 3.7.

Step 1. Apply different cooling rates to samples of steels A, B, C, and D.

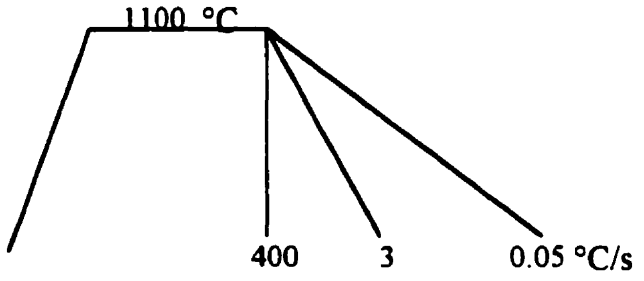

Step 2. Carry out aging index tests

Step 3. Carry out internal friction measurements on samples of steels B and C

Figure 3.7. The steps employed to compare the SSA behaviors of the 4 IF steels.

The effects of different reheat temperatures and cooling rates were investigated on steel A. The samples were reheated to five temperatures, 900, 950, 1050, 1150, and 1200 °C. They were then cooled to room temperature at the three rates mentioned above. Following this, the SSA behaviour was studied by carrying out aging index tests on the samples treated this way. This procedure is illustrated in Fig. 3.8.

Step 1. Apply different reheat temperatures and cooling rates to samples of steel A.

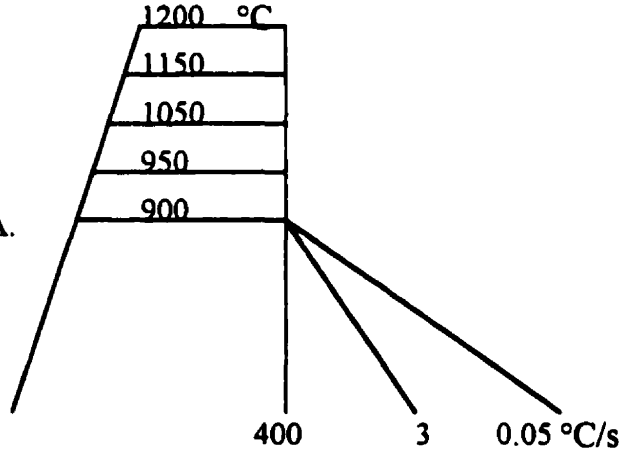

Step 2. Carry out the aging index tests

Figure 3.8. The treatments employed to study the effects of reheat temperature and cooling rate on the SSA behavior of steel A.

3.4.1.3. Quench Aging Tests

In order to follow the occurrence of aging phenomena during storing at room temperature, some specimens of steel A were rapidly cooled from 1050 and 900 °C using water (400 °C/s) and helium gas (50 °C/s). They were then tensile tested at 300 °C and 10^{-3} s^{-1}: i) immediately after quenching and ii) after storing at room temperature (24 °C) for three weeks.

3.4.1.4. Bake Hardening Tests

Three different approaches to testing the susceptibility of steel B for bake hardenability were investigated. The mechanical properties were then compared with regard to the amount of bake hardening and the possibility of an industrial application. Also, for each case, the optimum amounts of prestrain and temperature that give the maximum bake hardening were determined.

Samples of steel B were reheated to 900 °C, held for 60 s, and then cooled to room temperature at 12 °C/s (LFR). The aim was to obtain enough solute carbon for bake hardenability. The high annealing temperature, 900 °C, is necessary in the case of IF steels so as to produce a susceptibility for bake hardening [51, 52, 54, 55, 71]. All the tensile tests were then carried out at a strain rate of 10^{-3} s^{-1}.

3.4.1.4.1. Dynamic Bake Hardening (DBH) Method

In this new method, samples of steel B were prestrained 2, 4, 6, and 8% at 100, 150, 200, and 250 °C (i.e. they were bake hardened "dynamically"). After cooling in still air, they were tensile tested at room temperature. This procedure is illustrated in Fig. 3.9. The bake hardening values, yield strengths before and after baking were then obtained from the tensile test results. The

yield strength after baking is usually used to judge the dent resistance of metals [49, 125].

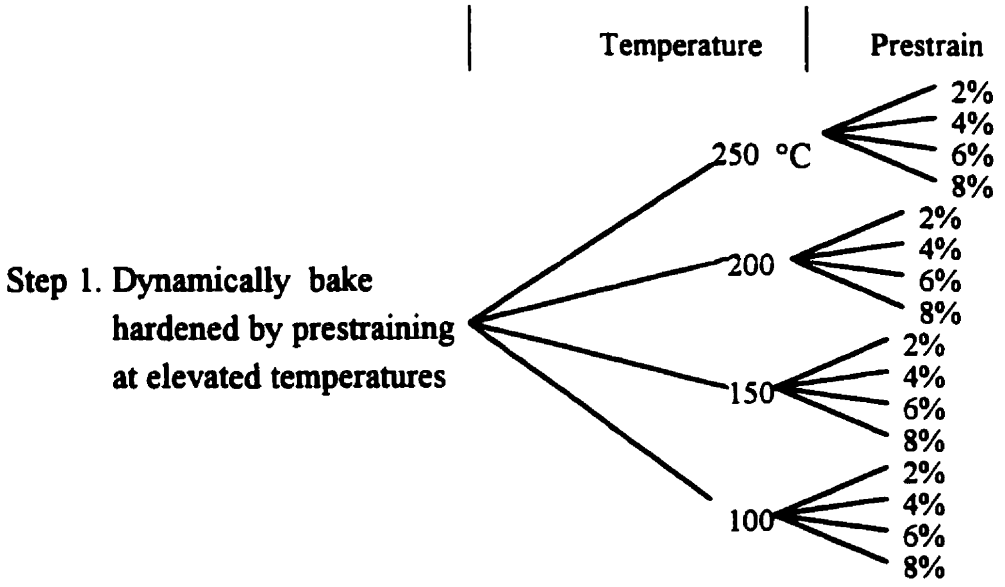

Figure 3.9. Schematic diagram of the DBH method.

3.4.1.4.2. Static (Conventional) Bake Hardening (SBH) Method

This method is exactly the procedure normally used to assess the bake hardenability of steels. Samples were prestrained 2, 4, 6, and 8% in tension and at room temperature. They were then aged at 100, 150, 200, and 250 °C for 20 min. Following this step, tensile tests were carried out at room temperature. These steps are summarized in Fig. 3. 10.

3.4.1.4.3. Dynamic-Static Bake Hardening (DSBH) Method

This method is another new technique introduced here regarding the susceptibility for bake hardening. Like the DBH process, in the DSBH method, samples were also dynamically bake hardened by prestraining 2, 4, 6,

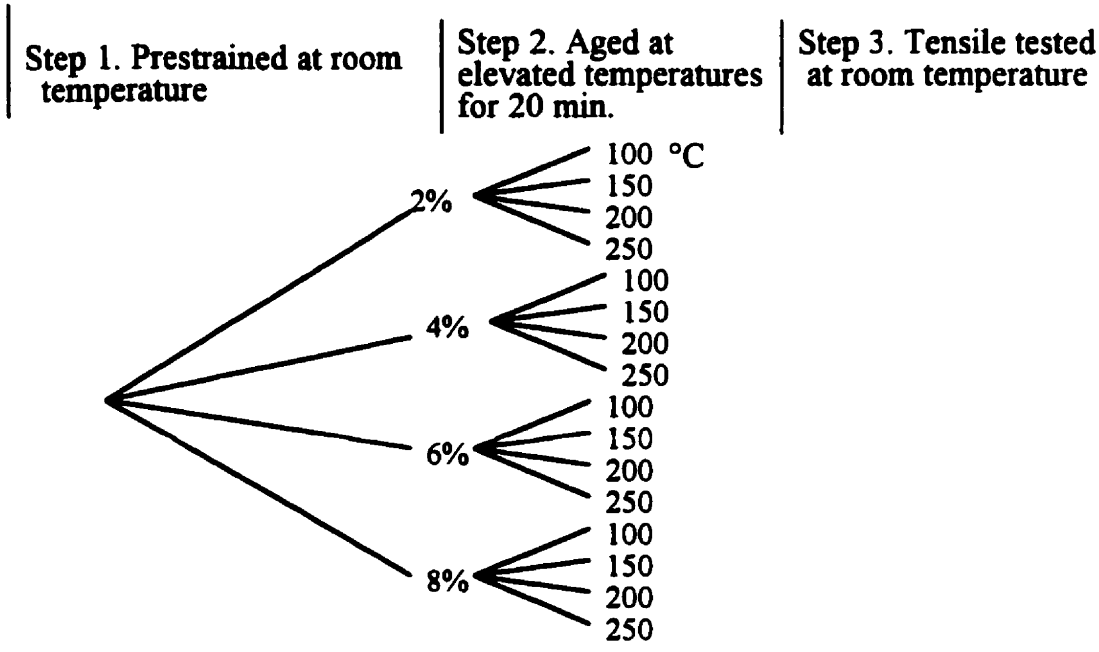

Figure 3.10. The steps of the SBH method.

and 8% at 100, 150, 200, and 250 °C. The only difference between the DBH and DSBH procedures is that, in the DSBH technique, the samples were subjected to another aging process: static strain aging at 170 °C for 20 min (this step is usually employed for the simulation of conventional bake hardening). Finally, they were pulled to fracture at room temperature. In fact, this method (DSBH) is a combination of the DBH and SBH techniques, as presented in Fig. 3.11.

3.4.2. Solute Carbon Measurement

In studying the aging behaviour of steels, it is important to know how much C is in solution during or after the manufacturing process. There are two common techniques for the measurement and estimation of the amount of solute carbon. The internal friction technique is the most popular method for measuring the amount of carbon in solution. This is the technique that was

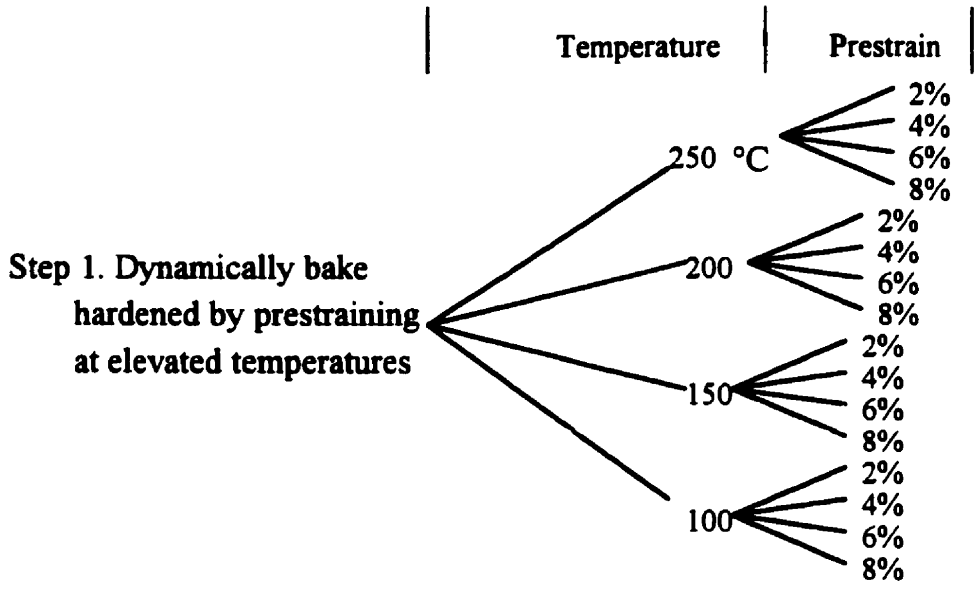

Step 2. Statically strain aged at 170 °C for 20 min.

Step 3. Tensile tested at room temperature

Figure 3.11. The steps employed in the DSBH method.

used in this study. As already mentioned in section 2.8, the conventional internal friction technique has a couple of disadvantages: i) at elevated temperatures, metallurgical reactions occur in the steel during the test, ii) at low frequency, the procedure is very time consuming. Consequently, the new method described in that section was used to measure the amount of carbon in solution. The advantage of this method is that the interstitial levels can be measured at room temperature using a wide range of frequencies.

3.4.2.1. Solute Carbon Estimation

In order to expedite the study of the aging behaviour and because the conventional internal friction method is not sufficiently accurate for very low carbon steels, a correlation has been established between the amount of carbon in solution and the aging index [61, 75, 104, 108]. This correlation was shown

in Fig. 2.16. Knowing the aging indices and using this correlation, the amounts of carbon in solution can be roughly estimated [61, 75, 104, 108].

3.4.3. Torsion

Torsion tests can be used to study the dynamic strain aging behavior of steels at high temperatures and high strains. For the first time, torsion tests were carried out to investigate the dynamic strain aging behaviour of a Ti IF steel (steel A) in the austenite and ferrite regions. The measured torque, T, and twist, θ, were converted to equivalent stress and strain using the following equations [117, 126].

$$\sigma = 3.3\ T\sqrt{3}/2\pi R^3 \qquad (3.7)$$

$$\varepsilon = \theta R/L\sqrt{3} \qquad (3.8)$$

where R and L are the radius and gage length of the specimen, respectively.

The A_{r3} temperature for IF steels with almost the same chemical composition is estimated to be about 900 [121, 127], 895 [68], or 890 °C [67, 128]. As for the A_{r1}, a value of 860 °C has been reported [67, 68, 121, 127, 128]. Therefore, in order to be conservative, the maximum temperature for testing in the ferrite range was chosen to be 850 °C. However, according to the following equation used to calculate the A_{r3} [129] based on chemical composition, this temperature for IF steels is close to that for pure iron, ≈ 910 °C [127, 130].

$$A_{r3} = 910 - 310C - 80Mn - 20Cu - 15Cr - 80Mo + 0.35\,(t-8) \qquad (3.9)$$

Here t is the plate thickness.

3.4.3.1. Hot Rolling Simulation

The pass strains and interpass times applied are presented in Table 3.3. This simulation involves seven roughing and seven finishing passes, along the lines of a typical industrial strip-rolling schedule [67, 68, 121, 128]. All the simulated passes were executed at a strain rate of 2 s^{-1}. The first roughing temperature was 1260 °C, while different finishing temperatures were employed. The roughing passes were carried out on the austenite phase, and the finishing passes in the ferrite region. However, in some cases, the first finishing pass was carried out in the austenite or in the $\gamma+\alpha$ and the rest in the ferrite region. In all cases, the serrations were initiated in the ferrite phase.

3.4.3.2. Warm Rolling Simulation

The same schedule, Table 3.3, was used in this case. The only difference with respect to the above program is that in this case both the roughing and finishing passes were carried out in the ferrite region. The first roughing temperature was 850 °C.

3.4.4. Coiling Simulation

The effects of coiling temperature and cooling rate after this process were investigated by employing one coiling temperature (650 °C) and two cooling rates (0.01 and 0.03 °C/s). This treatment was executed on samples of steels B and C.

The applied coiling temperature is a typical temperature normally used in the coiling of IF steels [48, 58, 59, 74, 131]. Recently, the demand for low-temperature coiling has increased because of the problems associated with the

Table 3.3. Schedule for the simulation of hot and warm rolling.

	Strain rate (/s)	Strain per pass	Interpass time (s)
R1	2	0.23	3.5
R2	2	0.25	8
R3	2	0.23	10
R4	2	0.29	12
R5	2	0.39	13
R6	2	0.75	18
R7	2	0.56	150
F1	2	0.41	3.5
F2	2	0.53	2.5
F3	2	0.55	1.7
F4	2	0.55	0.80
F5	2	0.55	0.80
F6	2	0.40	0.80
F7	2	0.40	

high-temperature coiling process. These problems are [3, 132-134]: i) decreases in the product yield, ii) increases in the oxide scale thickness, iii) the formation of coarse grains, which then cause surface defects, iv) the formation of large cementite particles, which can cause damage by cracking, v) variations in the mechanical properties along the coil length, mostly because of differences in cooling rate between the coil ends and the middle. That is the reason for employing the second cooling rate of 0.03 °C/s, while the cooling rate of 0.01 °C/s is mostly used in industrial applications [55, 135, 136].

As shown in Fig. 3.12, this simulation consisted of reheating to 1150 °C (which is a little above the finishing temperature of the present materials) and cooling to room temperature at 3 °C/s. Specimens were then reheated to 650 °C, held at this temperature for 15 min and then cooled to room temperature at 0.01 °C/s and 0.03 °C/s. This method resembles the technique that has been employed by most workers to simulate the coiling process [48,

55, 57, 65, 131, 137, 138]. However, some workers have applied another procedure, which consists of cooling down, after finishing, to the coiling temperature [139-141]. Finally, aging index tests were carried out on the samples and, from the aging indices obtained, the amount of carbon in solution was estimated.

It should be pointed out that, according to previous workers, coiling temperature does not have any significant effect on the subsequent mechanical properties, e.g. on bake hardening [48, 51, 59, 121, 125, 134, 135, 142, 143].

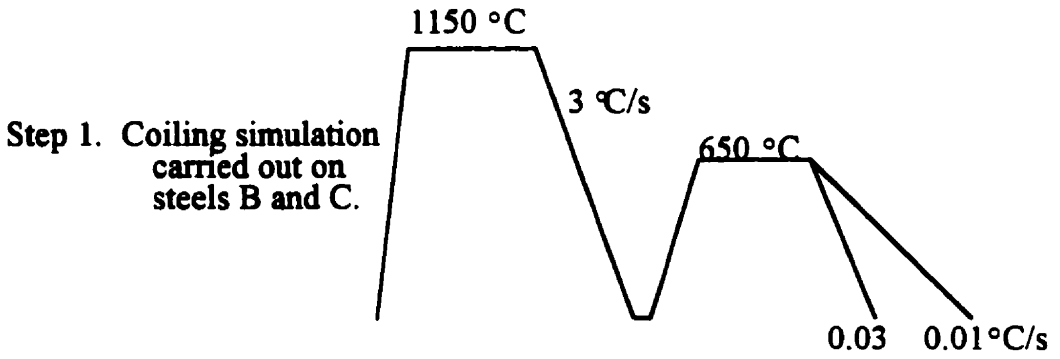

Fig. 3.12. Schematic diagram of the simulation of the coiling process.

3.4.5. Continuous Annealing Simulation

Since the amount of carbon in solution after coiling may affect the solute carbon level during continuous annealing, a coiling simulation was employed prior to simulating continuous annealing. After a laboratory cold reduction of about 75%, samples of steels B and C were reheated to three "annealing" temperatures (650, 750, and 850 °C). After holding for 60 s, they were cooled to room temperature at 0.03, 3, and 100 °C/s. Except for the

cooling rate of 0.03 °C/s, which was discussed in the previous section, the cooling rates employed after continuous annealing normally lie between 3 and 100 °C/s [49, 54, 56, 131]. However, some workers have reported still faster rates of about 50-400 °C/s [3], or ultrarapid rates of 1000 °C/s [3], and 2000 °C/s [55, 144]. Fig. 3.13 presents the steps employed for the continuous annealing simulation.

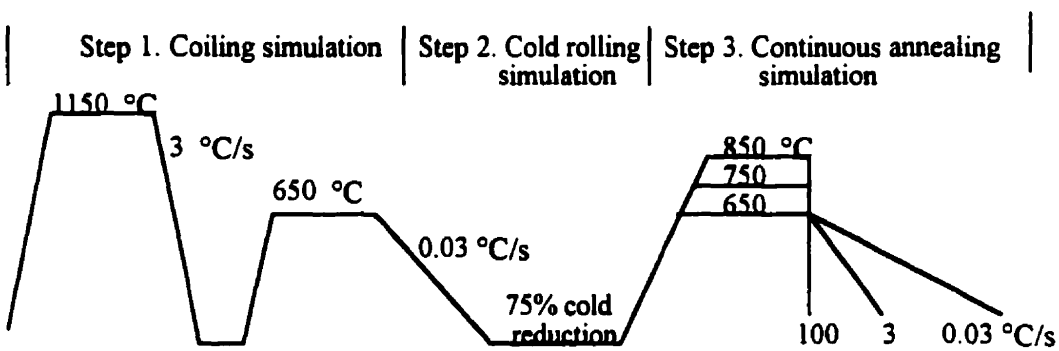

Step 4. Internal friction measurements and aging index tests.

Fig. 3.13. Schematic diagram of the simulation of the continuous annealing process.

It should be mentioned that the specimens which were prepared for the aging index tests did not receive any cold reduction. According to the past work, cold reduction ratios do not significantly affect the bake hardenability [48]. The tests of step 4 were carried out to compare the estimated and measured amounts of carbon in solution for each soaking temperature and cooling rate.

3.4.6. Flattening Simulation

The residual stresses present after heavy cold reductions result in irregular flatness across the strip width. Final flattening or removal of these non-uniform stresses is carried out by plastic extension of the strip during heating in the continuous annealing furnace. The applied strain rate is about 10^{-4} s^{-1} [145] under these conditions. Therefore, to simulate the flattening process, tensile tests were carried out on steels A, B, and C at this strain rate (10^{-4} s^{-1}) and at temperatures from ambient to 400 °C.

CHAPTER 4

Results

4.1. Dynamic Strain Aging

4.1.1. Effects of Chemical Composition, Reheat Temperature and Cooling Rate

Some typical stress-strain curves for specimens of steel A cooled at the six different cooling rates are illustrated in Fig. 4.1. It is evident that dynamic strain aging occurs after cooling from all reheating temperatures, except for the specimens that were furnace cooled. This implies that only furnace cooling allowed full or nearly full precipitation of the carbon as required by the decrease in carbon solubility with decreasing temperature. Even still air cooling resulted in a material that was supersaturated with carbon. The former case is in good agreement with the findings of other workers, who have suggested that, when coiling is carried out at high temperatures and high Ti/(C + N) ratios are employed, the solute carbon and nitrogen can be tied up by the Ti [59].

In Fig. 4.2, the UTS is plotted vs. the time required to cool to room temperature for all reheating temperatures and cooling rates. There are clear trends for the UTS values to increase with reheat temperature. For the specimen quenched in water after reheating to 1200 °C, the UTS exceeds 370 MPa. Under furnace cooling conditions, the UTS values converge to around 150 MPa. Note also that a particular value of UTS, e.g. 260 MPa, can be obtained by a combination of low reheat temperature and short cooling time, or high reheat temperature and longer cooling time.

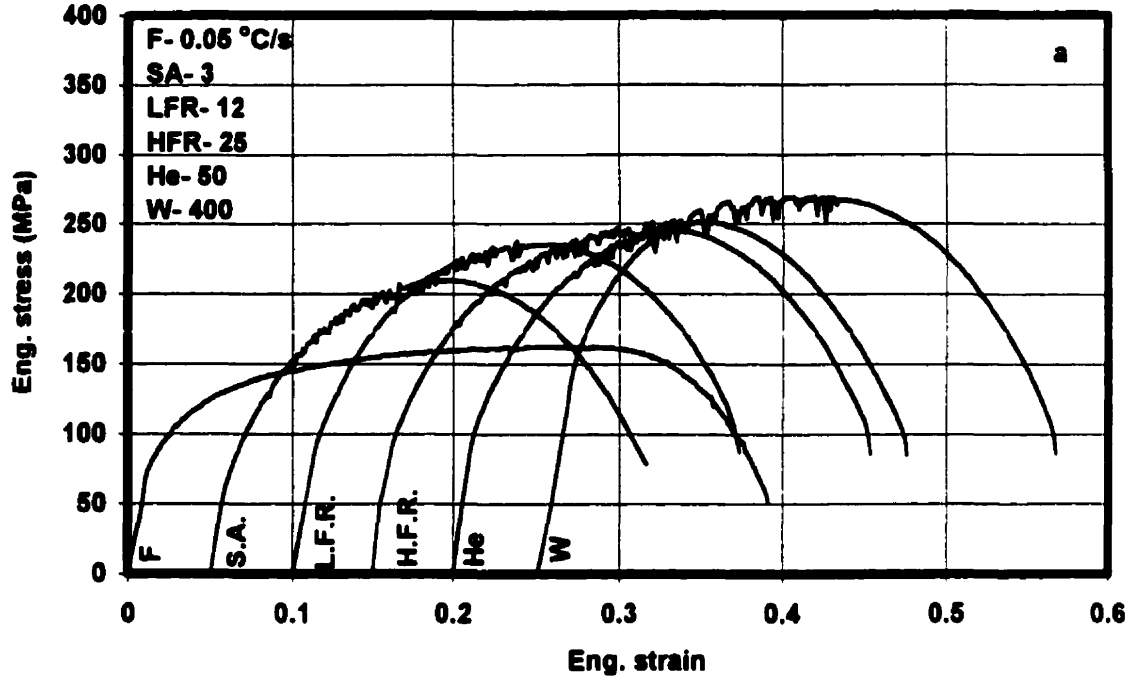

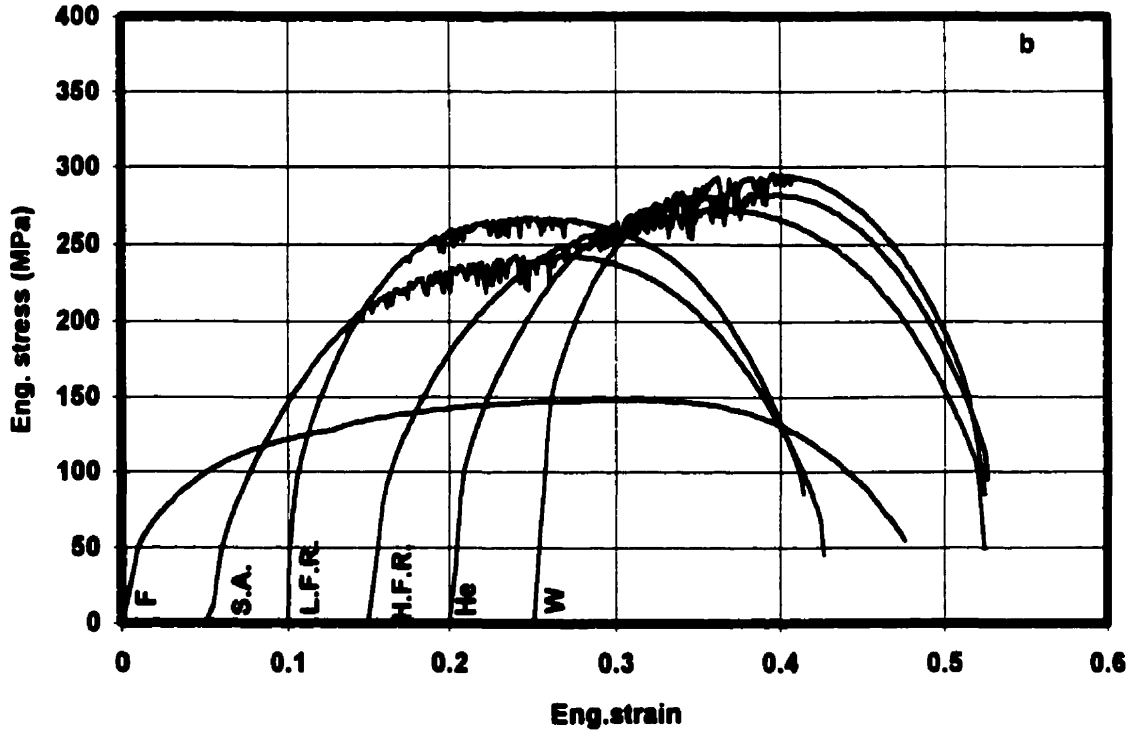

Fig. 4.1. Stress vs. strain curves of specimens cooled from a) 900, b) 1050, c) 1150, and d) 1200 °C at different rates and then tensile tested at 300 °C and 10^{-3} s^{-1}.

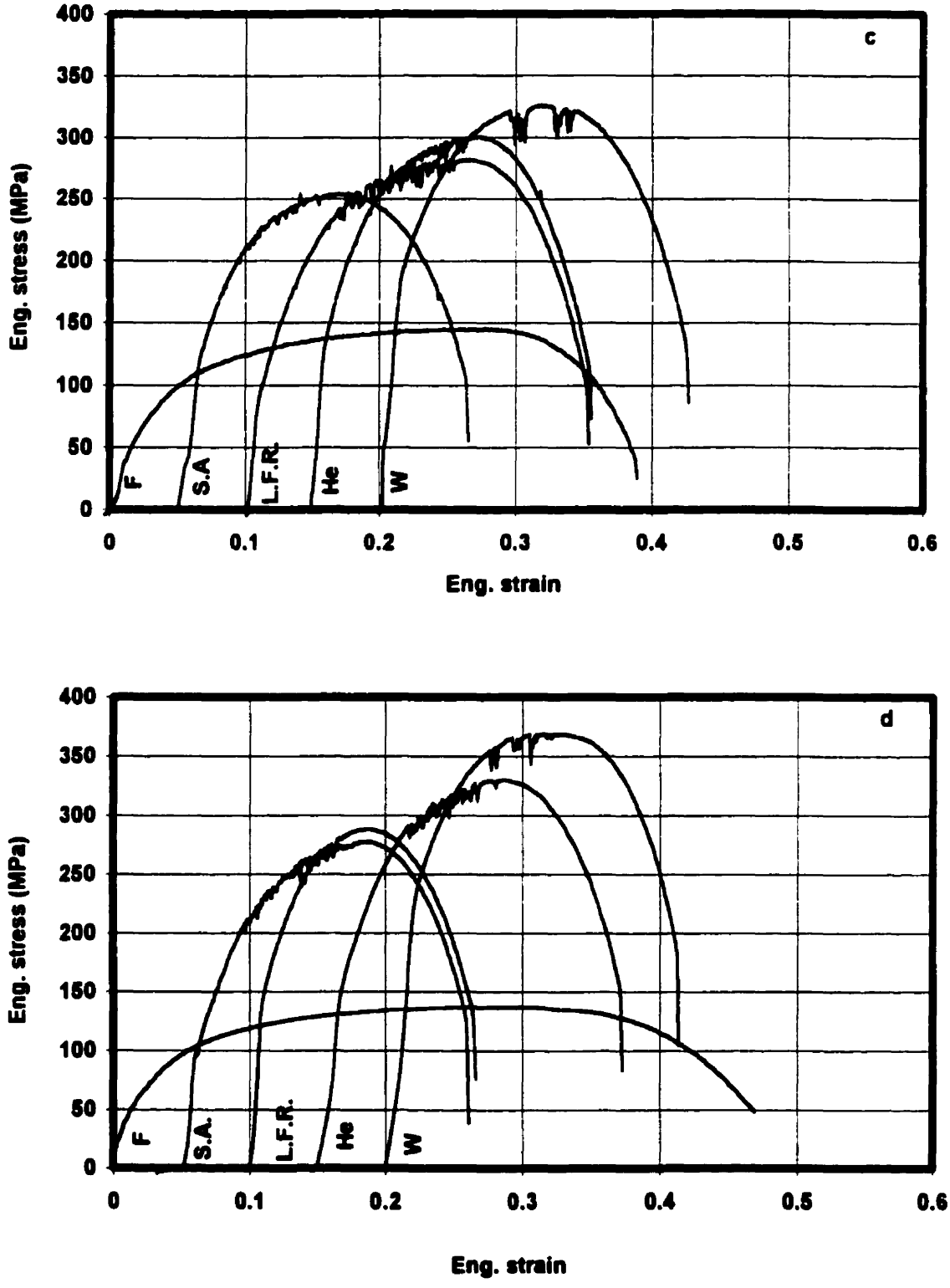

Fig. 4.1. Stress vs. strain curves of specimens cooled from a) 900, b) 1050, c) 1150, and d) 1200 °C at different rates and then tensile tested at 300 °C and 10^{-3} s^{-1}.

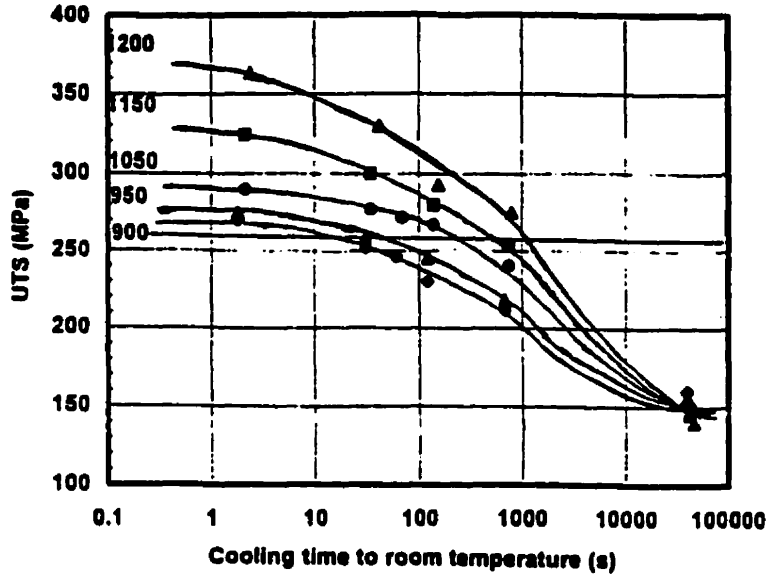

Fig. 4.2. UTS vs. cooling time to room temperature for various reheat temperatures and cooling rates.

In terms of the effect of chemical composition, some typical stress-strain curves pertaining to the specimens cooled from 1100 °C at the different rates are illustrated in Fig. 4.3. It is clear from these tests (carried out at 300 °C) that once again still air cooling (3 °C/s) resulted in significant amounts of carbon remaining in solution. Thus, dynamic strain aging took place at all values of Ti_{exc}, Ti^*_C/C, and Ti^*_S/S and in all four kinds of IF steel. Only after applying very slow cooling (0.05 °C/s), were the smooth curves observed that signify there is no carbon left in solution.

The effects of chemical composition and reheat temperature are presented in Fig. 4.4. In the cases of cooling from 900, 1000, and 1100 °C in still air (3 °C/s), considerable amounts of carbon remained in solution, leading to the occurrence of DSA. This happened whatever the chemical composition. Also, as the reheat temperature was increased, the UTS also increased.

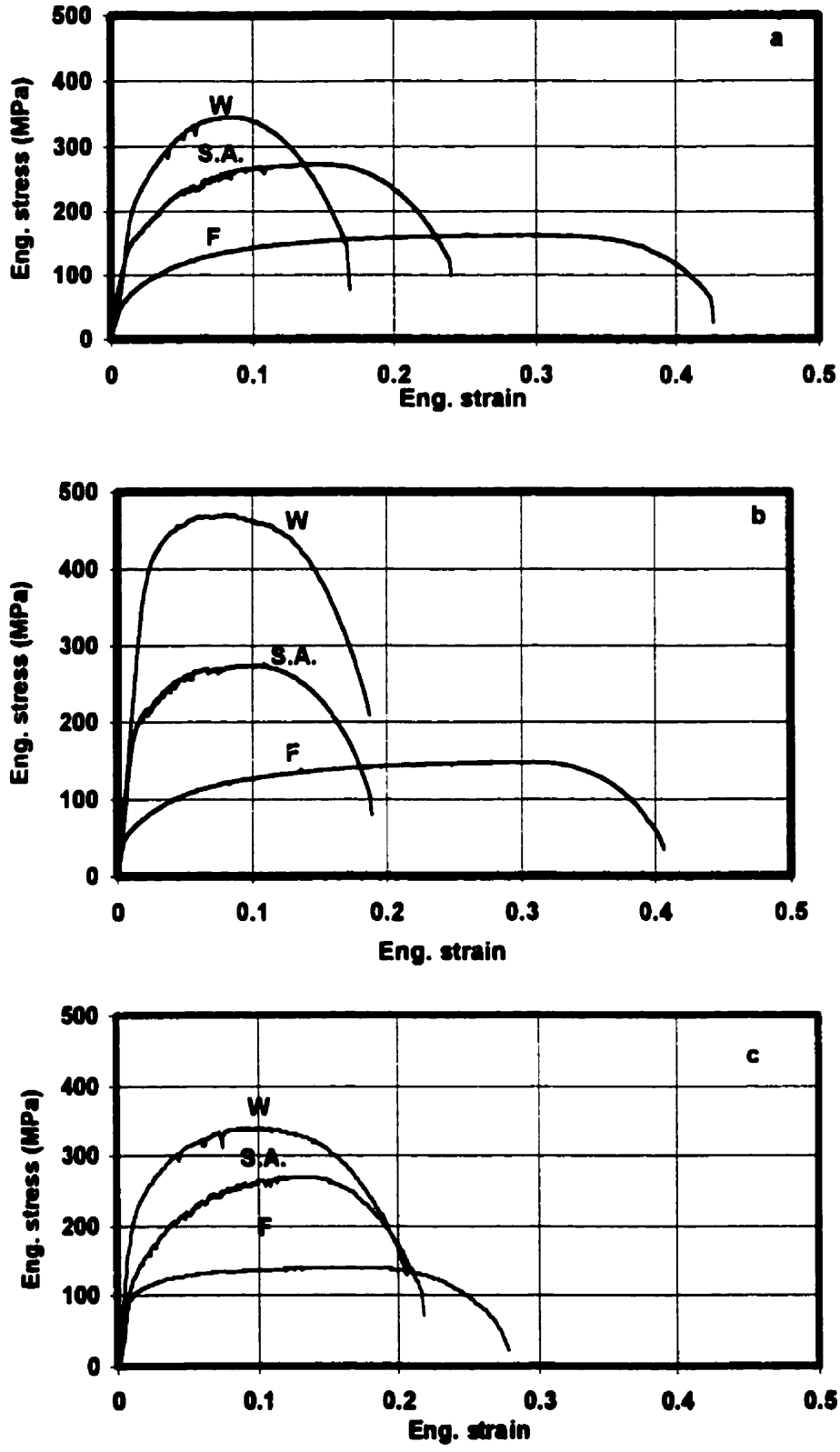

Fig. 4.3. Stress/strain curves of specimens cooled from 1100 °C at different rates and tested at 300 °C and 10^{-3} s^{-1}: a) steel B, b) steel C, and c) steel D.

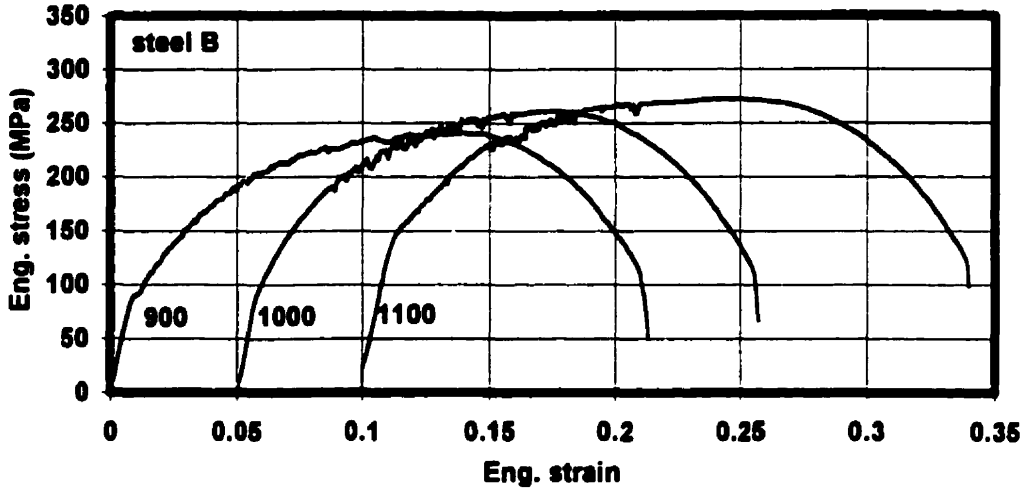

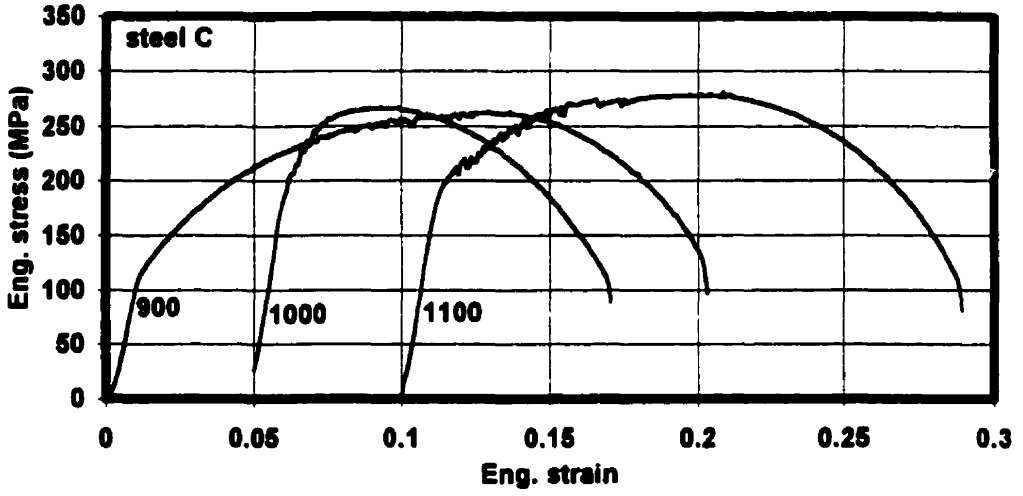

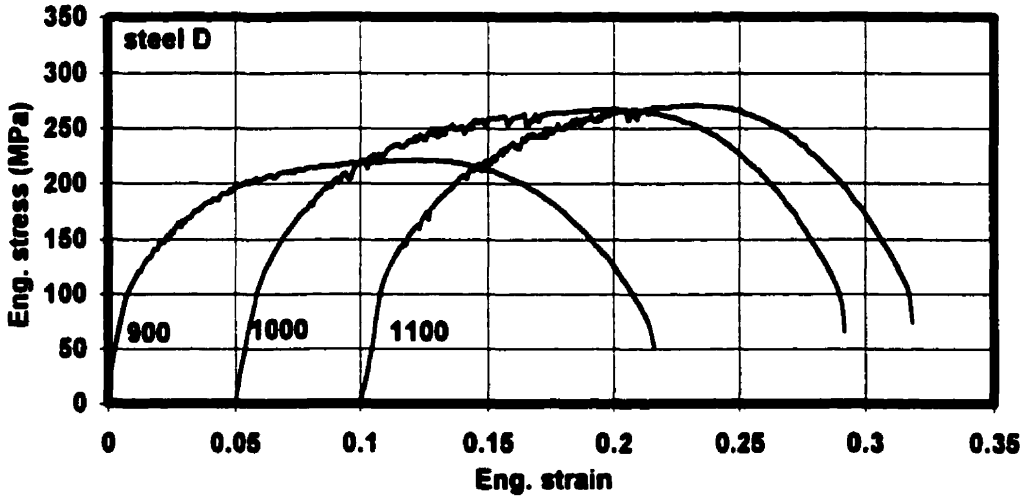

Fig. 4.4. Stress vs. strain curves of specimens cooled from different reheat temperatures in still air (3 °C/s), then tensile tested at 300 °C and 10^{-3} s^{-1}.

4.1.2. Effects of Chemical Composition, Tensile Strain Rate and Test Temperature

For steels A, B, and C, the flow curves obtained through the temperature range (25 to 450 °C) at strain rates of 10^{-3} to 10^{-1} s^{-1} are displayed in Figs. 4.5 to 4.7, respectively. At each given strain rate, the stress-strain curves undergo pronounced strengthening with increasing temperature, as past research on different kinds of steel has shown [22, 35, 146-151]. The temperature at which serrations first appear shifts from about 100 to about 220 °C as the rate is increased from 10^{-4} to 10^{-1} s^{-1}.

When the strain rate is increased, the temperature associated with the disappearance of the serrations increases from 350 to 425 °C. Within the serrated flow range, the magnitude and frequency of serrations increases to a maximum as the temperature is increased. This maximum is towards the high temperature side of the serrated flow range. Note also that the work hardening rates are steeper for the curves displaying pronounced serrations.

In the case of steel A, the yield and flow stresses are plotted versus temperature in Fig. 4.8 for all applied strain rates. The flow stress values go through a maximum at intermediate temperatures, then drop at higher temperatures. This flow stress behavior, common in all four steels, can be divided into three classes:

(i) the low temperature range, where little or no aging occurs;
(ii) the intermediate temperature range, which is characterized by the serrations and high rates of strain hardening;
(iii) the higher temperatures, where the serrations disappear and the rates of strain hardening fall.

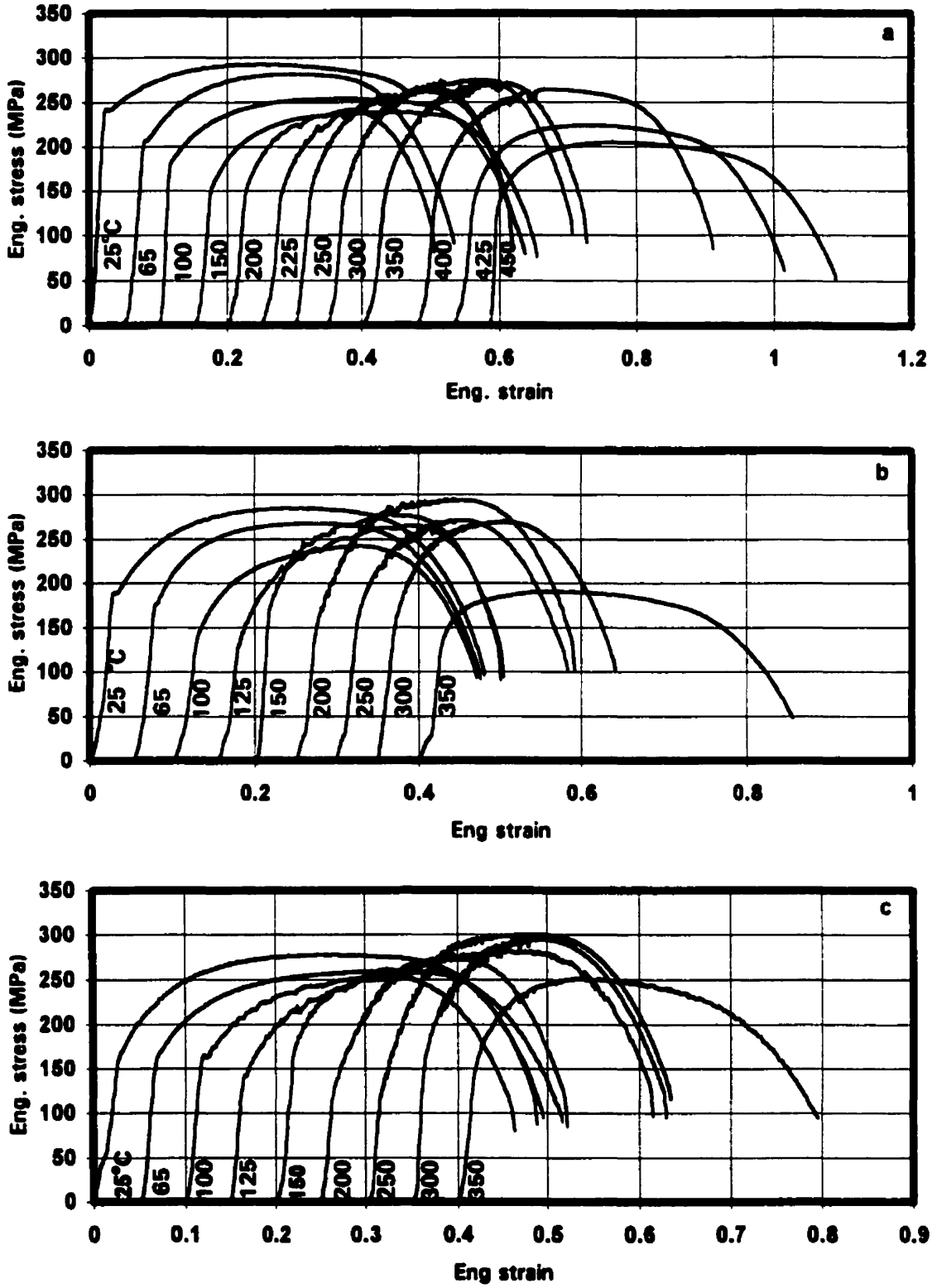

Fig. 4.5. Stress/strain curves of specimens tensile tested at different temperatures and strain rates of a) 10^{-1}, b) 10^{-2}, and c) 10^{-3} s^{-1} (steel A).

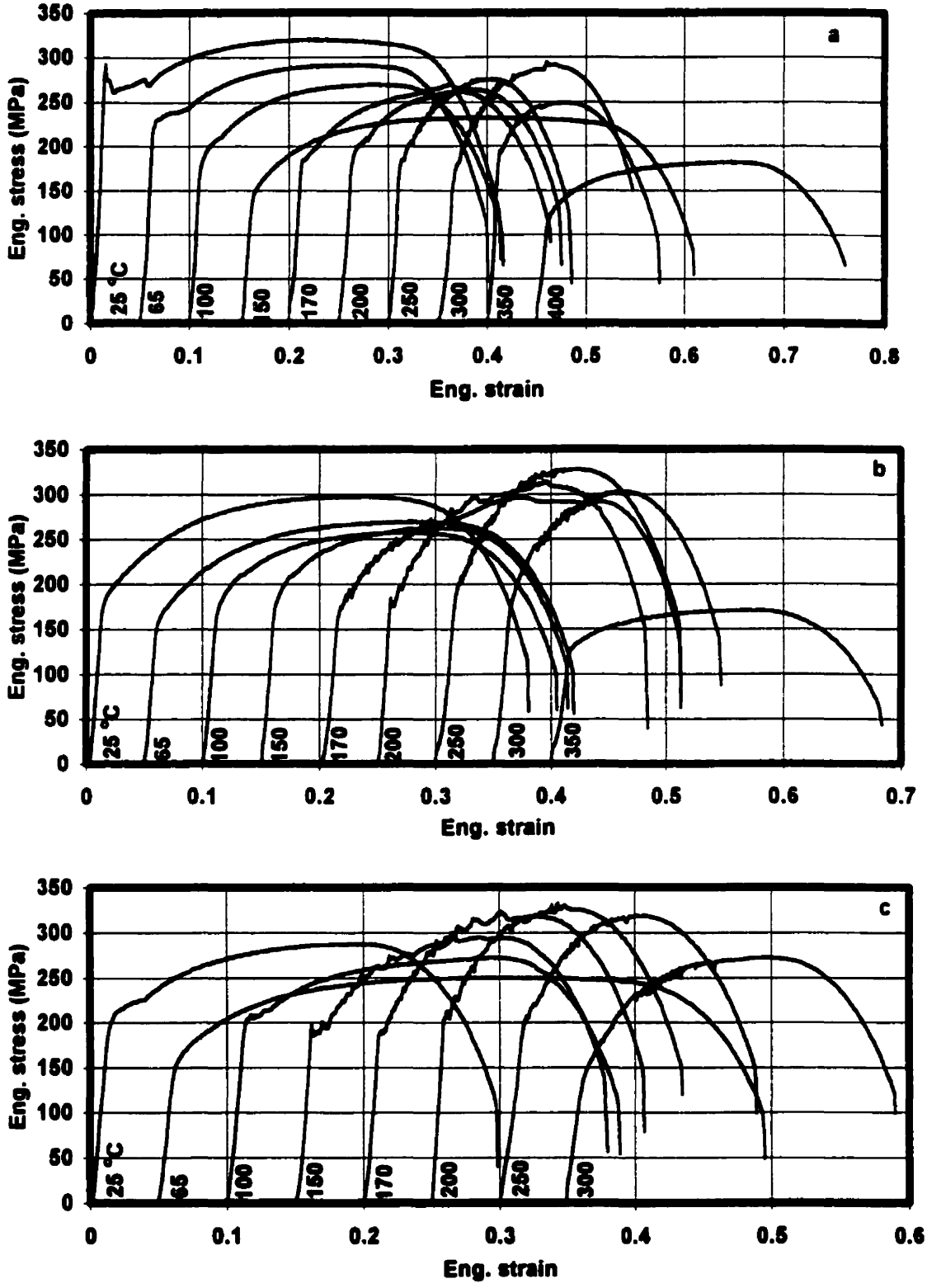

Fig. 4.6. Stress/strain curves of specimens tensile tested at different temperatures and strain rates of: a) 10^{-1}, b) 10^{-2}, c) 10^{-3} s^{-1} (steel B).

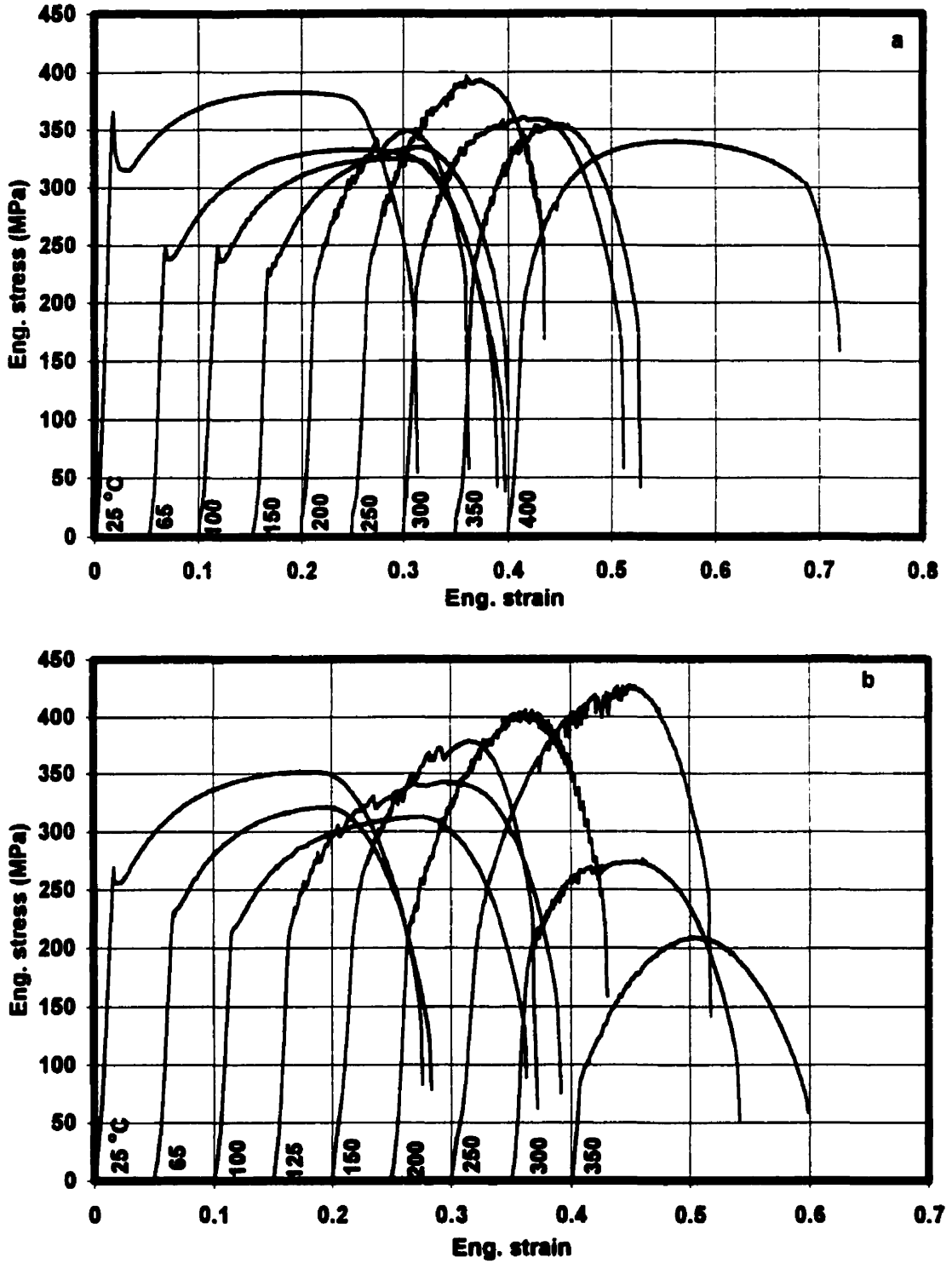

Fig. 4.7. Stress/strain curves of specimens tensile tested at different temperatures and strain rates of: a) 10^{-1} and b) 10^{-3} s^{-1} (steel C).

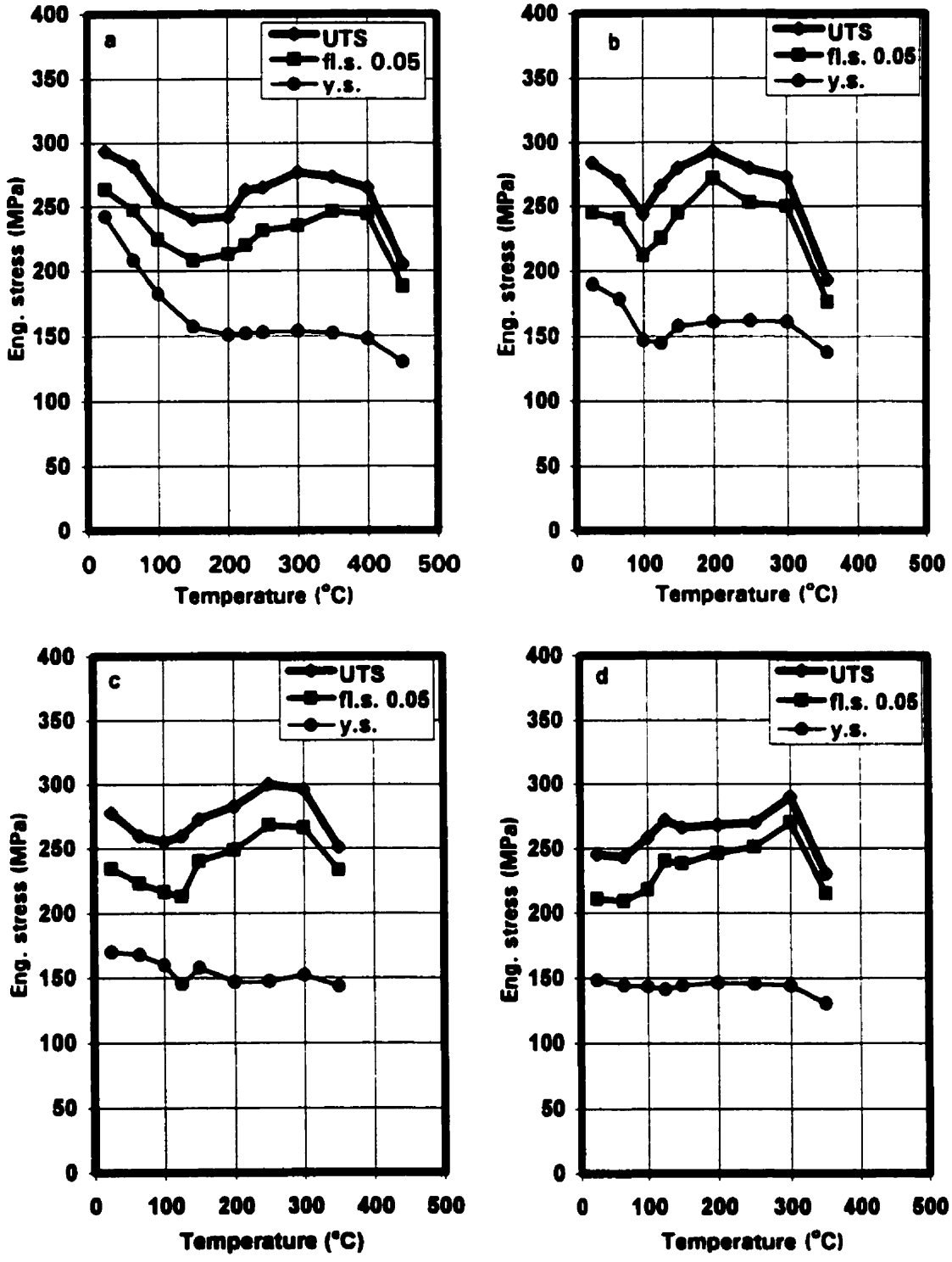

Fig. 4.8. Temperature dependence of the yield, flow, and ultimate stresses at strain rates of: a) 10^{-1}, b) 10^{-2}, c) 10^{-3}, and d) 10^{-4} s^{-1} (steel A).

A typical temperature dependence of the UTS at various strain rates is displayed in Fig. 4.9. Although this behaviour is plotted for steel A, the trends displayed are common to all four IF steels investigated. Here, best-fit polynomial equations were used to draw lines through the data points. For each applied strain rate, there is a maximum for the UTS, which generally shifts to higher temperatures as the strain rate is increased. For example, the position of the UTS maximum shifts from about 230 °C for 10^{-4} s^{-1} to about 340 °C for 10^{-1} s^{-1}.

Referring to Fig. 4.10, in which is plotted the temperature dependence of the fracture strain of steel A, it is evident that there is a significant reduction in ductility at intermediate temperatures. Once again, best-fit lines are plotted through the experimental results. At a strain rate of 10^{-4} s^{-1}, the minimum in fracture strain is at about 210 °C, while at a rate of 10^{-1} s^{-1}, this minimum shifts to about 310 °C. This dependence indicates that, with increasing strain rate, the minima in the fracture strain shift to higher temperatures, as reported by past workers on dynamic strain aging [35, 149, 152, 153]. In addition, as the strain rate is increased, the minimum in the fracture strain shifts to somewhat higher values. For example, at a rate of 10^{-4} s^{-1}, the fracture strain minimum is about 0.25, while at 10^{-1} s^{-1}, it is about 0.32. These are also behaviors that were common to all the IF grades.

Once again in the case of steel A, the strain rate dependences of the flow stress and UTS are illustrated for the temperatures below (25 and 65 °C) and within (150 and 200 °C) the serrated flow range in Figs. 4.11 and 4.12, respectively. At 25 and 65 °C, where no serrations were observed at the four applied strain rates, the flow stress and UTS display the normal positive rate dependence, Fig. 4.11. However, in the serrated flow range, the rate dependence of the flow stress is negative, Fig. 4.12. This negative strain rate sensitivity is a key characteristic of

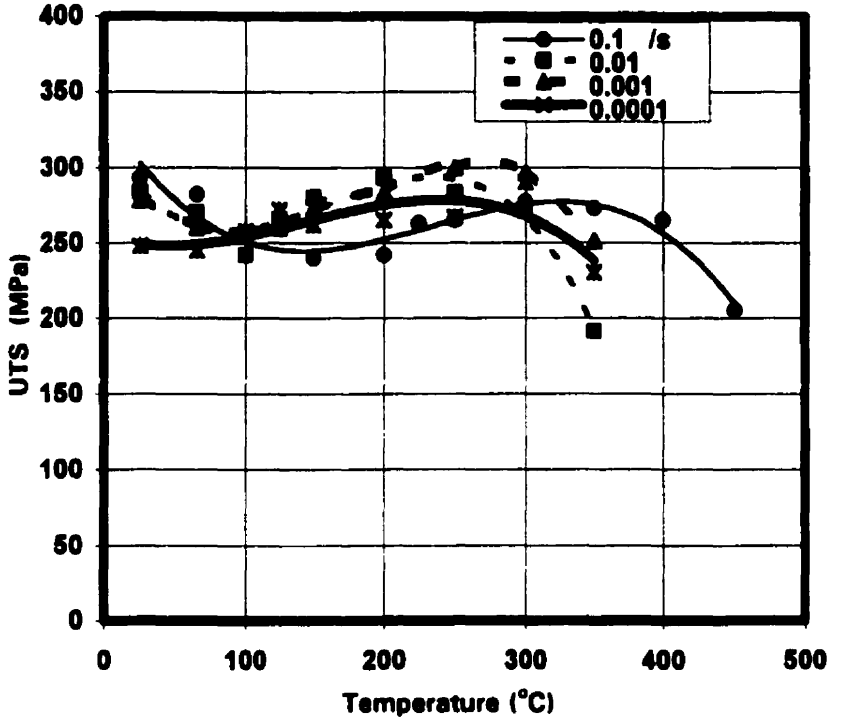

Fig. 4.9. Temperature dependence of the UTS at various strain rates (steel A).

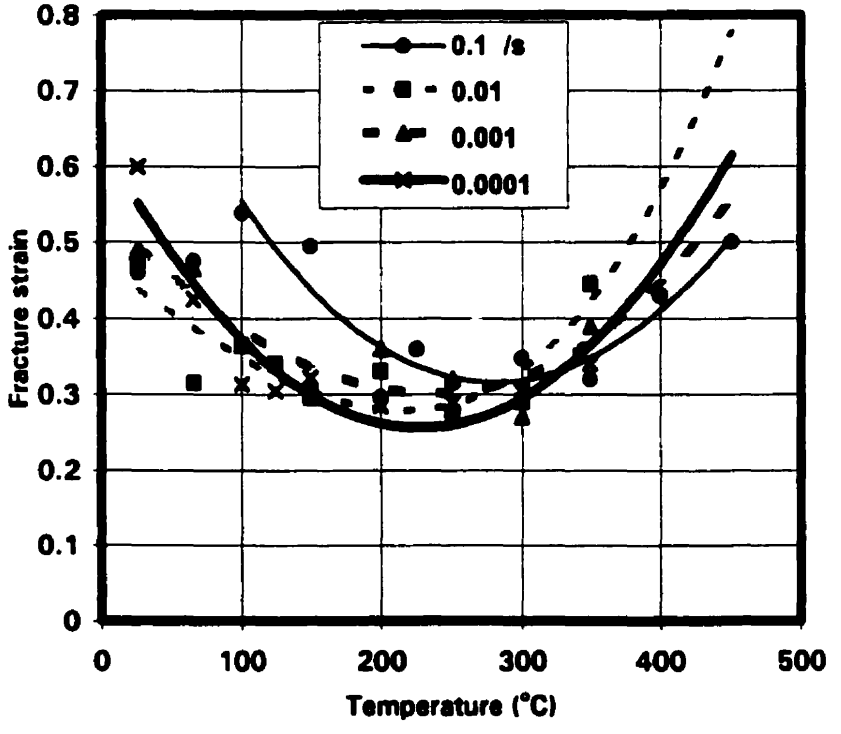

Fig. 4.10. Temperature dependence of the fracture strain at various strain rates (steel A).

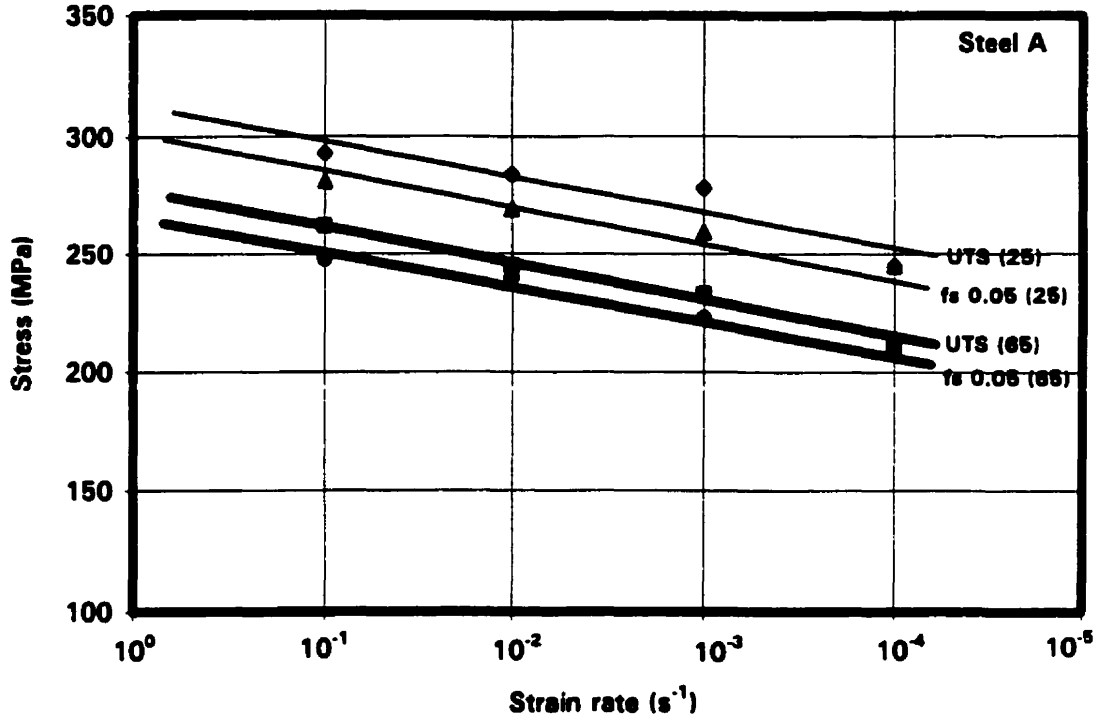

Fig. 4.11. Strain rate dependence of the flow stress and UTS at 25 and 65 °C.

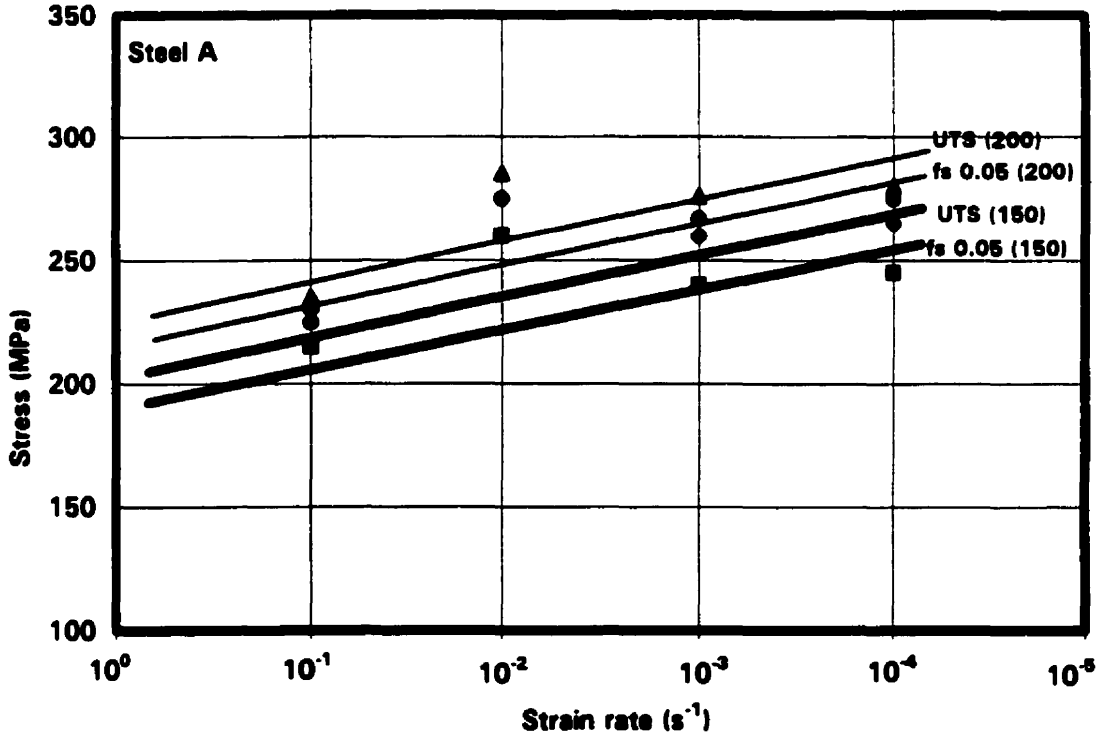

Fig. 4. 12. Strain rate dependence of the flow stress and UTS at 150 and 200 °C.

dynamic strain aging, and is responsible for significant reductions in ductility throughout the intermediate temperature range. In the case of steel D, the stress-strain curves associated with the specimens furnace cooled from 1100 °C are smooth, Fig. 4.13; this indicates that plastic deformation is homogenous and stable. The smooth decrease in flow stress with increasing temperature also demonstrates that the temperature-dependence of the flow stress is "normal", i.e. that no "peak" due to the occurrence of DSA is present, Fig. 4.14.

Figure 4.15 exhibits some typical stress-strain curves pertaining to specimens of steel D cooled from 900 °C in still air (3 °C/s), then tensile tested at different strain rates and temperatures. Although the reheat temperature was well above the calculated NbC solution temperature (866 °C), the magnitude of the serrations was lower than in the case of the three Ti IF steels.

4.2. Static Strain Aging

4.2.1. Effect of Reheat Temperature and Cooling Rate.

The stress-strain curves associated with some of the aging index tests carried out on specimens of steel A are displayed in Fig. 4.16. These samples had already been reheated to various temperatures and then cooled to room temperature at different rates. The effects of reheat temperature and cooling rate on the aging indices are shown in Fig. 4.17. There are clear trends for the AI values to increase with reheat temperature and cooling rate. These results are in good agreement with the past work, indicating the presence of more carbon in solution as the reheat temperature and cooling rate are increased [49, 154]. Under furnace cooling conditions (0.05 °C/s), the aging index amounts converge to around 5 MPa, which means this slow rate led to the almost complete stabilization of this IF steel. For example, in the case of cooling from 1200 °C at this rate, the AI value is zero. By contrast, the return of a sharp

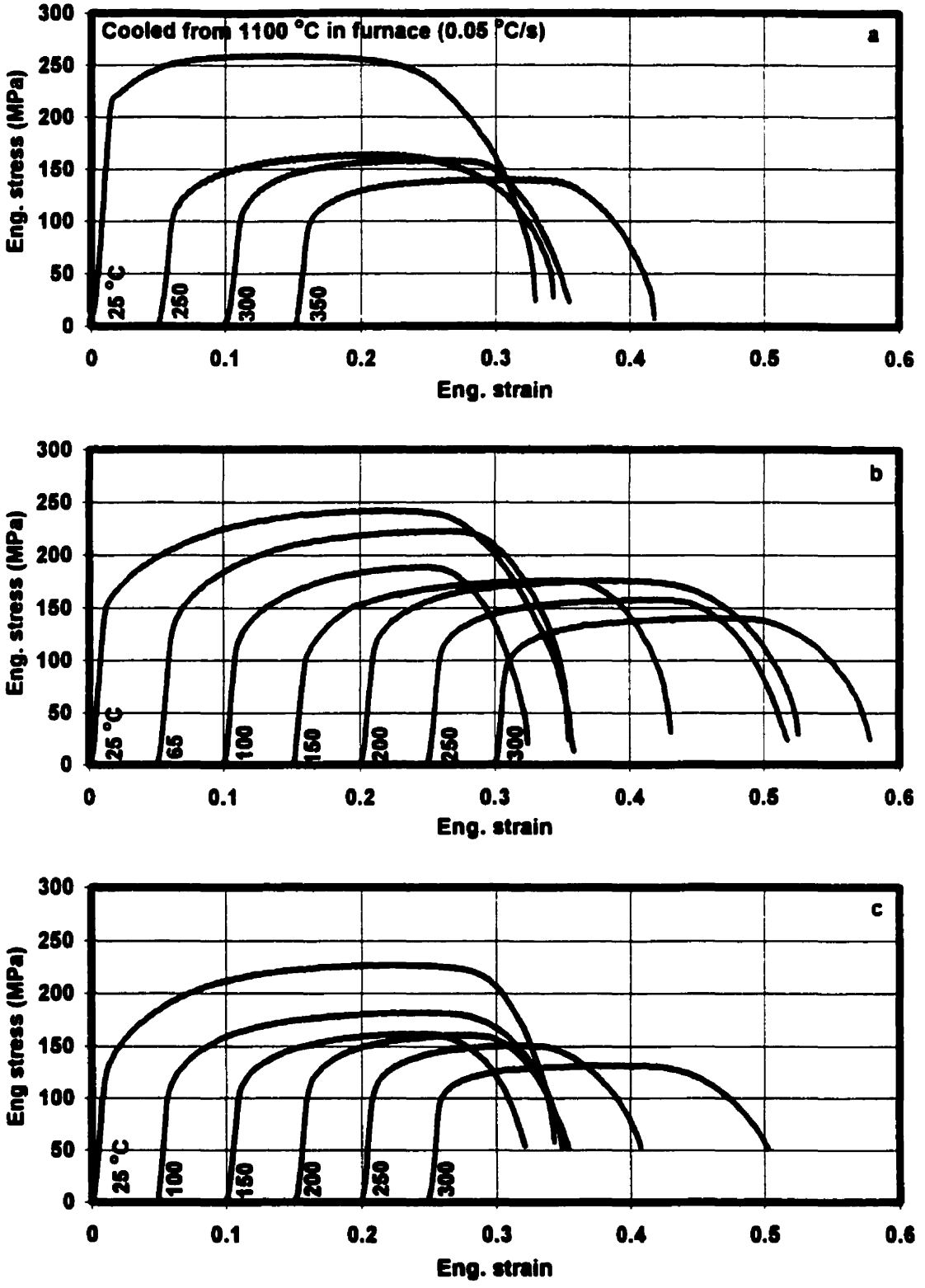

Fig. 4.13. Stress vs. strain curves for specimens tensile tested at various temperatures and strain rates of: a) 10^{-1}, b) 10^{-3}, and c) 10^{-4} s^{-1} (steel D).

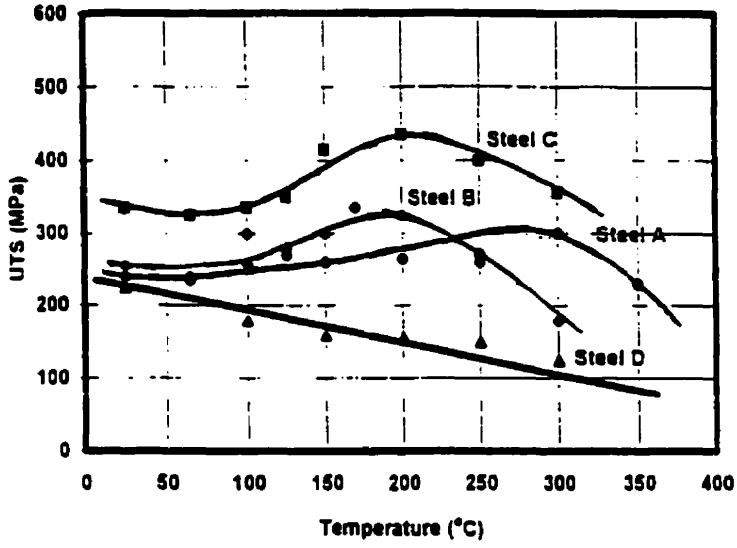

Fig. 4. 14. Temperature dependence of the UTS for steels A, B, and C (cooled in still air), and steel D cooled in the furnace from 1100 °C, then tensile tested at 10^{-4} s^{-1}.

yield point, considerable Luders strain and an increase in UTS all indicate that significant static strain aging can take place even in the case of still air cooling (3 °C /s). The estimated amounts of carbon in solution for each combination of reheat temperature and cooling condition are collected in Table 4.1.

Table 4.1. Aging index values and estimated amounts of carbon in solution for different reheat temperatures and cooling rates (steel A).

	Furnace Cooling		Still Air Cooling		Water Quench	
T (°C)	C ±1 (ppm)	AI ±3 (MPa)	C ±1 (ppm)	AI ±3 (MPa)	C ±1 (ppm)	AI ±3 (MPa)
900	0.5	5	1.5	15	4.5	28
950	0.5	5	2.5	20	5.5	30
1050	<0.5	3	4	26	7	36
1150	<0.5	3	6.5	33	8.5	40
1200	0	0	7	35	12	45

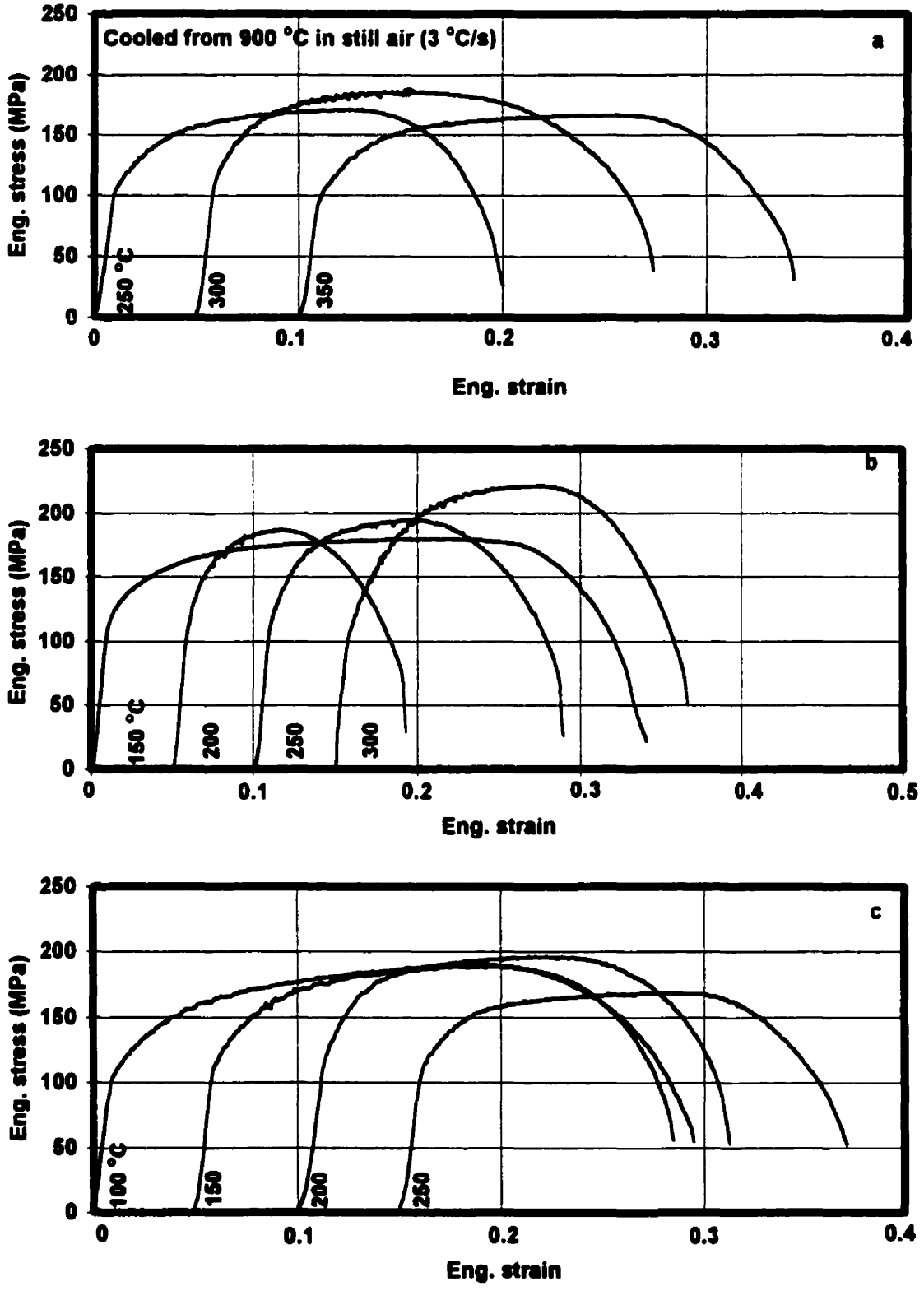

Fig. 4.15. Stress vs. strain curves for specimens tensile tested at various temperatures and strain rates of : a) 10^{-2}, b) 10^{-3}, c) 10^{-4} s^{-1} (steel D).

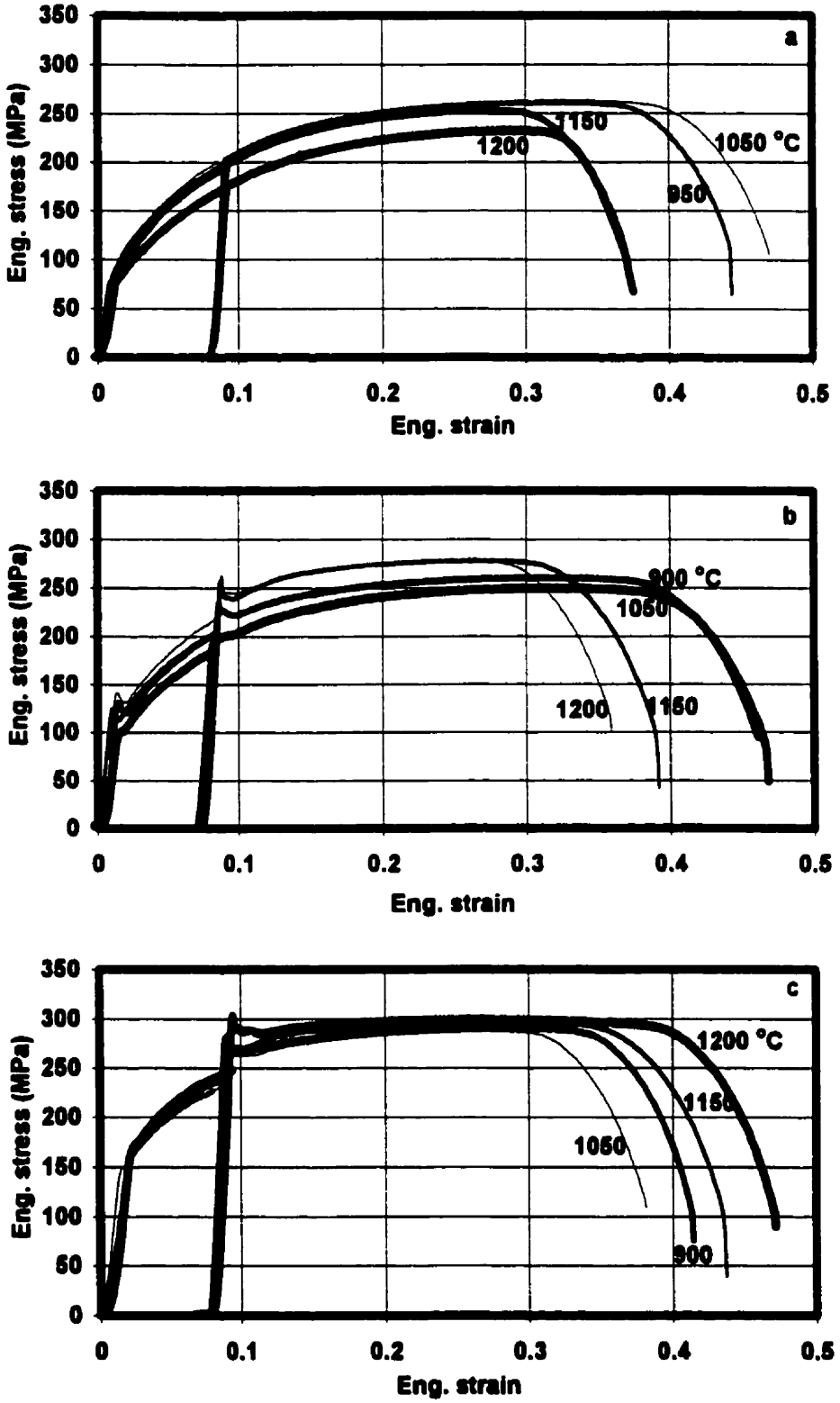

Fig. 4.16. Aging index tests on specimens cooled from different reheat temperatures at different rates: a) 0.05 °C/s, b) 3 °C/s, and c) 400 °C/s (steel A).

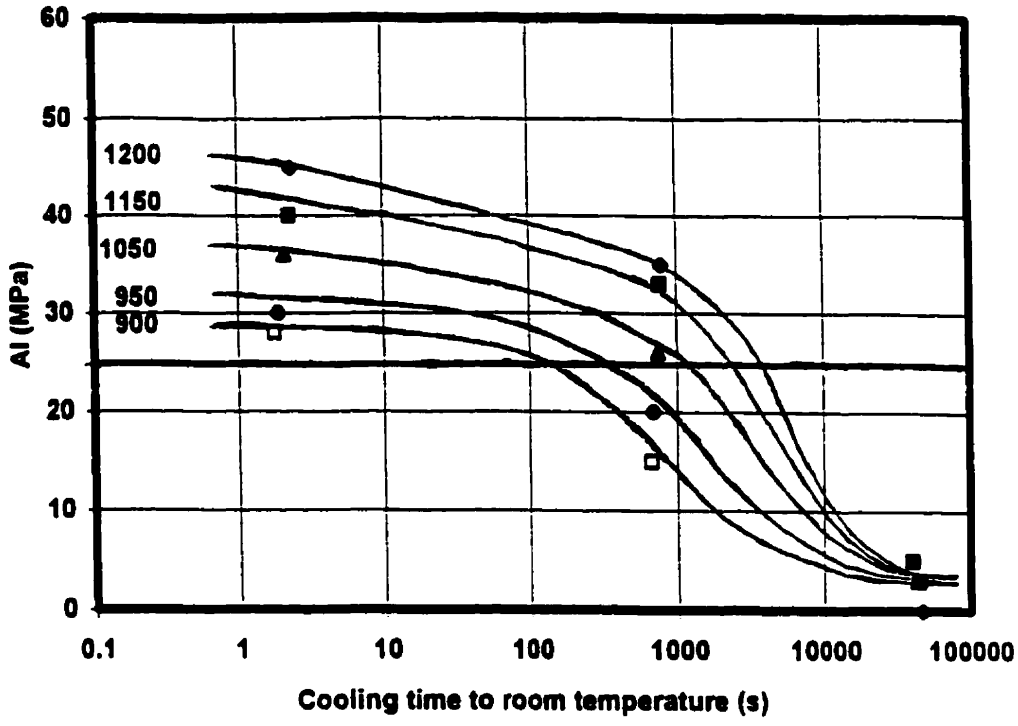

Fig. 4.17. AI vs. cooling time to room temperature for various reheat temperatures and cooling rates.

Note that a particular value of AI, e.g. 25 MPa, can be obtained by a combination of low reheat temperature and rapid cooling, or high reheat temperature and slower cooling, Fig. 4.17. The minimum and maximum AI values observed (0 and 45 MPa) correspond to reheating at 1200 °C following by i) furnace cooling and ii) water quenching to room temperature, respectively. Referring back to Fig. 2.16, these aging indices correspond to about 0 and 12 ppm of carbon in solution.

4.2.2. Effect of Chemical Composition and Cooling Rate

The effects of chemical composition and cooling rate on the static strain aging behaviors of the IF grades are plotted in Fig. 4.18. It is clear that two different behaviors are observed, one for the water quenched and still air

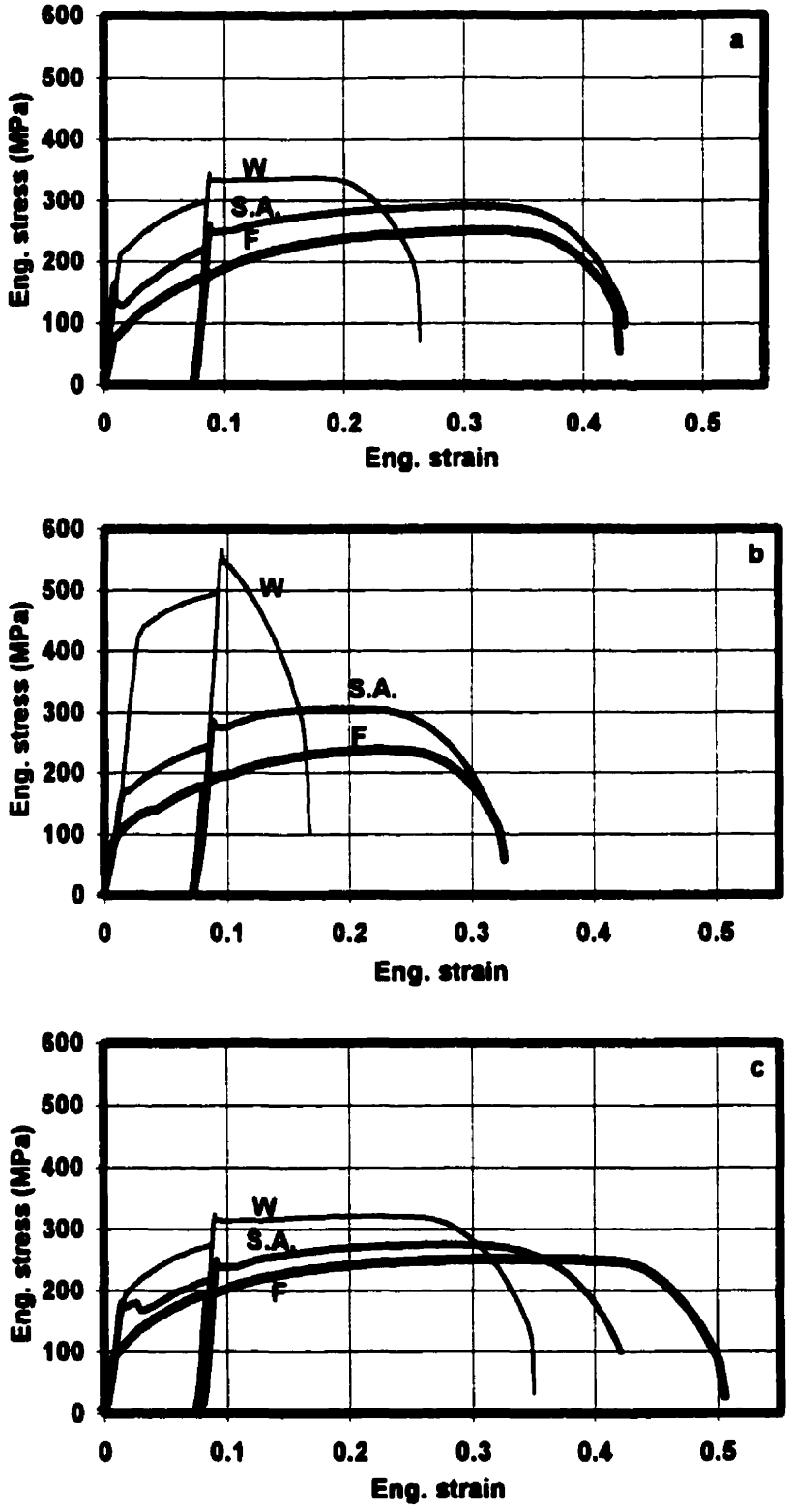

Fig. 4. 18. Aging index tests on specimens cooled from 1100 °C at different rates: a) steel B, b) steel C, and c) steel D. (W=400, S.A.=3, and F=0.05 °C/s)

samples, another for the furnace cooled specimens. For the water quenched and still air cooled samples, the aging indices increased with the Ti^*_s/S ratio; in the case of furnace cooling, the aging indices remained at zero whatever the IF steel.

The Ti^*_s/S ratio is a new parameter introduced here. So far, previous workers have investigated only the effect of Ti^*_c/C in their studies of IF steels. However, the former factor is closely linked to the probability of formation of TiS or $Ti_4C_2S_2$ at high temperatures, which then affects the amount of carbon in solution. Some aging indices determined and the estimated amounts of C in solution are listed in Table 4.2.

Table 4.2. Aging indices and the corresponding estimated amounts of carbon in solution (cooled from 1100 °C at different rates).

	Furnace Cooling		Still Air Cooling		Water Quench	
steel	C ±1 (ppm)	AI ±3 (MPa)	C ±1 (ppm)	AI ±3 (MPa)	C ±1 (ppm)	AI ±3 (MPa)
A	<0.5	3	5.5	30	8	38
B	0	0	4.5	28	7	36
C	0	0	7	35	15	53
D	0	0	3	22	8.5	40

These values correspond to samples that were cooled from 1100 °C in still air. It is of interest that steels A and B, which have the same values of Ti_{exc}, Ti^*_c/C, and Ti^*_s/S, exhibited the same aging behaviour, although the Ti and S levels in steel B were 1.5 times as high as in steel A. Steel C, with the

highest Ti^*_S/S and lowest S content, exhibited the highest aging index after water quenching and still air cooling, although it had the highest Ti^*_C/C value. This means that the Ti^*_S/S ratio is likely to be more important than the Ti^*_C/C ratio with respect to the removal of carbon from solution. By contrast, the aging behaviour of the Ti-Nb IF steel was similar to that of steels A and B.

4.3. Quench Aging at Room Temperature

The stress-strain curves determined on specimens quenched from 1050 and 900 °C using either water or helium and then tensile tested at 300 °C and 10^{-3} s^{-1} are illustrated in Fig. 4.19. In the case of the quench aged samples, the smooth stress-strain curves indicate the absence of carbon in solution after storing at room temperature for three weeks. Referring to Table 4.1, aging indices of about 28 and 36 MPa can be expected in the cases of water quenching from 900 and 1050 °C, respectively. These data suggest that considerable aging should take place during storage. When the samples were tensile tested immediately after quenching, dynamic strain aging occurred, as indicated by the presence of serrations in the stress-strain curves. It is of interest that the occurrence of either SSA or DSA led to the same increase in UTS and reduction in ductility or total elongation.

4.4. Bake Hardening

To estimate the amounts of solute carbon available for bake hardening, aging index tests were carried out. An average value of 26 MPa was obtained, corresponding to about 4 ppm carbon in solution. The maximum and minimum bake hardening values obtained with this amount of solute carbon were about 55 (DSBH method) and 3 MPa (SBH method), respectively. This means that, for a given solute carbon level, the dynamically and then statically aged

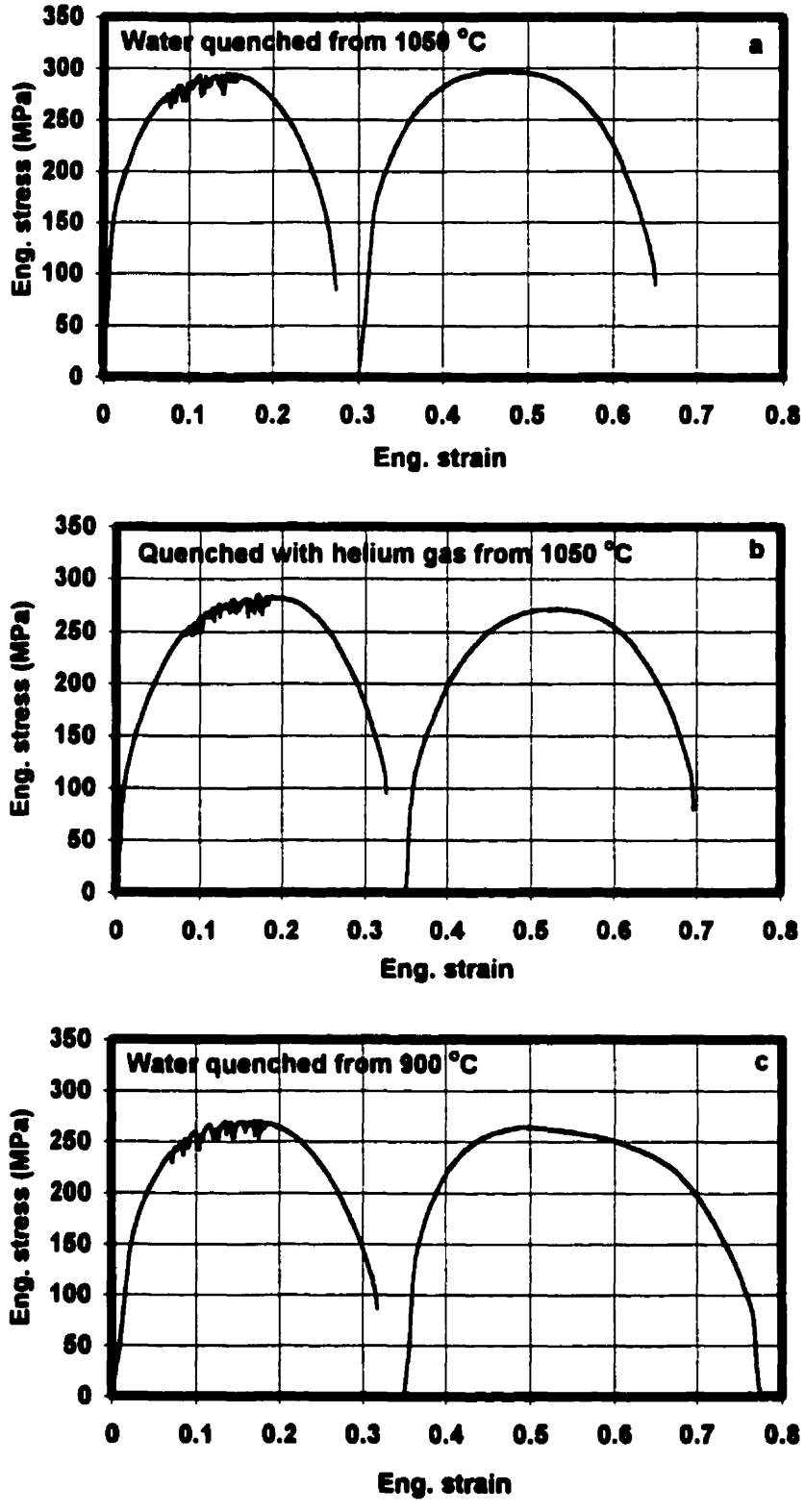

Fig. 4. 19. Stress vs. strain curves for specimens of steel A tensile tested at 300 °C and 10^{-3} s^{-1}: immediately after quenching (left) and after storing at room temperature for three weeks (right).

samples have much more capability to produce high bake hardening values than those that were bake hardened in the conventional way.

4.4.1. Dynamic Bake Hardening (DBH) Method

Figures 4.20 to 4.22 present the effects of prestrain and temperature on i) the amount of bake hardening, ii) yield strength before, and iii) after this process, respectively. Figure 4.20 illustrates how the DBH depends on temperature. The DBH amounts reach a maximum at around 170 °C, a position that does not change with prestrain. In terms of prestrain, the 2% prestrained samples exhibited the maximum amounts.

As shown in Fig. 4.21, the yield strength before baking remains fixed at about 95 MPa. This parameter increases with prestrain after DBH and reaches a plateau at the higher temperatures, as illustrated in Fig. 4.22.

4.4.2. Static (Conventional) Bake Hardening (SBH) Method

Figures 4.23 to 4.25 illustrate the effects of prestrain and temperature on i) the amount of bake hardening, ii) the yield strength before, and iii) after this method, respectively. According to Fig. 4.23, there is a maximum in the SBH value vs. prestrain, which shifts to lower prestrains as the temperature is increased, this is in agreement with the previous work [51, 52]. At intermediate temperatures (200 and 250 °C), three different behaviors are observed: (i) the bake hardening values increase with increasing prestrain at low prestrains, (ii) less bake hardening is observed with further increases in prestrain, and (iii) larger prestrains result in a plateau, or in a slight increase in the baking values. This is in good agreement with the findings of other investigators [5, 48, 51]. The maximum and minimum amounts of static bake hardening (26 and 3 MPa) were obtained in the cases of 4% and 2% prestrain followed by baking at 250 °C and, 100 °C respectively.

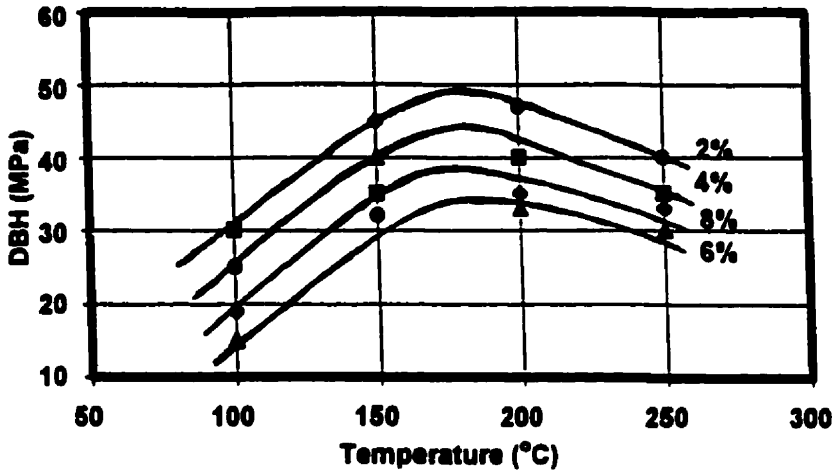

Fig. 4.20. Effects of temperature and prestrain on the DBH values.

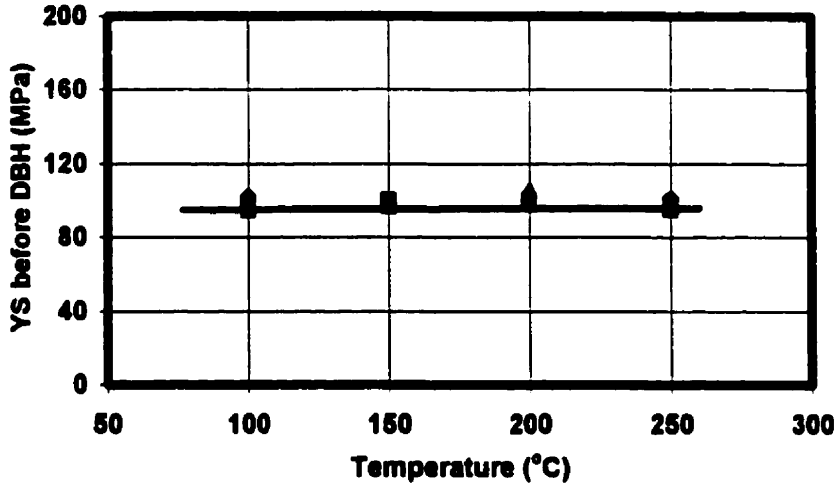

Fig. 4.21. Dependence of the yield strength before DBH on temperature.

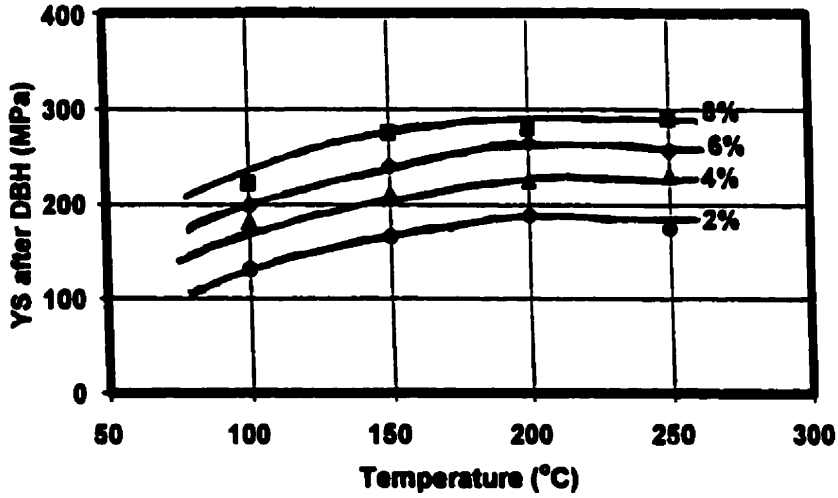

Fig. 4.22. Dependence of the yield strength after DBH on temperature.

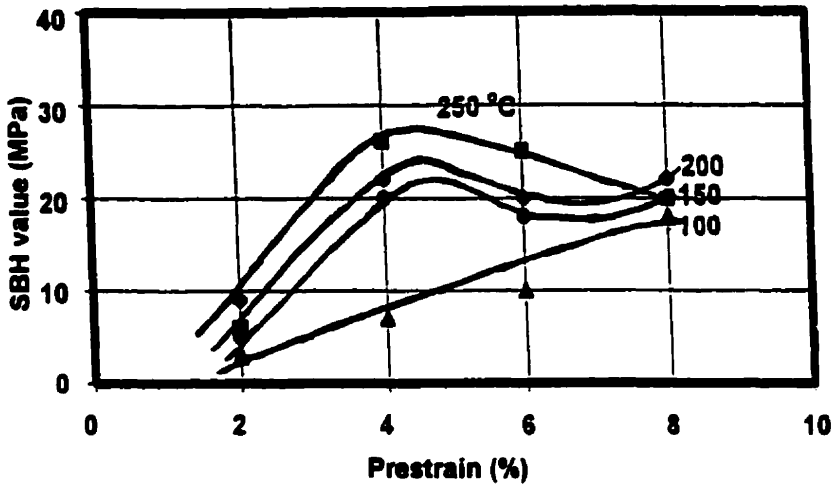

Fig. 4.23. Effects of temperature and prestrain on SBH.

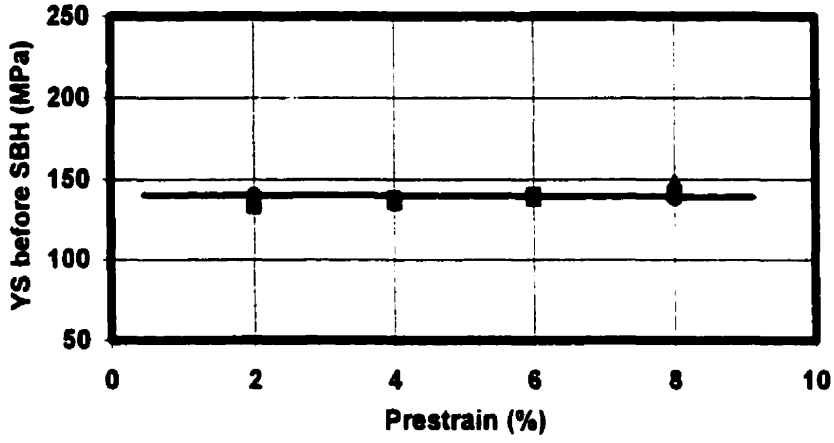

Fig. 4.24. Dependence of the yield strength before SBH on prestrain.

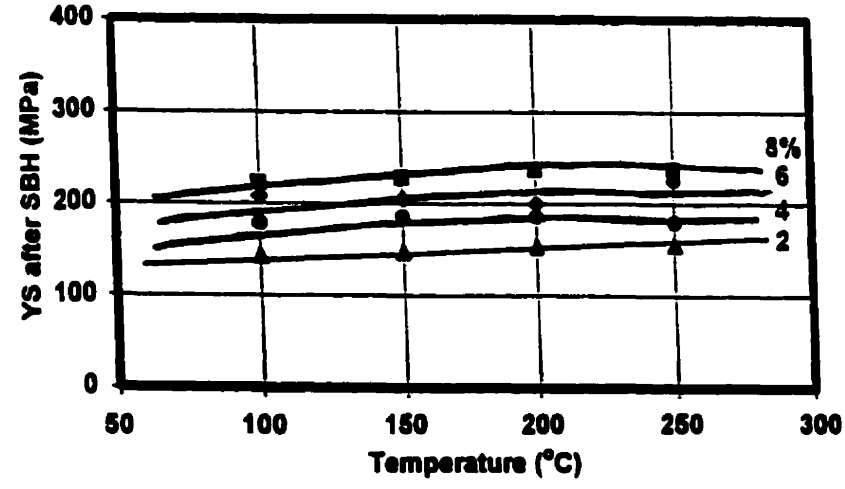

Fig. 4.25. Dependence of the yield strength after SBH on temperature.

Prestraining led to an increase in the yield strength until it almost reached a plateau. This happened between 200 and 250 °C, Fig. 4.25, and is in agreement with the results of past workers [43, 48, 115, 155]. By contrast, the yield strength before treatment remained constant at about 140 MPa, Fig. 4.24.

4.4.3. Dynamic-Static Bake Hardening (DSBH) Method

Figures 4.26 to 4.28 depict the effects of strain and temperature on i) the amount of bake hardening, ii) the yield strength before, and iii) after this technique, respectively. Two different behaviors were observed regarding the effects of strain and temperature on the amount of bake hardening, Fig. 4.26. When the subsequent aging temperature (170 °C) was higher than the temperature of dynamic aging (100 and 150 °C), the influence of dynamic aging was diminished. In this case, the effect of strain on the amount of bake hardening was almost the same as the behaviour observed in the SBH method for 150 and 200 °C. By contrast, when the former temperature was lower than the latter, the amount of bake hardening decreased with the strain. The maximum and minimum amounts of bake hardening (55 and 20 MPa) obtained with this method corresponded to straining to 4% and 8% at 150 and 250 °C, respectively.

Like the DBH method, the yield strength before the DSBH process remains constant at about 95 MPa, Fig. 4.27. By contrast, the yield strength after treatment increases with the amount of straining to essentially reach a plateau. The latter begins at a temperature between 150 and 200 °C, i.e. at approximately 170 °C, Fig. 4.28.

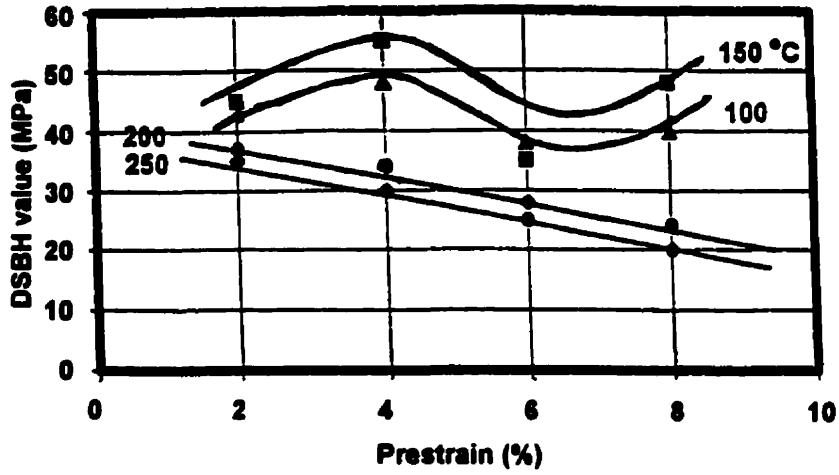

Fig. 4.26. Effects of temperature and prestrain on the DSBH values.

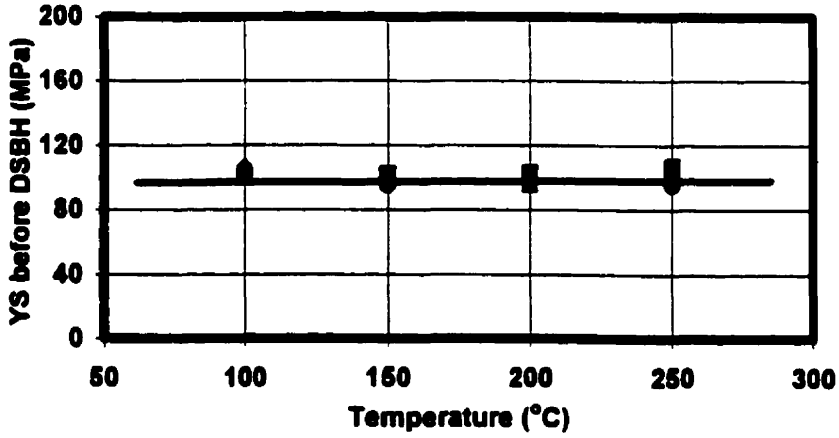

Fig. 4.27. Dependence of the yield strength before DSBH on temperature.

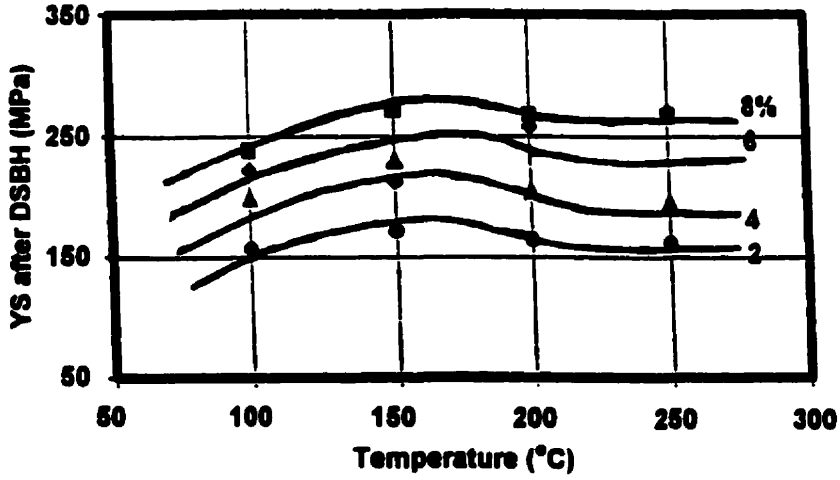

Fig. 4.28. Dependence of the yield strength after DSBH on temperature.

4.4.4. Comparison of the DBH, SBH, and DSBH Methods

The three methods of bake hardening steel B are compared in Figs. 4.29 to 4.33. It is evident that the dynamically aged specimens (the DBH and DSBH methods) produced the highest BH values, as well as pronounced work hardening rates, reduced Luders strains, lower yield strengths before prestraining, and significant increases in yield strength after baking. These factors can help to prevent buckling and wrinkling, necking in expanded zones, stretcher strains and spring back during press forming, and will lead to higher dent resistance after baking.

To avoid the above-mentioned defects in press forming, the yield strength should be as low as possible, the Luders strain should be almost zero, and the work hardening rate as high as possible. In addition, high yield points after baking confer high dent resistance. Referring to Figs. 4.29 to 4.33, all these properties can be improved by using a dynamic aging process.

The most important issues regarding the characteristics of the three bake hardening methods are the following:

i) The amounts of bake hardening in the cases of DSBH and DBH are much higher than those produced by the SBH (conventional) method. For example, in the case of a 2% strain at 100 °C, the amounts produced by the DSBH and DBH methods are about 15 and 8 times the SBH value, respectively. The minimum bake hardening value is about 3 MPa (2% prestrain at 100 °C with the SBH method) and the maximum value is about 55 MPa (a strain of 4% at 150 °C with the DSBH method). Generally speaking, the lowest bake hardening values were obtained in the case of SBH. Conversely, the highest amounts were observed in the case of the DSBH method when the temperatures of dynamic aging (100 and 150 °C) were

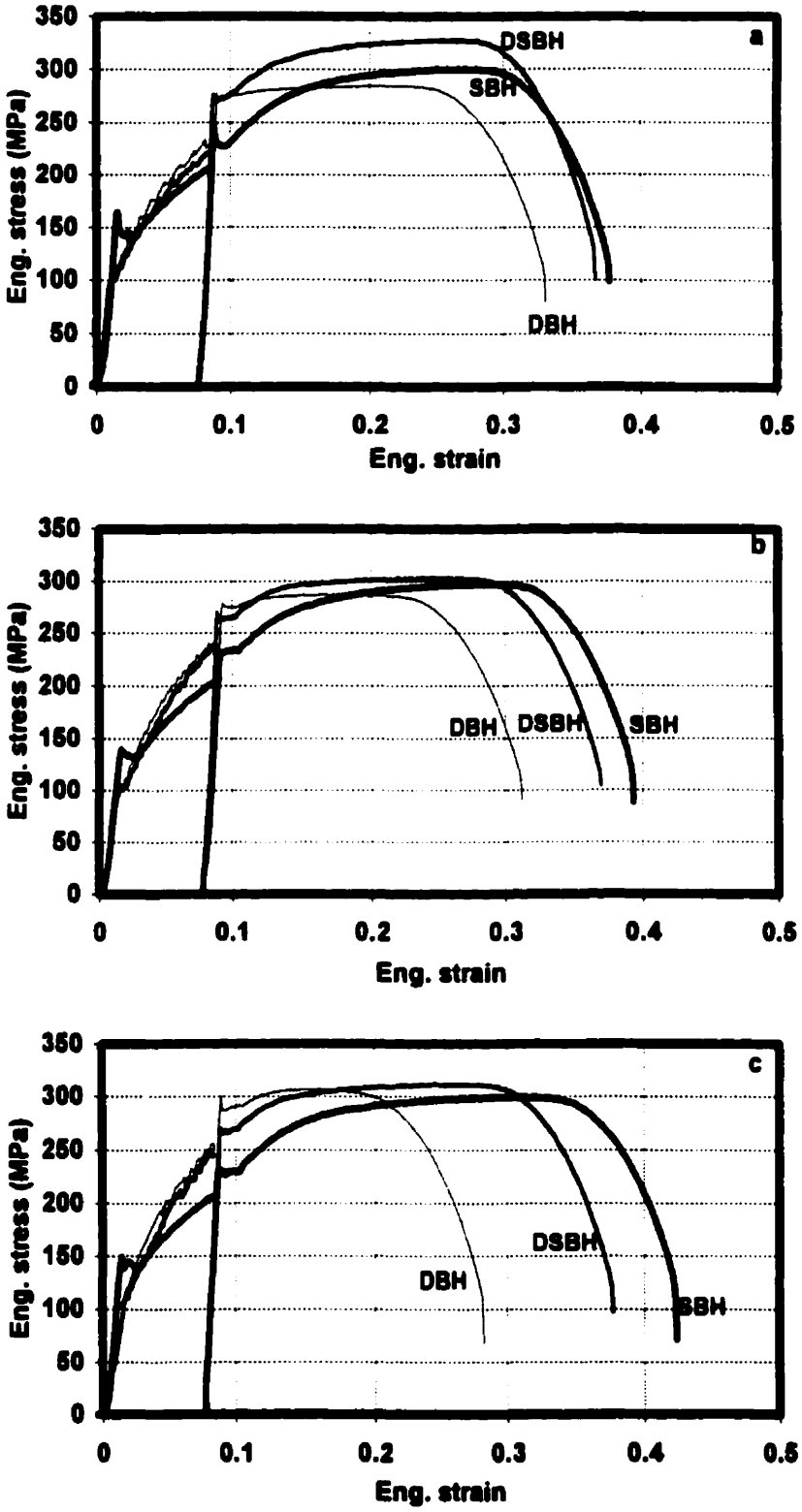

Fig. 4.29. Comparison of DBH, SBH, and DSBH values after an 8% prestrain at: a) 150, b) 200, and c) 250 °C (Steel B).

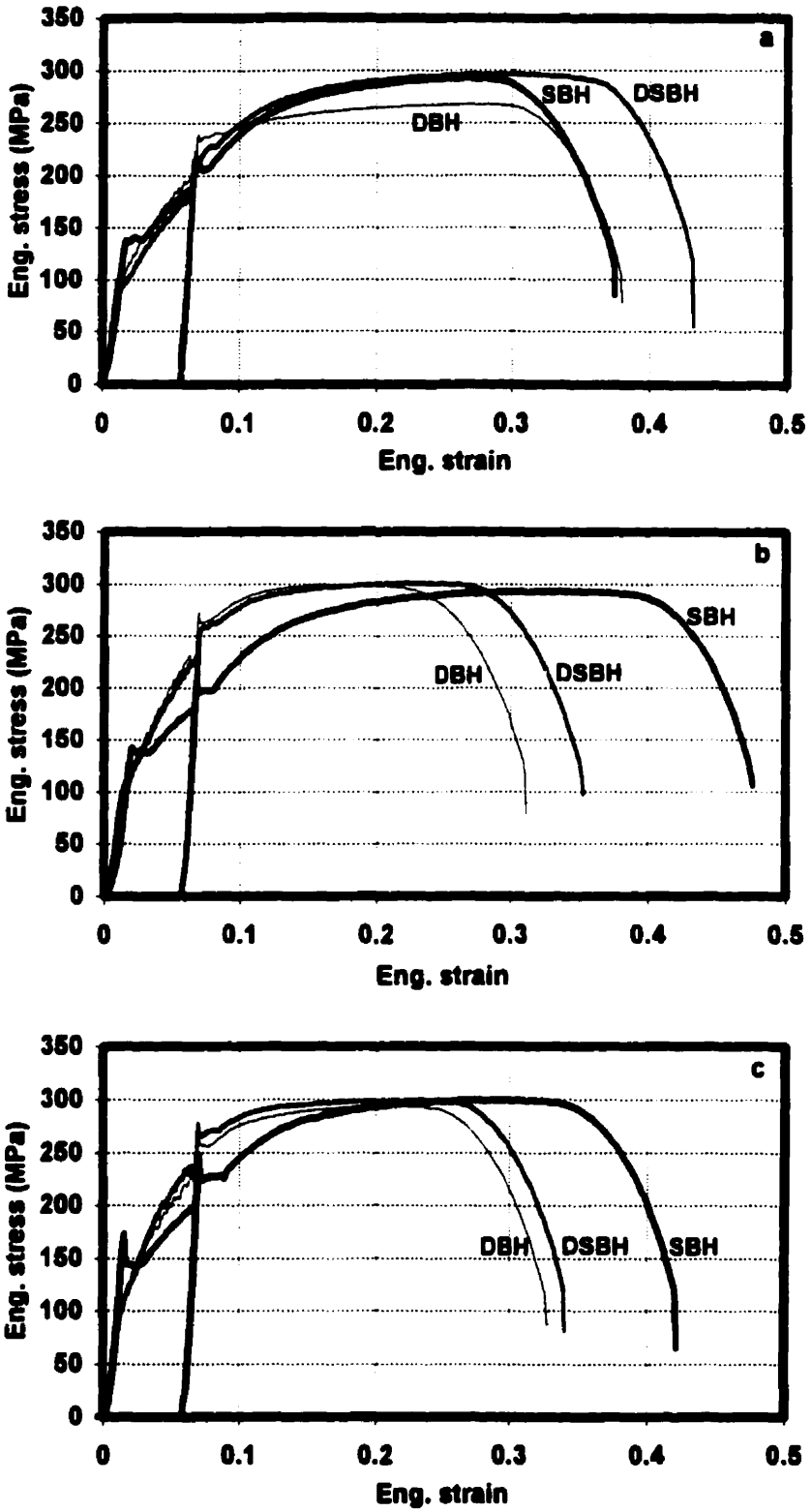

Fig. 4.30. Comparison of DBH, SBH, and DSBH values after a 6% prestrain at: a) 150, b) 200, and c) 250 °C (steel B).

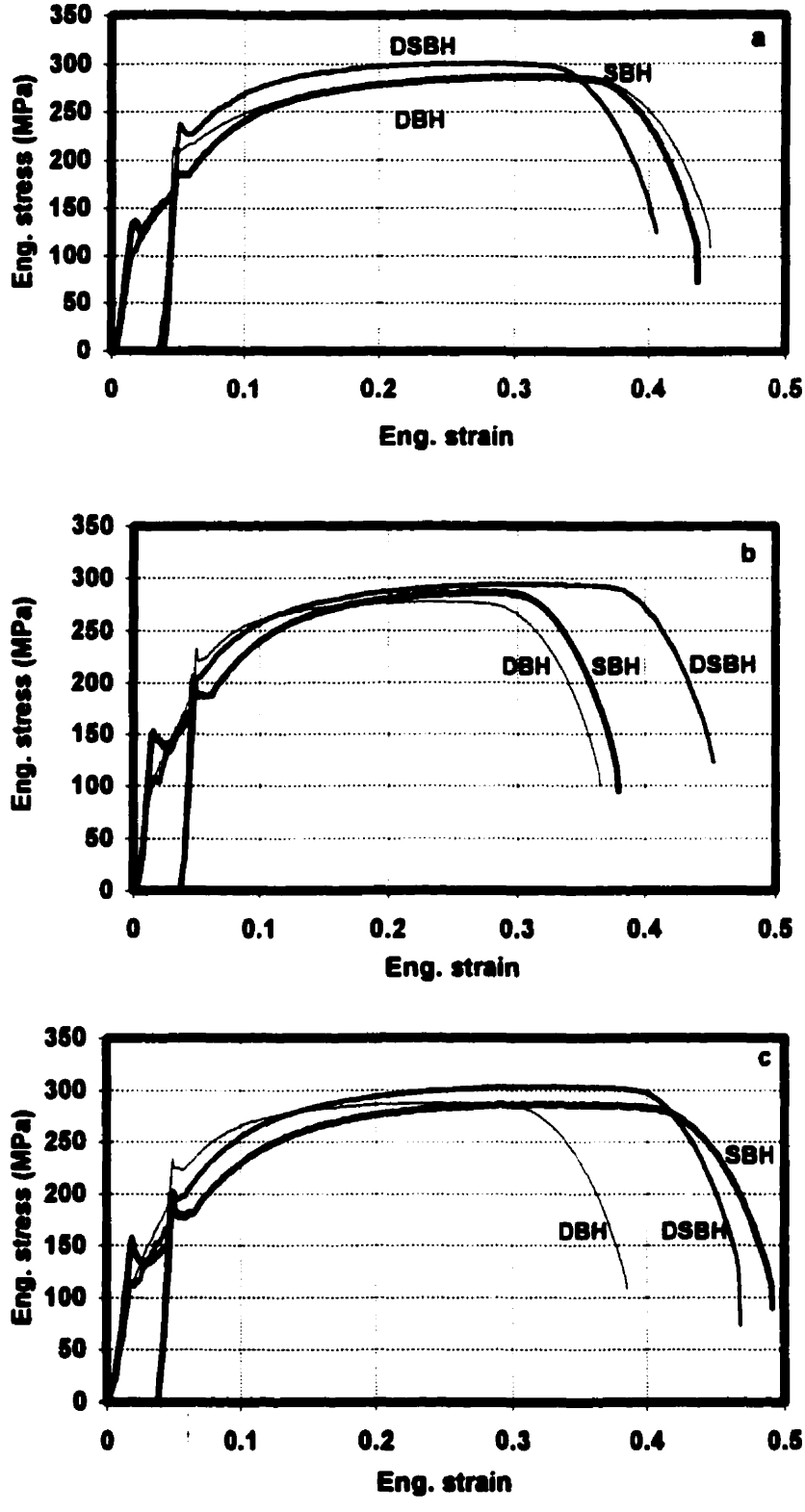

Fig. 4.31. Comparison of DBH, SBH, and DSBH values after a 4% prestrain at: a) 150, b) 200, and c) 250 °C (steel B).

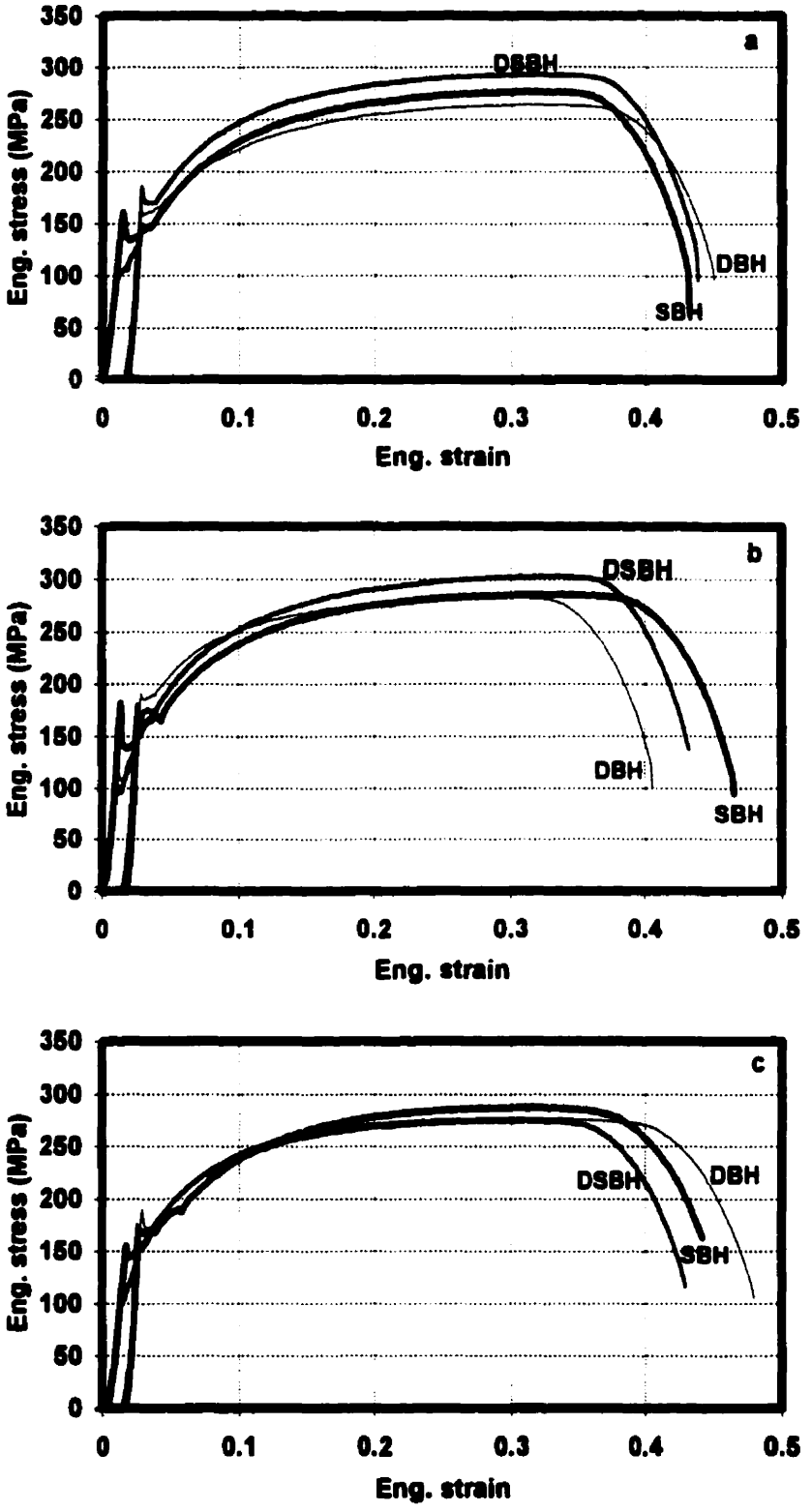

Fig. 4.32. Comparison of DBH, SBH, and DSBH values after a 2% prestrain at: a) 150, b) 200, and c) 250 °C (steel B).

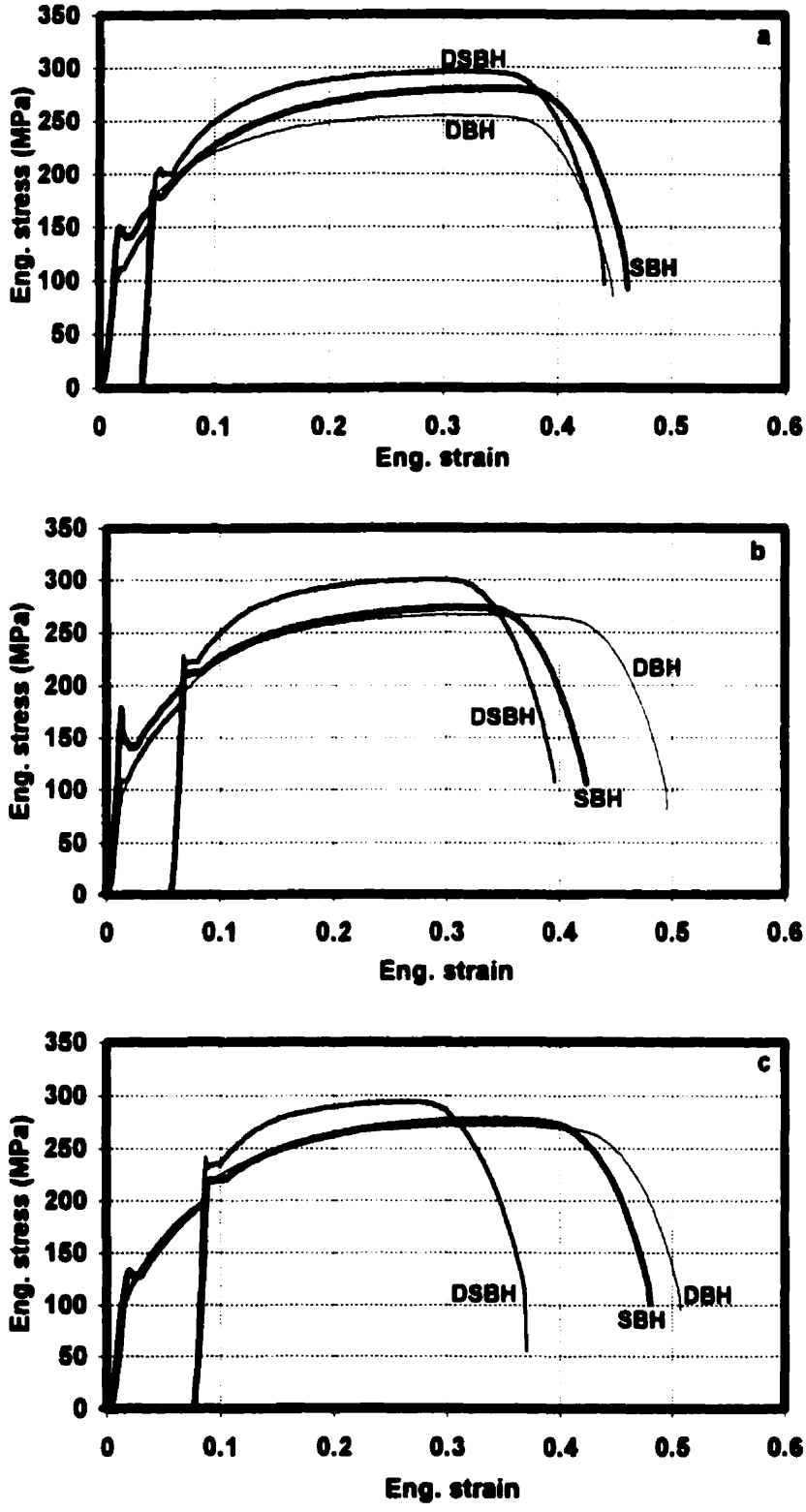

Fig. 4.33. Comparison of DBH, SBH, and DSBH values after prestraining at 100 °C to: a) 4% , b) 6%, and c) 8% (steel B).

lower than the temperature of subsequent static aging (170 °C). In other cases, it seems that the DBH method exhibited the higher values.

ii) There is no Luders strain during elevated temperature prestraining in the cases of the DBH and DSBH methods.

iii) In a similar manner, there is no sharp yield point when prestraining is carried out by the DBH and DSBH methods.

iv) The yield strength before baking in the DBH and DSBH methods is about 45 MPa lower than in the case of the SBH method.

v) The work hardening rate during prestraining is much higher in the DBH and DSBH methods than conventionally. This is because more pronounced work hardening rates are produced during dynamic strain aging than in the static strain aging case.

vi) The yield strength after baking is much higher when the DBH and DSBH methods are used.

vii) With increasing prestrain, the yield/tensile strength ratio increases until it almost attains unity in some cases of the DBH method.

viii) Although a sharp yield point and the Luders strain are rarely observed in the DBH method after baking, they are more significant for both the SBH and DSBH methods.

ix) The rise in UTS with prestrain is less pronounced than that of the yield strength, so that the UTS values are fairly close together (there is a maximum of about 45 MPa of difference between the various conditions of testing). Generally speaking, the DSBH, SBH, and DBH methods lead to average UTS values of 300, 290, and 280 MPa, respectively.

4.5. Torsion

4.5.1. Hot Rolling

As shown in Fig. 4.34, when both the roughing and finishing passes are carried out in the austenite phase, no serrations are observed in the stress-strain curves. When the first finishing pass was executed in the austenite region and the rest in the ferrite,

serrations manifested themselves in the flow curves of the passes carried out in the ferrite, see Fig. 4.35. In the third case when all the finishing passes were performed in the ferrite range, serrations were observed in all the flow curves, Fig. 4.36.

4.5.2. Warm Rolling

In this case, both roughing and finishing were carried out in the ferrite range. As presented in Fig. 4.37, serrations are observed during almost all the finishing passes. During each pass, they are initiated with a sharp yield drop, which is followed by the serrations. This phenomenon (DSA) can be attributed in this case to the substitutional elements, since the temperature and strain rate range in which the serrations are observed correspond to those reported for these elements [36, 93, 94, 156].

4.6. Coiling

The results of the aging index tests carried out on steels B and C (cooling from 650 °C at 0.01 °C/s) are presented in Figs. 4.38 and 4.39, respectively. The aging index values, along with the corresponding estimated amounts of solute carbon, are summarized in Table 4.3.

Table 4.3. Aging indices and estimated amounts of solute carbon resulting from the coiling simulation.

	Cooling Rate			
	0.01 °C/s		0.03 °C/s	
Steel	C ±1 (ppm)	AI ±3 (MPa)	C ±1 (ppm)	AI ±3 (MPa)
B	1.5	15	6	32
C	2.5	20	9	42

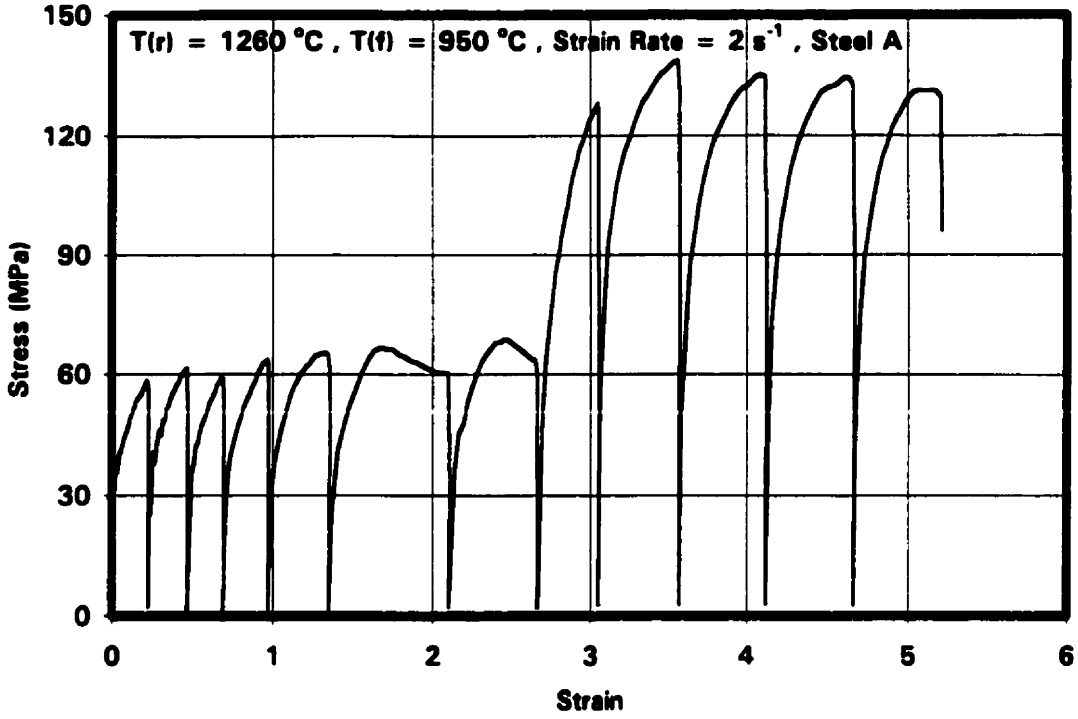

Fig. 4.34. Stress-strain curves determined in torsion when both finishing and roughing were carried out in the γ phase.

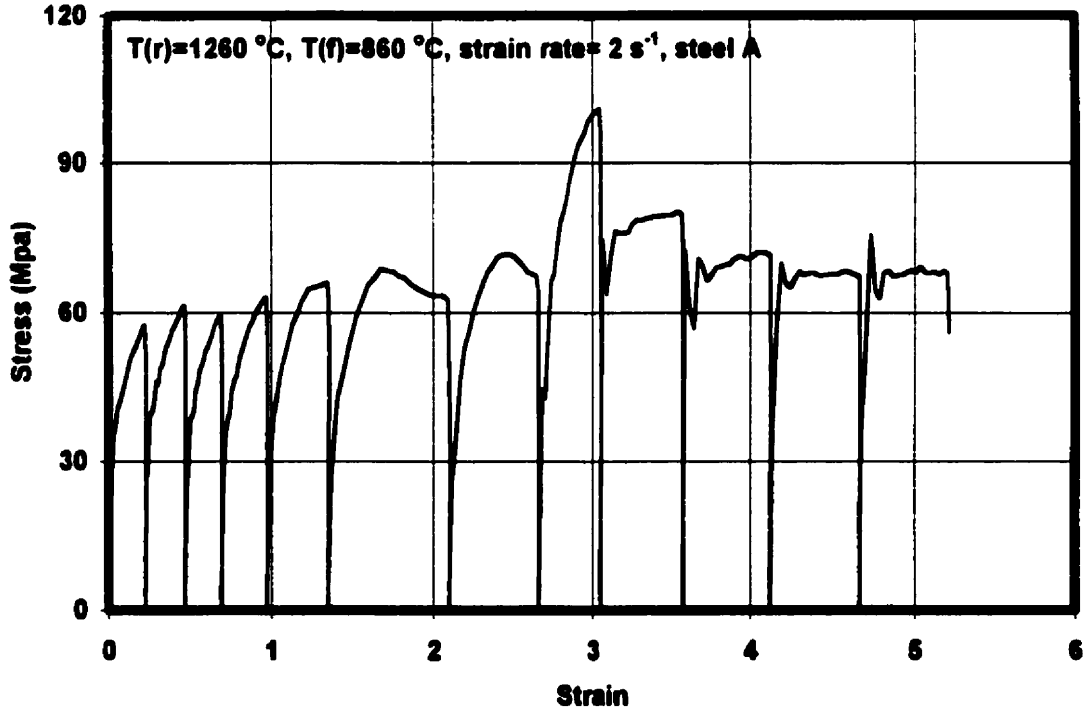

Fig. 4.35. Torsion stress-strain curves when the first finishing pass was carried out in the γ range and the rest in the α.

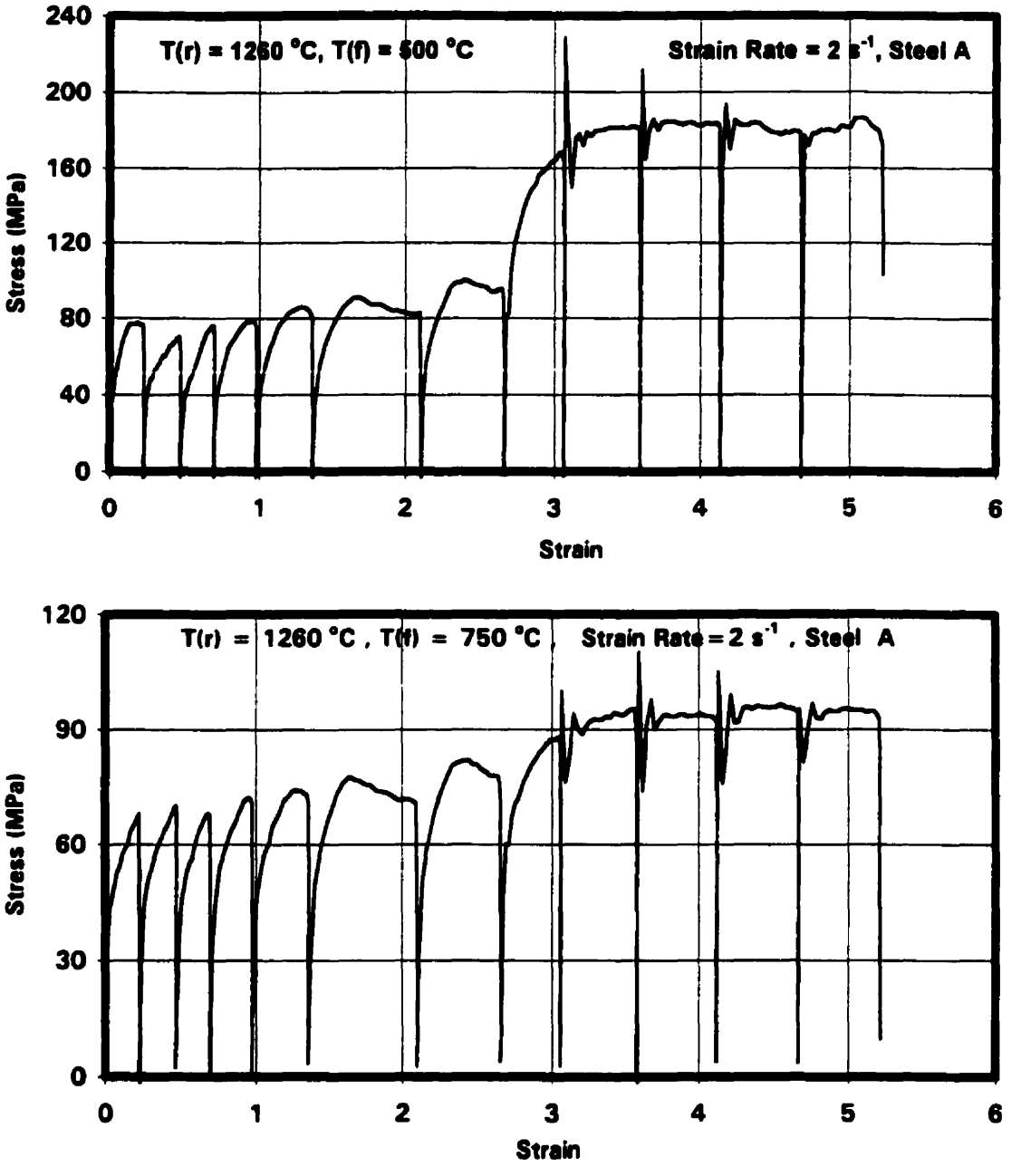

Fig. 4.36. Torsion stress-strain curves for cases where all the finishing passes were carried out in the α region with different finishing temperatures, T(f): 500 °C (above), 750 °C (below).

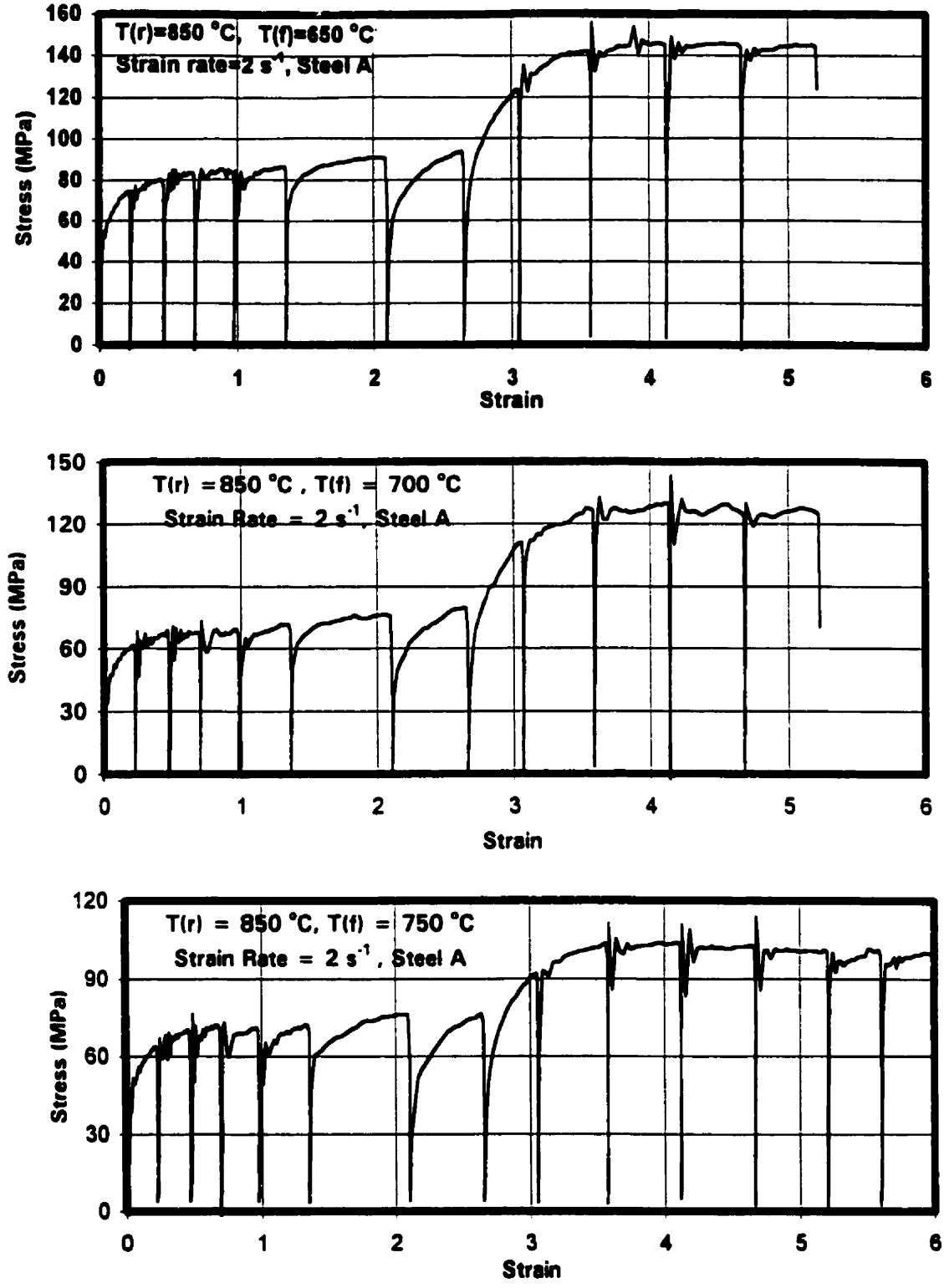

Fig. 4.37. Torsion stress-strain curves for the cases where both the roughing and finishing passes were carried out in the α range with different finishing temperatures T(f): 650, 700, and 750 °C.

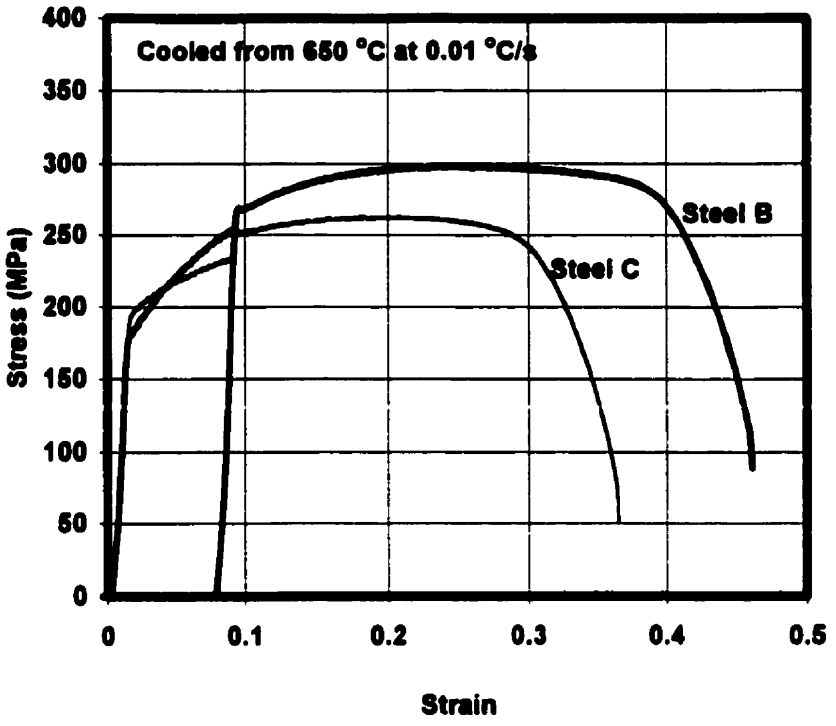

Fig. 4.38. Aging index tests on specimens cooled at 0.01 °C/s (coiling simulation).

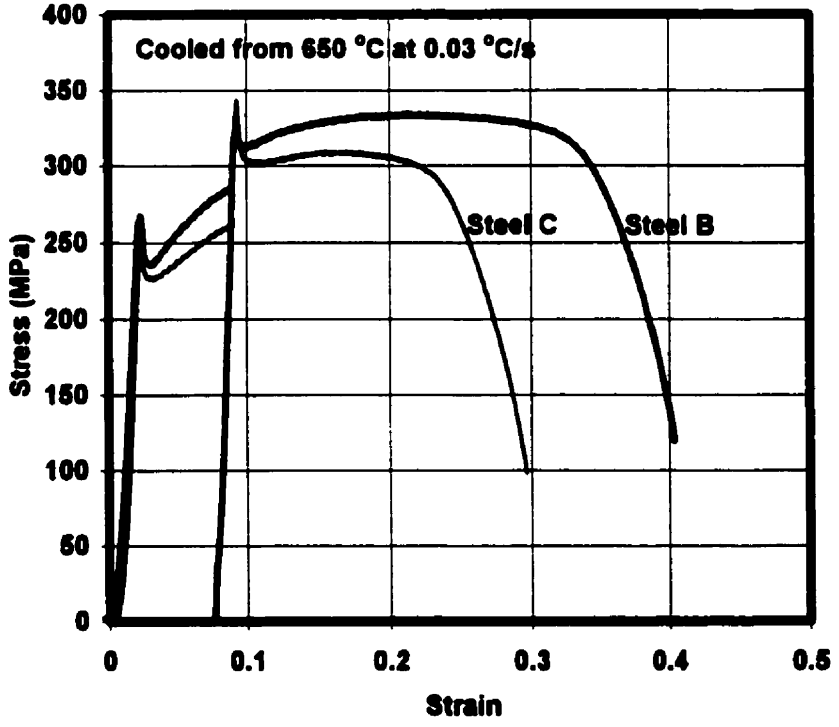

Fig. 4.39. Aging index tests on specimens cooled at 0.03 °C/s (coiling simulation).

These measurements show that, even after coiling, some amount of carbon will still remain in solution. Furthermore, when the second cooling rate of 0.03 °C/s was employed, even more solute carbon was obtained. The amount of carbon in solution at room temperature after coiling at typical IF steel temperatures (650-750 °C) was reported to be 3 ppm [157]. Other authors have found this amount to be 4 ppm after coiling at 750 °C [158]. In the present work, the aging indices and therefore solute carbon levels were highest for steel C, which had the lowest S content or highest Ti^*_f/S ratio.

4.7. Continuous Annealing

Some of the stress/strain curves obtained from the aging index tests carried out on steels B and C are illustrated in Figs. 4.40 and 4.41. The aging indices and their corresponding amounts of solute carbon are shown in Tables 4.4 and 4.5 for steels B and C, respectively.

Table 4.4. Aging indices and estimated amounts of solute carbon resulting from the continuous annealing simulation carried out on steel B.

steel B	Furnace Cooling		Still Air Cooling		Water Quench	
T (°C)	C ±1 (ppm)	AI ±3 (MPa)	C ±1 (ppm)	AI ±3 (MPa)	C ±1 (ppm)	AI ±3 (MPa)
650	3	22	4	25	5.5	30
750	2	17	3	22	4	25
850	0	0	0	0	0.5-1	5

Table 4.5. Aging indices and estimated amounts of solute carbon resulting from the continuous annealing simulation carried out on steel C.

steel C	Furnace Cooling		Still Air Cooling		Water Quench	
T (°C)	C ±1 (ppm)	AI ±3 (MPa)	C ±1 (ppm)	AI±3 (MPa)	C ±1 (ppm)	AI ±3 (MPa)
650	5.5	30	6.5	33	8.5	40
750	1.5	15	4	25	5.5	30
850	0	0	0	0	0	0

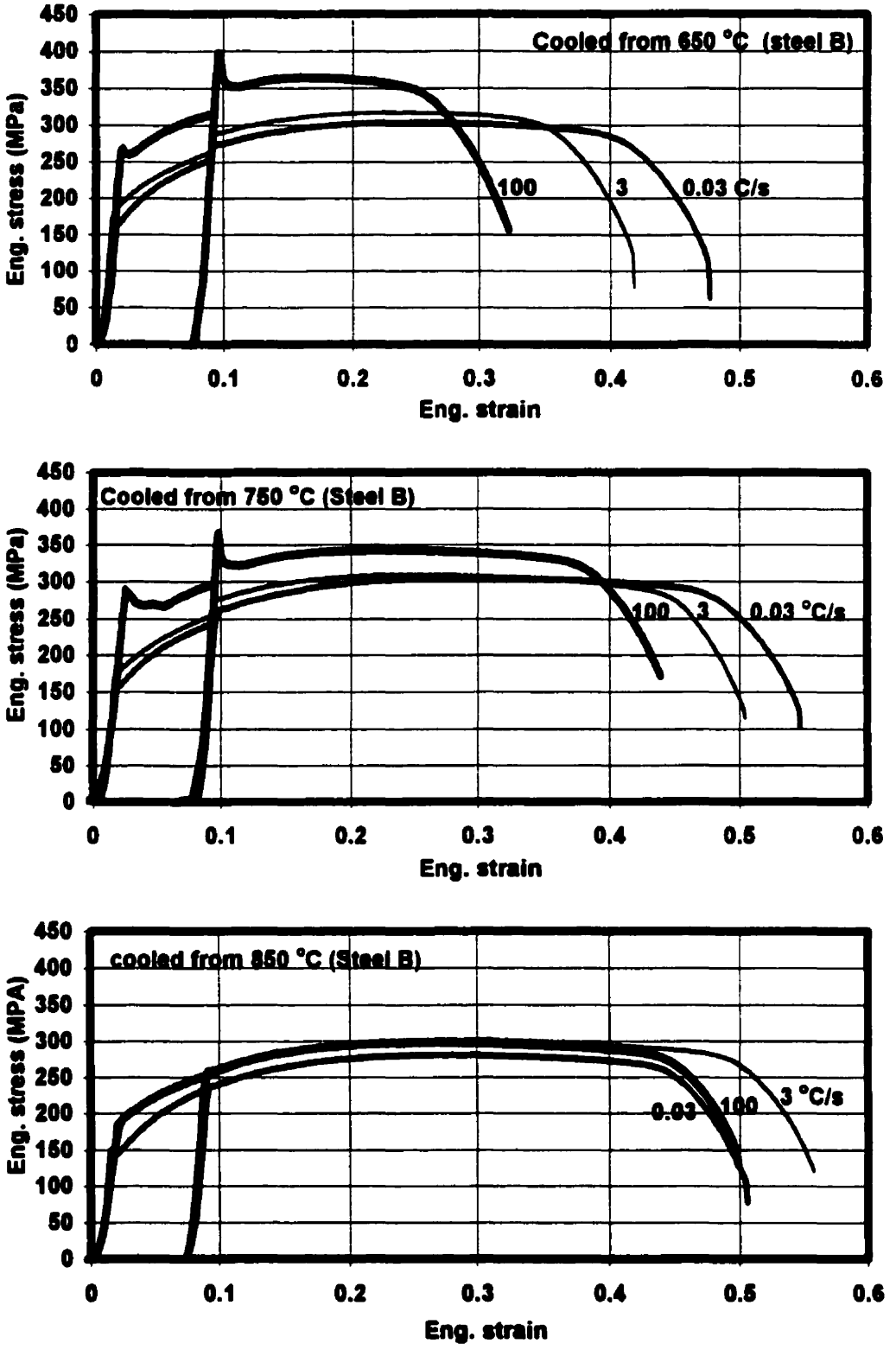

Fig. 4.40. Aging index tests carried out on specimens cooled from different annealing temperatures at different rates (continuous annealing simulation).

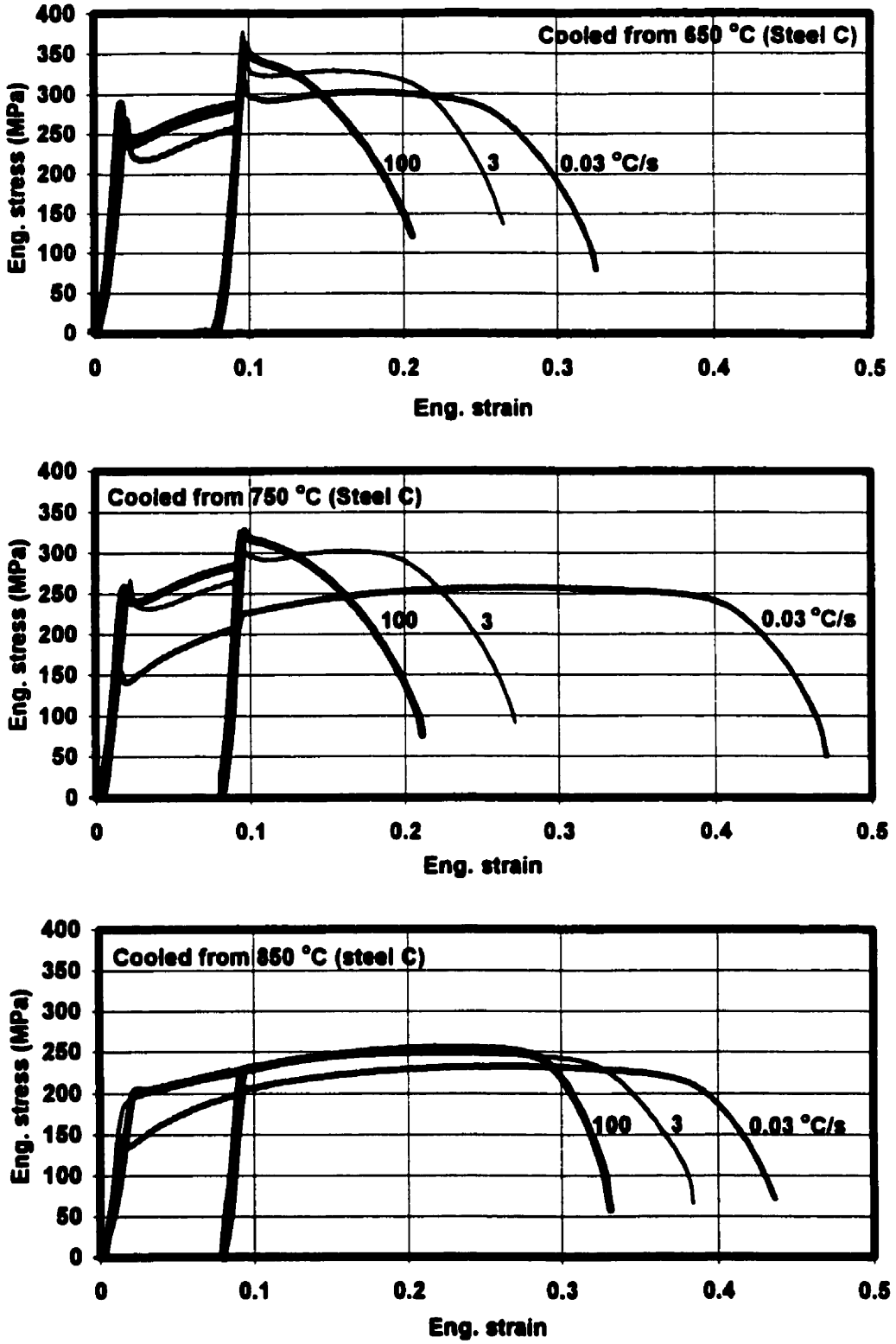

Fig. 4.41. Aging index tests carried out on specimens cooled from different annealing temperatures at different rates (continuous annealing simulation).

An interesting point is that the solute carbon and consequently the aging index values decrease with increasing annealing temperature, so that both converge to about zero at 850 °C. This result is in agreement with the findings of past workers who reported, in some cases, the effects of increasing the annealing temperature on the yield point, hardness, aging index, and/or solute carbon level [2, 45, 51, 55, 159, 160]. For example, the amount of carbon in solution for a 0.0019% steel was reported to be 4 ppm when continuous annealing was carried out at 800 °C (the cooling rate was unknown) [47]. The maximum amount of aging again pertained to the steel (C) that had the lowest S content and the highest Ti^*_f/S atomic ratio.

4.8. Internal Friction/Solute Carbon Measurements

Some of the results obtained from the internal friction measurements carried out on steels B and C are illustrated in Figs. 4.42 to 4.49. The measured and estimated solute carbon levels of the specimens cooled from 1100 °C at different rates are compared in Table 4.6. In the case of steel B, there is a small difference between the measured and estimated amounts of C in solution. The difference is somewhat more pronounced in the case of steel C.

Table 4.6. Measured and estimated amounts of solute carbon in samples cooled from 1100 °C at different rates.

	Furnace Cooling		Still Air Cooling		Water Quench	
Steel	Estimated +1 ppm	Measured +1 ppm	Estimated ±1 ppm	Measured ±1 ppm	Estimate ±1 ppm	Measured ±1 ppm
B	0	0	4.5	4.5	7	5
C	0	0	7	6.5	15	19

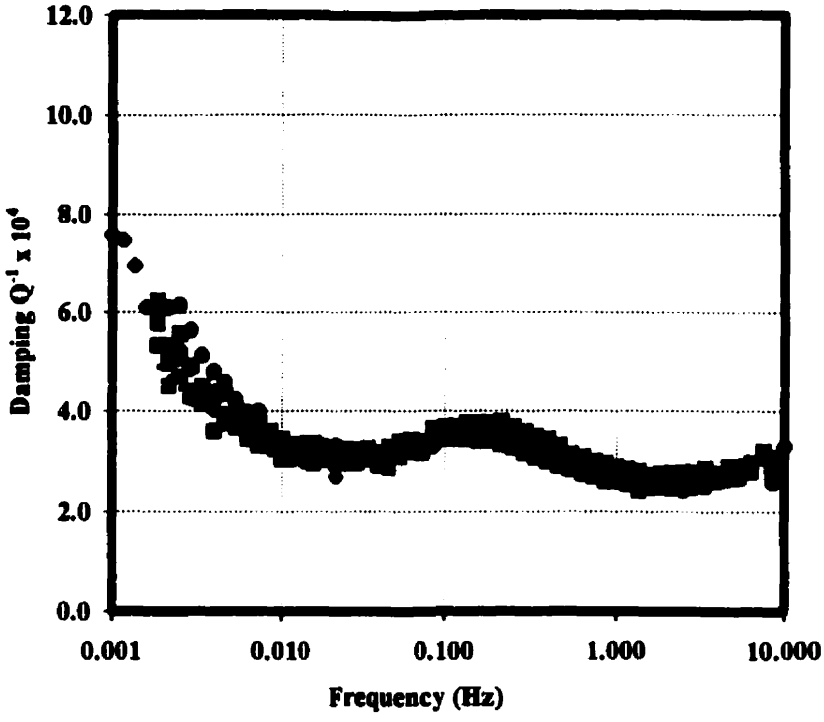

Fig. 4.42. Internal friction tests carried out on specimens cooled from 1100 °C in still air (steel B).

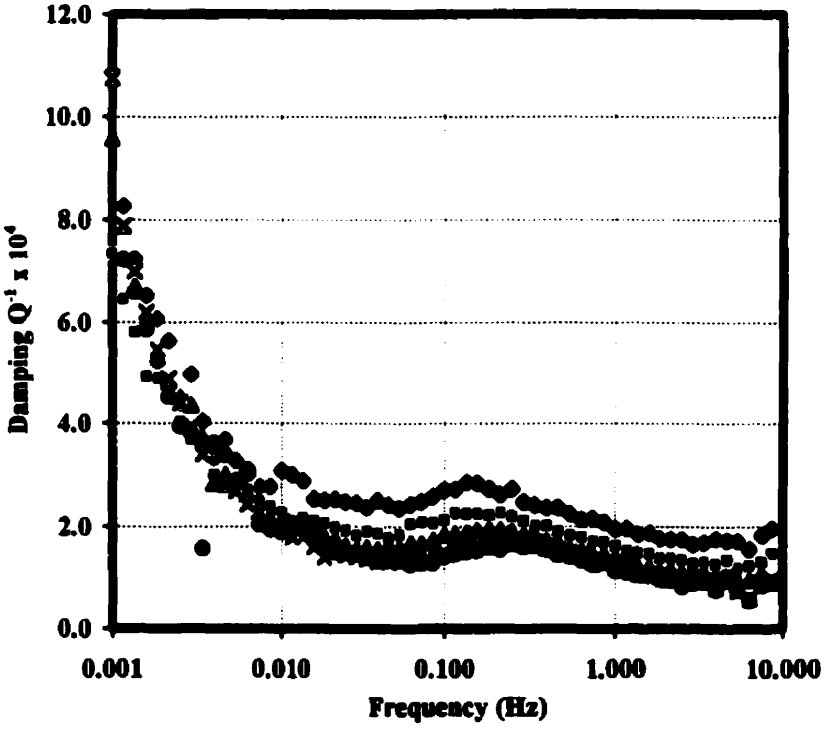

Fig. 4.43. Internal friction tests carried out on specimens water quenched from 1100 °C (steel B).

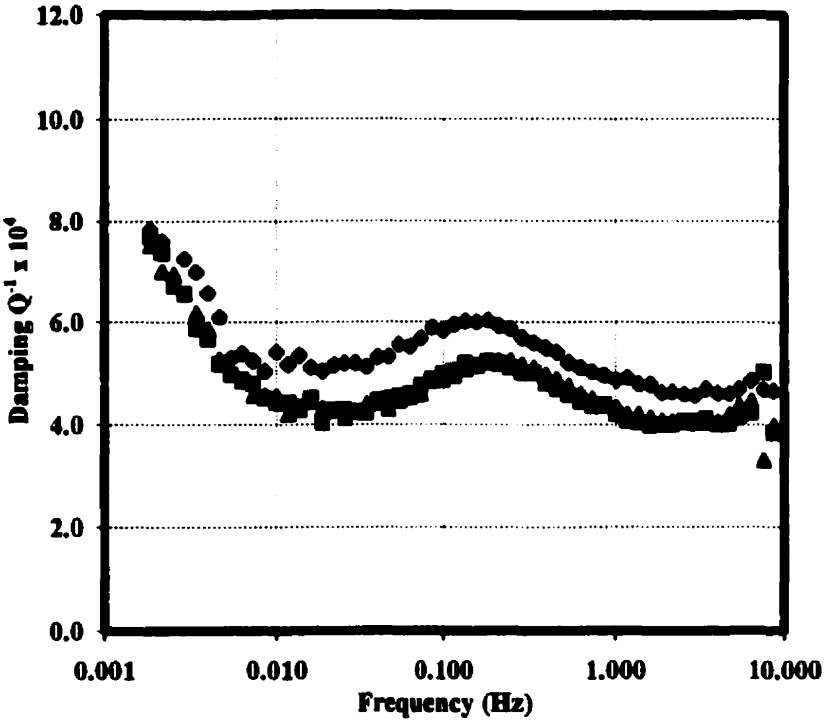

Fig. 4.44. Internal friction tests carried out on specimens cooled from 1100 °C in still air (steel C).

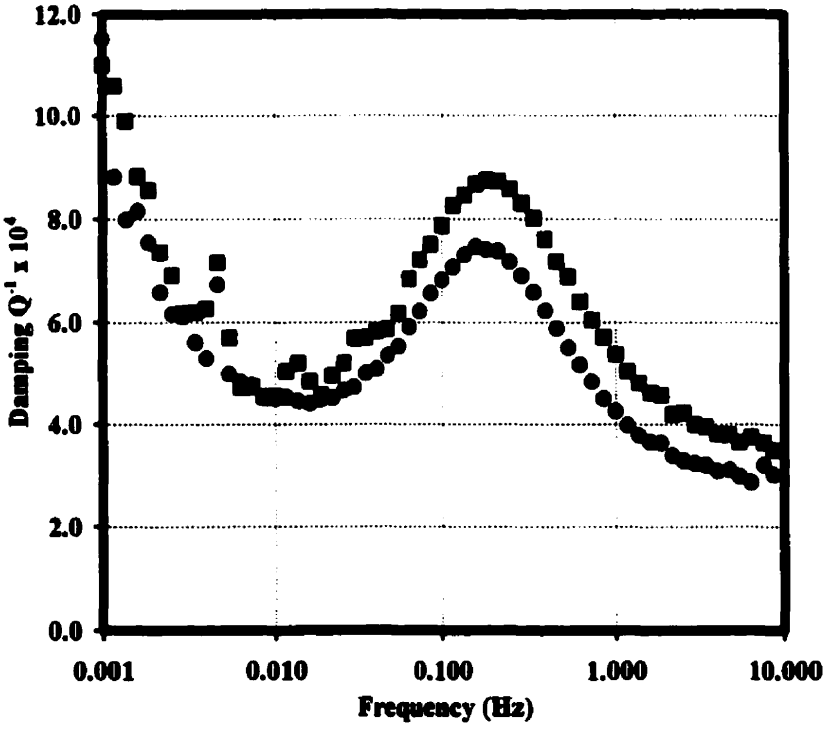

Fig. 4.45. Internal friction tests carried out on specimens water quenched from 1100 °C (Steel C).

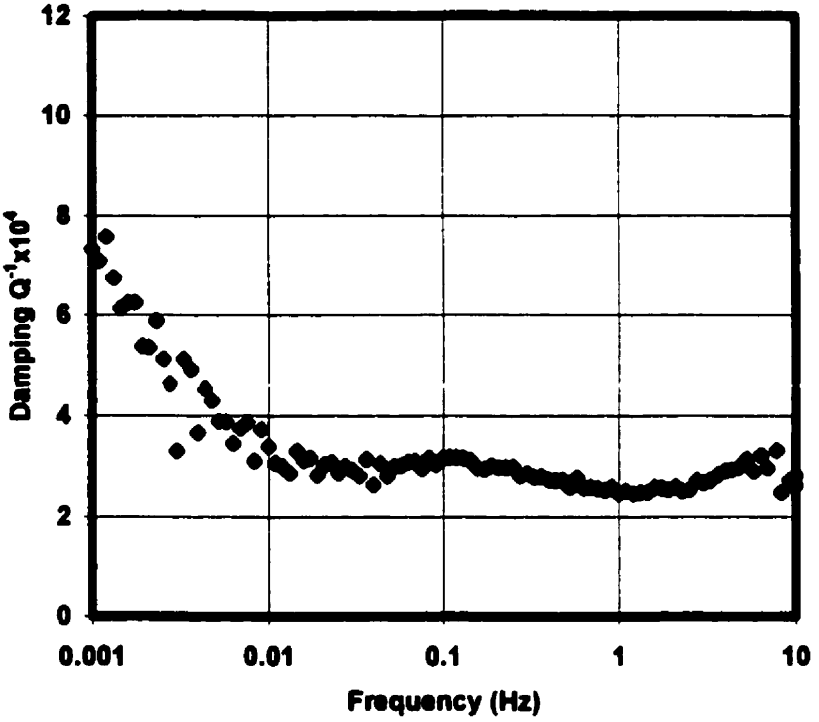

Fig. 4. 46. Internal friction tests carried out on specimens cooled from 750 °C in still air (steel B).

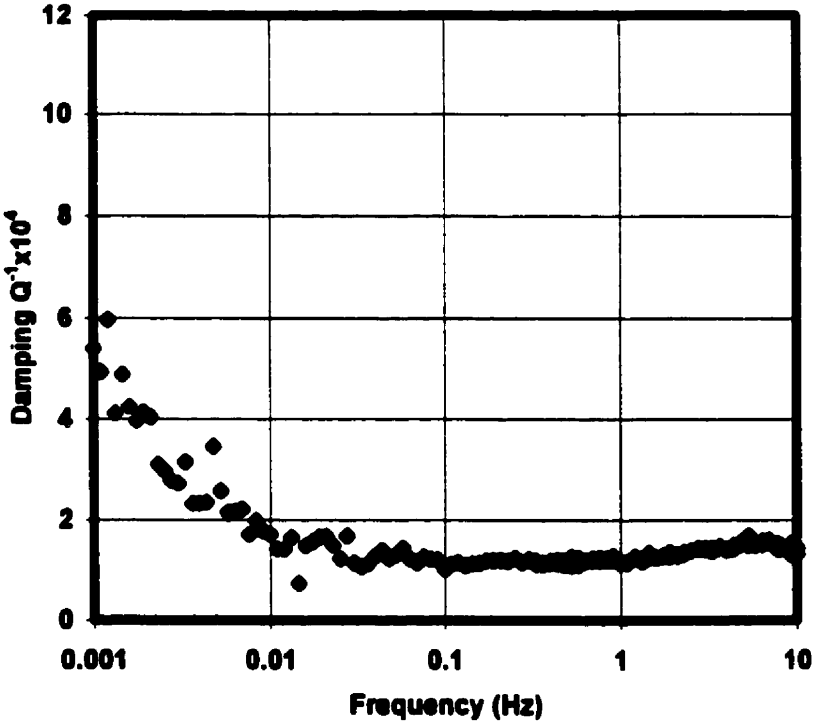

Fig. 4.47. Internal friction tests carried out on specimens cooled from 850 °C in the furnace (steel B).

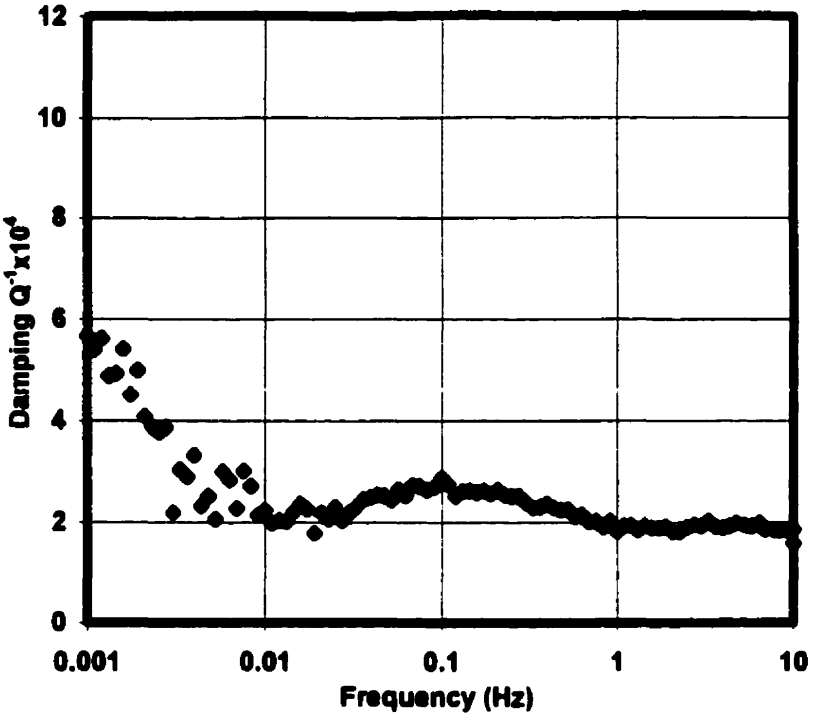

Fig. 4.48. Internal friction tests carried out on specimens cooled from 650 °C in still air (Steel C).

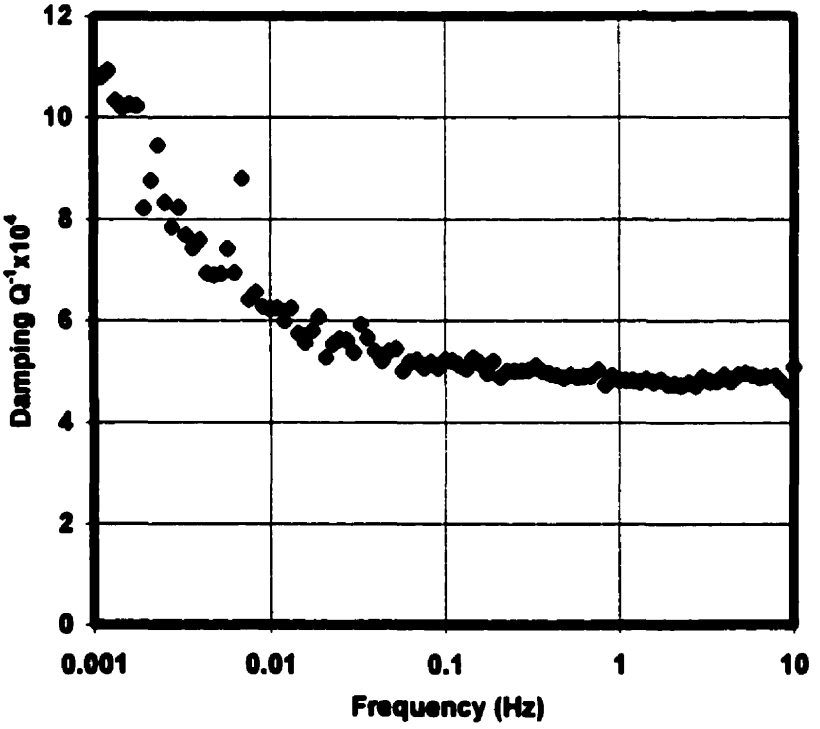

Fig. 4.49. Internal friction tests carried out on specimens water quenched from 850 °C. (Steel C).

The results for the samples cooled from 650, 750, and 850 °C (at three rates) are summarized in Table 4.7 for steel B.

Table 4.7. Measured and estimated amounts of solute carbon remaining in steel B after the continuous annealing simulation.

	Furnace Cooling		Still Air Cooling		Water Quench	
Steel B	Estimated ±1 ppm	Measured ±1 ppm	Estimated ±1 ppm	Measured ±1 ppm	Estimated ±1 ppm	Measured ±1 ppm
650 °C	3	5	4	15	5.5	10
750 °C	2	1	3	3	4	7
850 °C	0	0	0	1.5	0.5-1	4

4.9. Calibration between the Aging Index and Solute C Level

A calibration was established in this work between the aging indices and the amount of solute carbon present in the steels, see Fig. 4.50. This employed the results of the aging index and internal friction measurements and was based on averages for repeated tests. This calibration can be readily used to predict the aging behaviour of IF steels.

4.10. Flattening

Tensile tests were carried out on specimens of steels A, B, and C at the strain rate employed during flattening (10^{-4} s^{-1}). The flow curves obtained through the temperature range ambient to 350 °C at a strain rate of 10^{-4} s^{-1} are displayed in Fig. 4.51 for the Ti IF steels. In the blue brittleness range, the stress-strain curves show evidence of pronounced strengthening accompanied

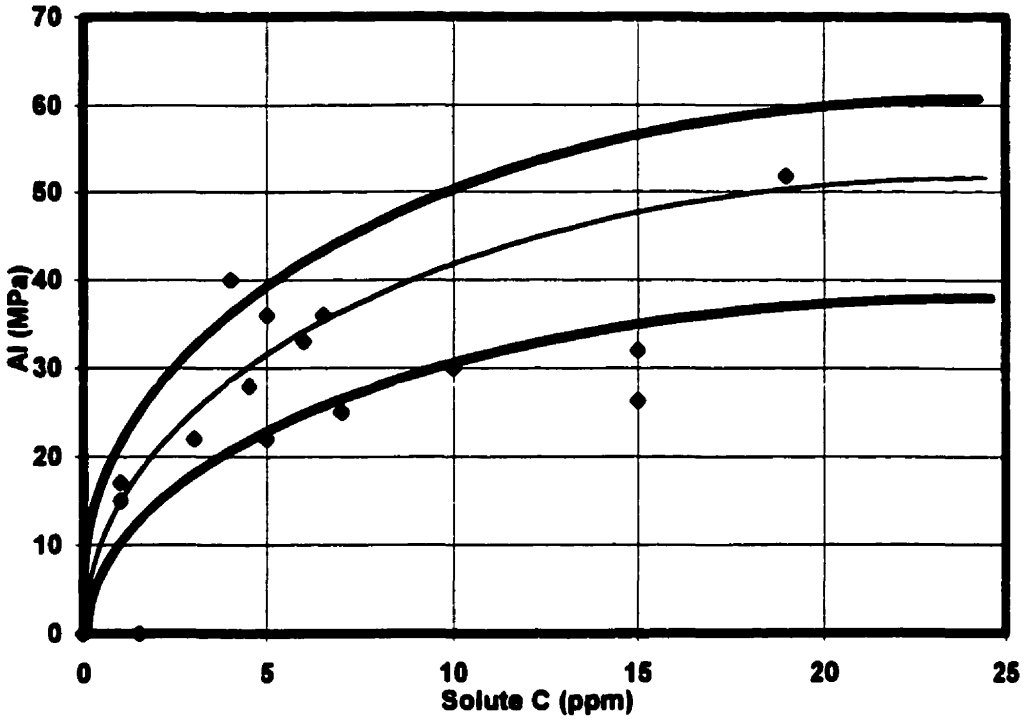

Fig. 4.50. Calibration between the measured aging indices and amounts of solute C in the present steels.

by a significant decrease in ductility. The temperature at which serrations first appear is less than 100 °C. Within the serrated flow range, the magnitude and frequency of the serrations as well as the work hardening rates increase to a maximum as the temperature is increased.

It is evident that, in some cases, for example at 200 °C, the serrations are initiated at very low strains, even less than 0.2% elongation. It should be noted that to remove irregularities along the strip width, the plastic strain required lies between 0.1% to 0.4% elongation [145].

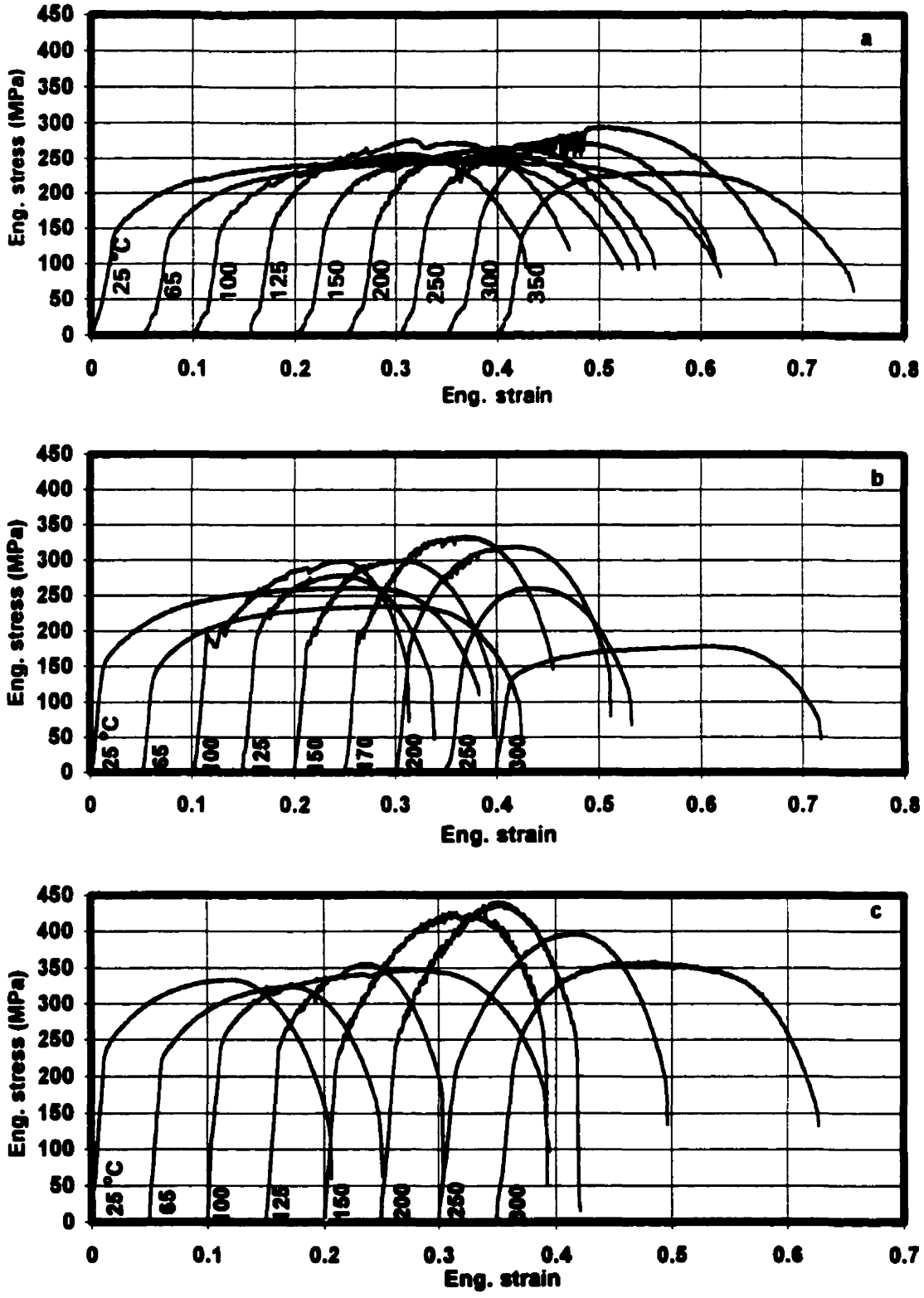

Fig. 4.51. Stress/strain curves determined on specimens tensile tested at different temperatures and a strain rate of 10^{-4} s^{-1}: a) steel A, b) steel B, c) steel C.

CHAPTER 5

Discussion

5.1. Effect of Cooling Rate

The effect of cooling rate on the amount of carbon that remains in solution at room temperature depends on several parameters. The foremost of these are the reheat temperature and total amount of carbon; the latter determines the maximum available amount of carbon. Also of importance are the type of particle that will act as a nucleation site for TiC and the size distribution and spacing of these nuclei. The length of the carbon atom diffusion path depends on the latter. Here it is important to recall that the nucleation rate is more important than the diffusion rate with respect to precipitation [40, 76] and that higher dislocation densities promote nucleation [76].

In terms of the type of particle required for nucleation, the precipitation of TiC on TiN nuclei has not been observed during cooling from high temperatures under the present conditions [69, 75, 101]. By contrast, TiS has been observed to act as a preferential site for the nucleation of TiC [57, 75, 102, 128]; this then leads to the formation of $Ti_4C_2S_2$. This appears to be the reason why Tsunoyama et al. [57] found that the amount of carbon in solution at room temperature depends inversely on the total amount of S in the steel. Upon cooling after annealing at high temperatures, they reported that a considerable amount of carbon remains in solution in Ti IF steels with low S levels. This was attributed to the lack of sufficient TiS nucleation sites for C

precipitation. Nucleation can also be promoted by the presence of pre-existing particles, or by the simultaneous precipitation of other particles [118]. Ti or Nb carbide can act as the nucleation site for iron carbide when the Ti/ C or Nb/C atomic ratio is less than unity [55]

During the continuous annealing of low carbon steels, MnS particles act as preferential nucleation sites for the precipitation of cementite, enabling the production of non-aging steels [3]. Elements like Mn or Ni can act as additional nucleation sites for carbide particles [161]. The rate of C precipitation in ternary alloys is also more rapid than in binary alloys; in the latter case, fewer precipitates are present to act as nucleation sites for the carbides [118]. In low carbon steels, epsilon carbides can serve as nucleation sites for the precipitation of Fe_4N [162].

As regards the *distribution* of particles, it is well known that finely dispersed sites are more effective in removing carbon from solution than widely dispersed sites. In the former case, the diffusion paths of carbon atoms to nuclei are shorter. Although this distance increases as the cooling rate is decreased, the time for diffusion becomes long enough to allow full precipitation of the carbon, thus following the equilibrium trend of decreasing carbon solubility with decreasing temperature. Chemical composition also affects the particle dispersion. For example, in the case of Ti IF steels, the precipitates are dispersed more coarsely than in Nb IF steels [59, 65].

With respect to the total amount of carbon, it has been reported that when the carbon content is high, e.g. 0.78%, the amount of carbon in solution at the reheat temperature is not retained, even after water quenching [163]. In this case, it appears that the closely spaced Fe_3C particles act as sites for

carbon precipitation during quenching, so that the amount of carbon in solution after quenching is reduced.

To achieve the same low solute carbon levels in lower carbon grades, e.g. 0.01 to 0.1%, Butler [164] applied a cooling rate four orders of magnitude slower than water quenching, 0.5 °C/min. However, he reported that this cooling rate was ineffective for the 0.01% C material. Evidently, insufficient precipitation sites were available, resulting in almost all the carbon remaining in solution. Considering the much lower carbon content in the present Ti IF steels, e.g. 0.0019% C, it can be expected that a still slower cooling rate will be required because of the still larger interparticle spacing. Nevertheless, keeping in mind that Butler's findings are related to plain carbon steels, it remains possible that carbide formers such as Ti can act as more effective scavengers by removing solute carbon, either by direct precipitation or by complex precipitation [5, 102].

Bleck et al. [50] found that, after batch annealing, the amount of carbon in solution in steels with <0.015% C is much more than in steels with >0.03% carbon. The amount of solute C in the former was up to 12 ppm compared to 1 ppm for the latter.

In the present work, even still air cooling resulted in a material that was supersaturated with carbon. This can be attributed to the very low carbon content, as discussed above, and also to the lack of sufficient time for Ti or C diffusion. Baird [5] has suggested that slow cooling is not the most effective way to precipitate C or N because of the wide separation of nucleation sites and the consequent long diffusion distances. Others have also noted that the

precipitation of carbon is less complete in alloys with very low carbon contents because of the sparseness of carbide nucleation sites [102, 165, 166].

With regard to the furnace cooled samples, it can be concluded that, in practice, control of the level of carbon in solution can be achieved by choosing an optimum coiling temperature. This temperature should be low enough for the equilibrium solubility of carbon to be low, but high enough to allow sufficient time for precipitation and diffusion. Although high coiling temperatures promote favorable texture development, they also promote the formation of large cementite particles, which can then cause damage by cracking [134]. There are other disadvantages of high coiling temperatures, such as the presence of thicker oxide layers along the strip edges, and greater differences in cooling rate between the coil ends and the middle [132]. Bleck et al. have therefore suggested that lower coiling temperatures should be used, which would lead to higher yield strengths as a result of the carbon in solution [59].

As will be discussed later, the effectiveness of Ti in removing carbon from solution depends on the amount of Ti remaining after reaction with N, S, O, and some of the P. However, it should be noted that, upon cooling after continuous annealing [55, 57, 141], some dissolved carbon can remain in solution in Ti IF steels, even when the excess Ti is greater than zero [57].

In summary, the most important factors that determine the effectiveness of a particular cooling rate in removing carbon from solution are: the reheat temperature, the initial amount of carbon in solution, the type of particle acting as a nucleation site, and the diffusion distance between nucleation sites. The

latter depends, in turn, on the mean size of the particles that act as nuclei [61, 164].

5.2. Effect of Chemical Composition

Some workers [113] have reported that sufficient solute C is not easily obtained through the dissolution of carbide formers, even when high annealing temperatures are employed. Furthermore, annealing at high temperatures is not economical or practical. It is easier to adjust the amount of solute carbon instead by controlling the chemical composition, especially in the case of the bake hardenable steels.

The chemical composition is important because the solubility products of the various precipitates are modified by the presence of alloying elements [62, 63]. In IF steels, for example, elements such as S, P, and Mn can affect the amount of C in solution, regardless of the cooling rate.

Alloying elements can influence the precipitation process by a) changing the C activity and consequently the solubility of carbon, b) affecting the density of nucleation sites, and c) changing the composition of the final precipitate. Manganese, for example, decreases the activity of carbon, resulting in the formation of a metastable carbide; conversely silicon stabilizes the carbide because it increases the activity [167, 168]. Phosphorus has almost the same effect as silicon [161, 169].

The effects of the various alloying elements on nucleation are summarized in Table 5.1.

Table 5.1. Relation between type of particle and nucleation site.

particle or element	nucleation site for
TiS	TiC
TiC/NbC	iron carbide
MnS	cementite
Mn/Ni	carbides
epsilon carbide	Fe_4N
particles in ternary and other alloys	carbides

In terms of changing the composition of the carbide, when the P content is high, FeTiP forms in place of $Ti_4C_2S_2$ and TiC, as the former is more stable than the latter two compounds [131]. By increasing the Mn content in IF steels, the formation of $Ti_4C_2S_2$ is suppressed. This reaction is also retarded when the S content is extremely low [131]. In both cases, the aging index can be increased because of the increased availability of C in solution. Finally, the amount of $Ti_4C_2S_2$ increases when the sulfur content is increased. This leads to a decrease in the amount of TiC, and therefore in the solute carbon that is produced by the dissolution of TiC during annealing. Thus, the bake hardenability should decrease when the sulfur content is increased [170].

In the absence of solute carbon, the presence of phosphorus deteriorates the mechanical properties by segregating to ferrite grain boundaries [62, 66, 159]. Thus, when the aging index increases (indicating that more solute C is present), the transition temperature is also decreased [66]. In the absence of Mn, only Ti(C, N) and $Ti_4C_2S_2$ can form, while with 1 pct Mn, MnS and TiC replace $Ti_4C_2S_2$ precipitation. Thus, increasing the Mn content can leave

more carbon in solution available for bake hardening [62]. Boron can also migrate to grain boundaries and in this way prevent phosphorus segregation [171]. Thus, the addition of boron can improve the mechanical properties when the phosphorus content is high.

In general, the higher the effective atomic ratio of (Ti*+Nb)/C, the lower the aging index. This means that increasing the ratio, when the P content is high, should lead to more P segregation at the grain boundaries. Therefore, in P-alloyed IF steels, the (Ti*+Nb)/C ratio must be maintained at a low level [62].

In addition to its effect on the amount of C in solution, chemical composition can also change the mechanical properties by affecting the extent of grain refinement, the precipitate size distribution, the texture and anisotropy, etc. For example, solute carbon affects the formation of favorable textures for deep drawability [64]. Furthermore, the amount of Ti and therefore the cost of alloying increase with the C level. For these reasons, the N content is usually of subordinate importance in IF steels [59]. Compared to Nb IF steels, the precipitates are dispersed more coarsely in Ti IF steels [59, 65]. Finally, finer grains can be produced in Ti-Nb IF steels than Ti IF steels [66].

5.3. Work Hardening Rate, Strain Rate, and Temperature

As was shown in Figs. 4.5 to 4.7, dynamic strain aging (DSA) is accompanied by a large increase in work hardening rate, attributable to the multiplication of dislocations [10]. It is generally assumed that the dislocations become immobilized by solute pinning and fresh dislocations have to be produced as the deformation progresses [8]. In other words, rapid strain aging of the mobile dislocations makes the creation of new dislocations necessary in

order to reach the required strain [172]. Locking of these strain-aged dislocations leads to the observed increase in flow stress, which may also be partly due to precipitation on dislocations and/or the formation of interstitial (Cottrell) atmospheres [5, 8, 50, 152, 172]. This process of pinning and unpinning, repeated many times during deformation at elevated temperatures, leads to serrations in the stress-strain curves and to the observed increase in the work hardening rate. Each rise in flow stress is associated with the primary Luders band being temporarily locked by strain aging, while each fall is associated with unlocking and the Luders band moving forward again [5]

In the present work, as the strain rate was increased, the temperatures of the flow stress maximum and the ductility minimum shifted to higher temperatures (see Figs. 4.9 and 4.10), in agreement with the literature [35, 173-176]. Cottrell [177, 178] suggested that, at a given strain rate, the minimum temperature at which serrations appear is that at which the diffusion coefficient (in $cm^2\ s^{-1}$) of the solute species is about:

$$D \cong 10^{-9} \times \text{strain rate} \qquad (5.1)$$

indicating that the process is controlled by the diffusion of solute atoms. Substituting the diffusion coefficient of carbon, the equation is:

$$\text{strain rate} = 2 \times 10^{7} \exp(-20{,}100/RT) \qquad (5.2)$$

where R is the gas constant and T the absolute temperature. According to this relation, for strain rates of 10^{-4}, 10^{-3}, 10^{-2}, and $10^{-1}\ s^{-1}$, the minimum temperatures at which jerky flow takes place are 113, 150, 196, and 252 °C,

respectively. Baird and Jamieson [152] later suggested that the pre-exponential factor for the onset of serrated flow is somewhat higher (~10^8). This leads to minimum temperature values for the onset of serrations of: 91, 123, 163, and 211 °C, respectively, which are in reasonable agreement with the present results.

5.4. Aging Index Tests

The changes in mechanical properties produced by baking, i.e. the aging-index treatment, are due to the process of static strain aging [49]. During the initial stages of static strain aging, Cottrell atmospheres are formed by the segregation of the carbon to dislocations, thereby anchoring them [8, 49, 118]. The increase in the upper and lower yield points arise from the additional force needed to separate dislocations from these atmospheres and to move them. Therefore, among the various properties that change during strain aging, the increase in yield strength is probably the most reliable sign of aging [84].

Hundy [179] suggested the following equation as a means of calculating the time of strain aging at room temperature from results that were obtained at higher temperatures:

$$\log (t_r/t) = 4400(1/T_r - 1/T) - \log T/T_r \qquad (5.3)$$

Here t_r is the aging time at room temperature T_r (K), and t is the time at an elevated temperature T. Considering the present results generated at T = 100 °C and t = 1 hr, some equivalent aging times at room temperature and at elevated temperatures are listed in Table 5.2. It should be noted that this expression is applicable for predicting the effect of aging temperature on a

certain steel, containing a certain amount of carbon in solution, after a given prestrain. However, it may not be correct above 150-200 °C, because the level of carbon in solution may increase when the temperature is raised above 200 °C [179-181], or even above 100 °C [182, 183].

Table 5.2. Aging times required to give rise to the same amount of aging as observed after 60 min at 100 °C.

10 °C	16 °C	20 °C	40 °C	60 °C	80 °C	120 °C	150 °C
6 months	3 months	7 weeks	6 days	1 day	4 hr	15 min	2.5 min

Okamoto et al. [184] reported that, for a material to resist aging at room temperature for three months, the upper limit of dissolved carbon is approximately 10 ppm. However, according to the present results, even 1.5 ppm carbon in solution in samples cooled from 900 °C in still air can lead to significant static strain aging at room temperature during this time and to dynamic strain aging at elevated temperatures, Figs. 4.1 and 4.16.

Tsunoyama et al. [57] found that when the concentration of S was at normal levels (~0.01%), the AI was small, whereas when the S content was decreased, the AI increased up to 30-40 MPa. As will be discussed later in more detail, this is because, when the S content is low, there are too few TiS precipitates to act as nucleation sites for the TiC. Irie et al. [55] investigated the effect of soaking temperature in continuous annealing on the aging indices of a series of Ti-IF steels with 0.07% P. A constant cooling rate of 70 °C/s was applied to all the steels. As the Ti_{eff}/C, atomic ratio (Ti_{eff} = Total Ti - 1.5[S] - 3.43[N]) was increased from 0.4 to 4.6, they found that, in a steel with Ti_{eff}/C

= 0.4, the AI of about ~53 MPa was independent of soaking temperature. By contrast, the aging indices were low, in the cases of $Ti_{eff}/C = 1.1$ and $Ti_{eff}/C = 4.6$, when soaking temperatures no higher than 830 and 920 °C, respectively, were employed. Finally, the aging indices increased markedly and rapidly at soaking temperatures above 830 and 920 °C for the latter two steels. They concluded that, if the AI was less than 30 MPa, the mechanical properties would change by only a small amount after storing for three months at temperatures of about 40 °C. Brun and Pansera [154] reported similar results: after annealing at temperatures above 820 °C, the AI was increased. This increase was higher for rapid cooling and low Nb/C ratios. The present results are in good agreement with these findings: an increase in both the reheat temperature and cooling rate produced higher AI values.

As for the Nb IF steels, after annealing at 830 °C for 40 s, Hashimoto et al. [185] found that, when the amount of Nb was more than 7.8%C - 0.01, the aging index was less than 30 MPa. It was concluded that this value of aging index can guarantee that the mechanical properties will not change during storage for three months in the summer. In case of Nb/C = 0.6, even with slow cooling, the aging index was higher than 40 MPa. With Nb/C = 1, the aging index was lower than 20 MPa when the cooling rate was less than 2 K/s.

Katoh et al. [61, 186] found that an AI value of about 30 MPa corresponded to approximately 5 ppm C in solution. This is in good agreement with the present results in the case of water quenching from 900 or 950 °C. In these cases, the amounts of solute carbon were approximately 4.5 and 5.5 ppm for AI values of about 28 and 30 MPa, respectively. Satoh et al. [2] reported

that, for this amount of carbon in solution (5 ppm), the aging index was approximately 40 MPa.

Ushioda et al. [3] suggested that an aging index of 30 MPa can be considered as a non-aging value for steel and 20 MPa as a target for the complete absence of aging properties. In the present work, the maximum aging index value obtained for a non-aging steel was about 5 MPa corresponding to less than 1 ppm (about 0.5 ppm) carbon in solution. According to this result and in agreement with other workers [9, 187], a steel with a solute carbon level below 1 ppm (less than 10 MPa of AI value) can be considered as a non-aging steel. However, if a threshold level of 30 MPa is selected for the aging index, the situation is completely different. This value corresponds to about 5.5 ppm C in solution, an amount that can cause significant dynamic and static strain aging, Figs. 4.1 and 4.16.

As for the aging index tests at a constant temperature, 100 °C, McIvor [102] has reported that 5 to 300 min of aging at this temperature is equivalent to 3 days to half a year of aging at room temperature. He concluded that a treatment consisting of a 10% tensile prestrain followed by aging for 30 min at 100 °C should be equivalent to about 3 weeks of aging at room temperature.

5.5. Activation Energies

In the case of dynamic strain aging, the strain rate can be related to the test temperature by the well known Arrhenius equation [35, 155, 176, 188, 189].

$$\text{strain rate} = A \exp(-Q/RT) \qquad (5.4)$$

where A is a frequency factor and Q is the activation energy for dynamic strain aging. From the slopes of the lines in Fig. 5.1, activation energies of about 82 and 132 kJ/mole are obtained for the minimum and maximum temperatures associated with the appearance and disappearance of serrations, respectively. These findings are in good agreement with those of other workers for plain C steels [9, 10, 35, 189-193]. In addition, the activation energy for the appearance of serrations matches well with the activation energy for the diffusion of carbon in α-iron, indicating that the process is controlled by the diffusion of this element. The higher activation energy for the *disappearance* of serrations has been attributed to the binding energy of interstitial atoms to the dislocations [9, 10, 194].

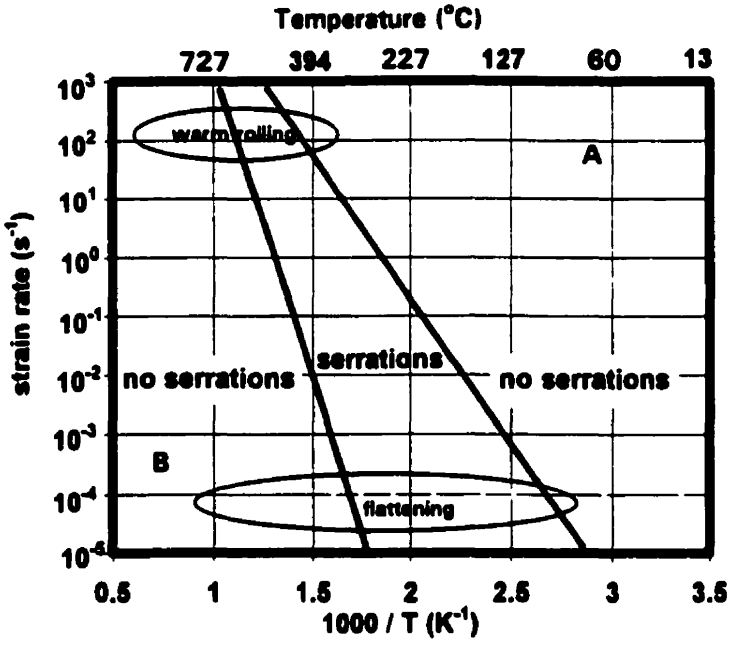

Fig. 5.1. Temperature and strain rate range over which serrations are observed.

Referring to Fig. 5.1, the two lines corresponding to the low temperature/low activation energy side and to the high temperature/high activation energy side divide the domain into three regions. In region A,

corresponding to high strain rates and/or low temperatures, plastic deformation is uniform and stable; hence the stress-strain curves are smooth. The central region is the serrated flow region, where the dislocation velocity remains approximately equal to the solute diffusivity, leading to pinning and unpinning. In region B, which corresponds to low strain rates and/or high temperatures, plastic flow is also homogeneous, and smooth curves are obtained because of the positive strain rate dependence. The lines in Fig. 5.1 can be extrapolated to predict whether or not dynamic strain aging will occur at the strain rates and temperatures involved in the processing of IF steels. This is a topic to which we will return later.

As for the specimens cooled from different reheat temperatures, the activation energy for the occurrence of dynamic strain aging can be determined from the time required to attain a UTS of, for example, 260 MPa at the various cooling rates that led to DSA. These times were deduced from Fig. 4.2 and then plotted against the inverse of the absolute reheat temperature in Fig. 5.2. This method resembles that employed by Cottrell and Churchman [195] to obtain the activation energy that applies to the static strain aging of a low carbon steel. The slope of the fitted line in Fig. 5.2 leads to an activation energy of about 160 kJ/mole. This value is in good agreement with the activation energies reported by previous workers for the interaction of interstitials with dislocations and for the occurrence of dynamic strain aging: 134 to 184 kJ/mole [194], 167 kJ/mole [196-198], 163 kJ/mole [199], 156 kJ/mole [200], 153 kJ/mole [189], 128 to 153 kJ/mole [9], 126 to 153 kJ/mole [10], 138 kJ/mole [201, 202]. and 135 kJ/mole [35].

Mura et al. [194], Leslie [9], and Keh et al. [10] attributed the higher activation energy (than that of C diffusivity) to the binding energy of interstitial

atoms to dislocations. Kawasaki et al. [196] concluded that such relatively high activation energies might be observed in cases where the diffusion rate of a *substitutional* element is likely to be the rate-controlling factor. However, their observed value of 163 kJ/mole is far less than the activation energy for the diffusion of substitutionals in iron, (288 kJ/mole for Fe [203], 281 kJ/mole for Ni [204]). Baird [8] believed that solute drag, which slows down dislocation movement, is responsible for the higher activation energy. Clough et al. [200] attributed the higher activation energies and their discrepancies to the complexities of DSA, which involves simultaneous deformation and aging.

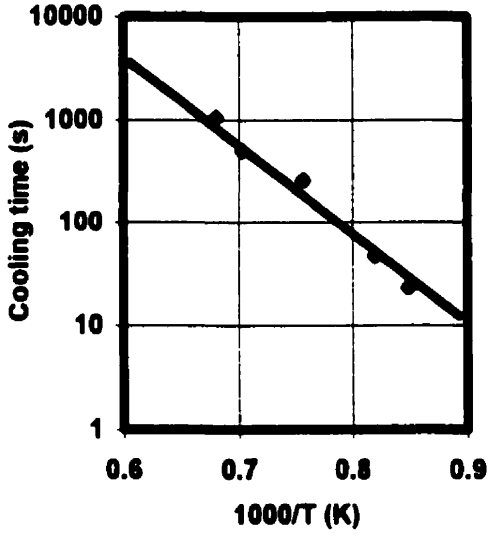

Fig. 5.2. Cooling times associated with a UTS of 260 MPa vs. inverse reheat temperature.

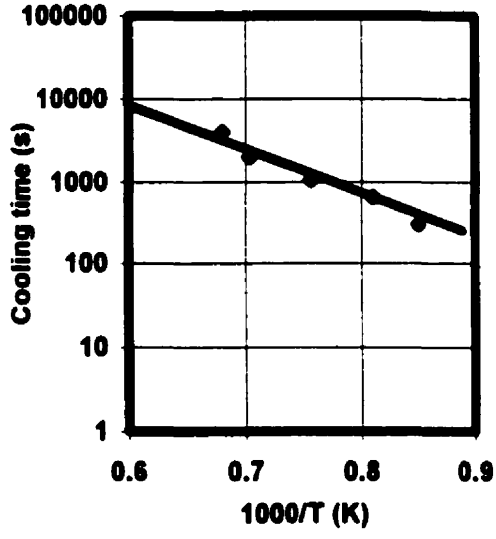

Fig. 5.3. Cooling times pertaining to an AI value of 25 MPa vs. inverse reheat temperature.

In addition to the above explanations for the higher activation energies, there could be another explanation. It is well known that an increase in cooling rate leads to a higher concentration of carbon-vacancy pairs [9, 205] as well as a higher dislocation density. This association of carbon atoms with vacancies,

reported during fatigue deformation, has been observed to lead to additional strengthening [206]. In this case, the activation energy for diffusion should include the energy required for vacancy formation as well as that for vacancy migration [203]. It is therefore possible that the higher activation energies for the specimens cooled at higher rates are due to the presence of higher densities of carbon-vacancy pairs. Thus, the higher activation energies could be related to the reduced mobility of the carbon atoms that are combined with vacancies. Note also that the activation energy for carbon-vacancy pairs interacting with dislocations was reported to be 143 kJ/mole [207].

The activation energy for the occurrence of *static* strain aging during the present aging index tests was determined from the time required to attain an AI value of 25 MPa after applying the various cooling rates from the different reheat temperatures. These times were deduced from Fig. 4.17 and then plotted against the inverse of the absolute reheat temperature in Fig. 5.3. The slope of the fitted line in this figure leads to an activation energy of about 105 kJ/mole.

Regarding the activation energy for static strain aging, the present finding is also in agreement with past works on the activation energy needed for this process and for the formation of Fe_3C. On studying the static strain aging behaviour of low carbon steels, Cottrell and Churchman [195] found activation energies of 67 to 92 kJ/mole and attributed them to the precipitation of Fe_3C. However, they reported that the range of activation energy may also have been linked to the possibility that more than one solute was taking part in the process [195].

It has been concluded [208] that the activation energy for static strain aging increases up to about 100 kJ/mole with increasing manganese content in the range 0.66-1.2% Mn. Gladman and Pickering [209] attributed their high activation energy, 97 kJ/mole, to precipitation in high-manganese ferrite, in which case the additional 20 kJ/mole is considered as the binding energy of the interstitials to manganese atom pairs. Leslie [9] also found that this value could be about 87.1± 10 kJ/mole.

Leslie [93] concluded that substitutional atoms in α-iron can cause strain aging at 300 °C or above. Although their effects are small compared to those of interstitial atoms [93], this may be another reason why the activation energies are higher in the case of DSA but not of SSA.

It has been proved by means of TEM studies that NbC or TiC can act as nucleation sites for iron carbide when the Ti/C or Nb/C (atomic ratio) is less than unity [55]. Brun and Pansera [154] also reported that when the Nb/C (atomic ratio) was less than unity, cementite particles were observed in the hot-rolled and coiled structure. The number of cementite particles decreased with increasing Nb/C ratio. This could be the reason why Hwang et al. [210] found that the AI value was approximately zero for a steel with an Nb/C (atomic ratio) less than unity, 0.55, which was coiled at 700 °C. At first, they found it difficult to understand why there was no solute carbon despite the small amount of carbide that was formed. However, later [113], they attributed the low level to the formation of some kind of Nb-C atomic complex or cluster. Nevertheless, this still cannot explain what happened to the extra solute C.

The formation of iron carbide has been reported even though the Ti/C or Nb/C atomic ratio was more than unity [141, 211]. This happened when there was supersaturated carbon present because a rapid cooling rate was employed, followed by coiling. Fonstein and Girina [211] attributed the maximum in solute C at 650 °C to the dissolution of these iron carbides during annealing, while Brun et al. [141] concluded that the solute C led to the formation of cementite during coiling. This is more likely to be the case in the present work.

5.6. Application to Mill Processing

Messien et al. [212] reported that the mean resistance to hot deformation of a Ti-stabilized IF steel increased when the rolling temperature was decreased. However, the increase was greater in the case of a low carbon steel. This is probably because more dynamic strain aging takes place in the latter steel. Their findings are in good agreement with the summary of the present results presented in Fig. 5.1 According to this figure, at strain rates of 50 and 200 s^{-1}, which are typical of strip rolling, the predicted temperature ranges for the occurrence of dynamic strain aging are about 390-590 °C and 480-660 °C, respectively.

Using the equation discussed earlier:

$$\text{strain rate} = 10^8 \exp(-20{,}100 / RT) \qquad (5.5)$$

the minimum temperatures at which jerky flow is initiated are 410 and 490 °C for strain rates of 50 and 200 s^{-1}, respectively. These values are consistent with the experimental results obtained here. The critical strain rate at which serrations are initiated at a particular temperature can be obtained from the following equation [192]:

$$\text{critical strain rate for init. of DSA} = (\alpha C_0/C_1)^{3/2} (L\rho_m U_m D/RTb) \quad (5.6)$$

where $\alpha \cong 3$, C_0 is the solute concentration of the alloy, C_1 is the concentration required at the dislocation for it to be locked, L is the average distance between the locked dislocations, ρ_m is the mobile dislocation density ($\rho_m = 1.85\times10^{14}\ \varepsilon^{0.72}\ m^{-2}$ [192]), D is the diffusion coefficient of the relevant interstitial, *b* is the Burgers vector, T is the absolute temperature, R is the gas constant, and U_m is the solute-dislocation binding energy. For an average $\varepsilon = 0.2$ per pass during rolling in the ferrite region, C_1 must be about 0.1 in order for the results of Fig. 5.1 to fit this equation. This can be interpreted to indicate that when the solute atoms occupy every tenth possible site, then dislocation pinning allows DSA to take place [35]. Note also that C_1 has been reported to fall between 0.5 and 1 for static strain aging [213].

Although the minimum temperature and maximum strain rate at which DSA is initiated have been relatively well characterized, much less is known about the conditions under which the irregular curves return to their normal smooth shapes. Sleeswyk [191] suggested the following equation for the critical strain rate at which this second transition takes place:

$$\text{critical strain rate for termination of DSA} = C(D^*/RT) \quad (5.7)$$

where C is a physical parameter that depends on the material properties and D^* is defined as follows:

$$D^* = D_o \exp(-Q^*/RT) \quad (5.8)$$

Here D_o is the diffusion frequency factor and Q* is the sum of the diffusion activation energy and the binding energy of the relevant interstitial to the dislocations. A value of 10^{20} J/m^{2}mole employed here for C in equation (5.7) calls for the serrations to disappear at temperature/strain rate combinations of 590 °C/40 s^{-1} and 660 °C/240 s^{-1}. At temperatures above and strain rates below these values, the deformation is again expected to be homogenous.

Barnett et al. [214] and Barnett and Jonas [215] studied the possibility of replacing cold by warm rolling in the case of low carbon steels. It was concluded that mobile atmospheres of C atoms form at warm rolling temperatures, leading to the occurrence of dynamic strain aging. Such aging can occur when the temperature is sufficiently low, e.g. below 630 °C, and the strain rate sufficiently high (i.e. above about 100 s^{-1}) [216, 217]. Although less than 0.003 sec is available at 100 s^{-1} for strain aging, the temperature appears to be high enough to permit this to take place [216, 217].

The increase in flow stress attributable to the occurrence of DSA must also be considered. This contribution to the flow stress increases the energy required for rolling. By contrast, the dynamic recovery that also takes place during ferrite rolling leads to softening. Messien et al. [212] suggested that the following equation describes the flow stress of a Ti IF steel during rolling in the ferrite region.

$$\sigma = \alpha G b \left[(h_o/1+r)(e^{\varepsilon} - e^{-r\varepsilon})\right]^{1/2} \qquad (5.9)$$

Here $\alpha \approx 1$ for bcc metals, G is the shear modulus, and h_o and r are, respectively, the strain hardening and softening parameters. They strained a Ti

IF and a low carbon steel up to $\varepsilon = 0.45$ in the temperature range 50-800 °C at 10^{-1} s^{-1} to obtain h_0 and r as functions of the strain under their conditions. In the Ti IF steel, they attributed the observed strengthening to an increase in dislocation density, as it was not yet known that DSA can indeed take place in IF steels.

At 200 °C, for example, the h_0 and r values they determined are about 2×10^{15} m^{-2} and 7, respectively [212]. Substituting these quantities into equation (5.9), a value of about 300 MPa is obtained for the flow stress of ferrite during warm rolling. This high level is shown here to be due to the occurrence of DSA, which is in turn responsible for the increase in dislocation density, see Figs. 4.5-7 and 4.51.

5.7. Implications with Regard to Flattening

The final flattening of strip is produced by its plastic extension during heating up in the continuous annealing furnace. The applied stress must be controlled to prevent heat buckles, necking (narrowing), and strip breaks [145]. The average extension or strain needed to flatten the sheet is about 0.002 m/m or 0.2% [145].

The applied strain rate depends, in turn, on the time that the sheet is subjected to a given temperature during reheating or soaking. For example, for a typical soaking time of 25 s, the relevant strain rate is [145]:

$$\text{strain rate} = 0.002/25 \approx 10^{-4}\ s^{-1} \qquad (5.10)$$

Although DSA cannot occur at the soaking temperatures employed during continuous annealing, it will be observed between about 100 and 350 °C at a strain rate of 10^{-4} s^{-1}, Fig. 4.51. At a still air cooling rate of about 3 °C/s, the overall time required for the sheet to pass through this temperature interval is therefore 84 s. This time is long enough for significant DSA to take place, as discussed in more detail below.

In addition, DSA can also occur when annealing and flattening are carried out simultaneously. The time required for a carbon atom to diffuse over a distance d towards a dislocation is given by [218]:

$$t = d^3 kT / (8AD) \qquad (5.11)$$

where d is twice the atomic distance *b*, k is Boltzmann's constant, and A ≈ 1.5×10^{-29} J.m depends on the physical properties of the material. At 200 °C, for example, this time is about 3.8×10^{-6} sec, while at room temperature (27 °C), it increases to about 0.76 sec. The time for aging to take place is the time necessary to *saturate* the dislocations. This is expressed by [219]:

$$t_a \cong (C_1 / \alpha C_0)^{3/2} (RTb^2 / 3DU_m) \qquad (5.12)$$

where at 100 °C and 200 °C, for example, the saturation times are about 14 and 0.067 sec, respectively. Thus, when a typical average heating rate of 7 °C/sec [3, 6, 52, 113, 159, 220, 221] is employed, significant aging can readily take place and sufficient time is available for C atoms to diffuse and lock the dislocations. Note also that, at this heating rate, the overall time required for the sheet to pass through the serrated flow interval is 36 s.

Manjoine [216, 217] investigated the resistance to plastic deformation of steels over a wide range of strains at various rates and temperatures. When the strain was 0.2% (e.g. in the case of flattening), he reported the occurrence of DSA, leading to maxima in flow stress at about 380, 420, and 550 °C at strain rates of 8.5×10^{-4}, 0.5, and 300 s^{-1}, respectively. At such low strains, higher temperatures are required to produce dynamic strain aging. This generalization is expected to apply to the case of flattening.

Similar results have been reported by McCormick [192]. He stated that the critical strain for the initiation of serrations can be even less than 0.001 (0.1% extension). According to his findings, at a constant rate of 10^{-4} s^{-1}, the critical strain for the initiation of serrations decreases from 0.05 (5% extension) at 80 °C to less than 0.0005 (0.05% extension) at about 130 °C. These observations are in good agreement with the present results obtained at intermediate temperatures and $\dot{\varepsilon} = 10^{-4}$ s^{-1}, Fig. 4.51.

The critical strain for the initiation of serrations can be calculated at each temperature and strain rate using the following equation [192]:

$$\varepsilon_c^{0.72} = (C_1/\alpha C_0)^{3/2} (RTb\dot{\varepsilon} / LKDU_m) \qquad (5.13)$$

where L is the average distance between the locked dislocations and K is a constant equal to 1.85×10^{14} m^{-2}. For steel A at 200 °C and 10^{-4} s^{-1}, this value is predicted to be about 0.00022 (0.022% extension), which is far less than the strain applied for flattening.

Finally, with regard to the solute C available to produce aging, it has been reported that holding for 10 s at 450 °C can lead to the solution of 25 ppm of interstitials in a 0.08% C steel [222]. According to the present results, even 1.5 ppm of C in solution can cause significant static and dynamic strain aging. Thus, cooling from temperatures above 450 °C at rates such as those described above (e.g. 3 °C/s) can produce steels that are susceptible to aging.

In brief, it appears from Fig. 5.1 that conditions are compatible with the occurrence of DSA during ferrite (warm) rolling. If it does indeed take place, it is expected to be more deleterious to the mechanical properties and more difficult to prevent or control than SSA. Figure 5.1 also indicates that DSA effects are likely to be observed at the temperatures and strain rates that correspond to flattening. This in turn can be expected to influence the formability and workability properties of the sheet.

From an industrial point of view, the magnitude of the elongation to fracture gives a direct measure of the ductility [176]. Significant reductions in ductility within the serrated flow region result from the unstable deformation that is associated with negative rate sensitivity [223-226]. These reductions, in turn, can be due to the presence of carbon in solution [227].

5.8. Stabilization of Interstitials in IF Steels

5.8.1. Stabilization by Chemical Composition

The precipitates that are expected to appear in Ti-IF steels are the carbides, nitrides, sulfides, and carbosulfides [228-231]. Among these, the precipitation temperatures of the nitrides, sulfides, and carbosulfides are the highest, while that of TiC is the lowest [232-235]. It appears that the formation of $Ti_4C_2S_2$ is principally responsible for removing carbon from solution [69,

74, 228, 229] while the TiS provides preferential nucleation sites for TiC and $Ti_4C_2S_2$ precipitation [69, 72, 131, 231, 234].

Compared to TiC, TiN has a low solubility product in austenite [57, 102, 104, 236] and its precipitation temperature is relatively high. During cooling, titanium nitride precipitates first [131, 237] and, as long as sufficient Ti is present, it appears that no N remains in solution at ambient temperatures. Thus, the dynamic strain aging reported in the present study probably arises from the presence of solute C.

In addition to the carbides, nitrides, sulfides, and carbosulfides, it has been shown that Ti precipitates in the form of FeTiP at about 700 to 750 °C [55, 131, 141], and is more stable than both $Ti_4C_2S_2$ and TiC, see Fig 5.4 [131]. Oxygen also causes some of the Ti to be lost because of its strong affinity for this element [75, 81, 82, 87, 92, 93, 104]. At high temperatures, e.g. 1600 °C, Ti will oxidize to TiO_2, while at low oxygen contents, or in iron deoxidized by Ti, Ti_2O_3 is formed [81]. In IF steels, the amount of O should be less than 20 ppm in order to prevent the formation of oxide inclusions [237].

Therefore, considering Ti as a scavenger for C and S (as TiS, TiC and $Ti_4C_2S_2$), N (as TiN), O (as Ti_2O_3), and some of the total phosphorus, P*, (as FeTiP), the values for Ti_{stab}, Ti^*_C, and Ti_{exc} are given by the following equations (wt%):

$$Ti_{stab} = \frac{2\times 48}{3\times 16}[O] + \frac{48}{32}[S] + \frac{48}{14}[N] + \frac{48}{12}[C] + \frac{48}{31}[P^*] \qquad (5.14)$$

$$= 2[O] + 1.5[S] + 3.42[N] + 4[C] + 1.55[P^*]$$

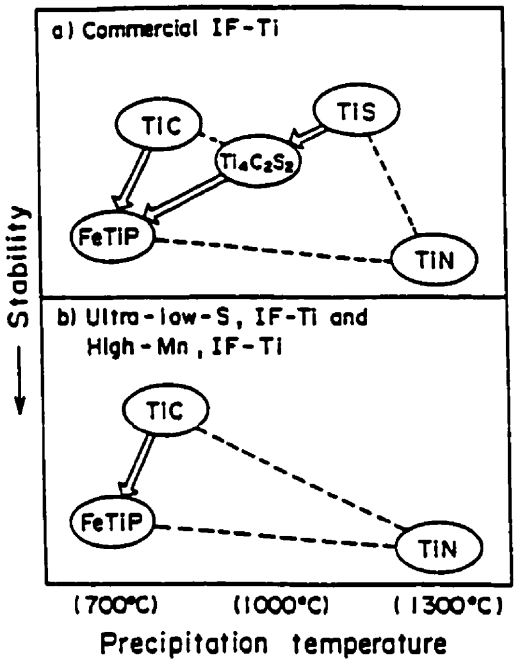

Fig. 5.4. Stability and precipitation temperatures of Ti compounds in IF steels [131].

$$Ti^*_C = \text{Total Ti} - 2[O] - 1.5[S] - 3.42[N] - 1.55[P^*] \quad (5.15)$$

$$Ti_{exc} = \text{Total Ti} - Ti_{stab} \quad (5.16)$$

Here, Ti_{stab} (the Ti needed for stabilization) is the amount of Ti required to fully stabilize the O, S, N, C, and some of the P. Ti^*_C refers to the Ti available to combine with C after the O, S, N and P have been scavenged. Ti_{exc} (excess Ti) refers to the amount of Ti that remains in solution after stabilization; this must be greater than zero for full stabilization. However, because Ti is added after deoxidizing the steel with Al [55, 75], the expressions for Ti_{stab} and Ti^*_C used in our calculations are as follows :

$$Ti_{stab} = 1.5[S] + 3.42[N] + 4[C] + 1.55[P^*] \quad (5.17)$$

$$Ti^*_C = \text{Total Ti} - 1.5[S] - 3.42[N] - 1.55[P^*] \quad (5.18)$$

Brun et al. [141] reported that the value of P* lies between 10 and 50% of the total P. Recently, Shi et al. [238] found that FeTiP forms in IF steels even if the P content is low, e.g. ≤0.01%. Therefore, in the cases of steels A and B, for example, assuming that respectively 45% and 30% of the P combines to form FeTiP, Ti_{exc} is zero and the Ti^*_C/C (atomic ratio) is unity. This means that, in the cases where more than 45% and 30% of the total P precipitates as FeTiP, there is not enough Ti to stabilize the C and some carbon will therefore remain in solution in these two steels.

If, however, one assumes that the FeTiP does not precipitate, Ti_{exc} is positive and the value of Ti^*_C/C is above unity, indicating that the complete stabilization of C is possible, provided the cooling rate is slow enough during processing [75].

In addition to the cooling rate, the amount of carbon in solution depends directly on the chemical composition and especially on the total amount of S. The effect of the chemistry of IF steels was discussed in section 5.2; however, some other points are mentioned below regarding the stabilization of IF steels by control of this factor.

If the S content is low, the amount of $Ti_4C_2S_2$ that forms is insufficient to remove all the carbon from solution [57]. In a very low S steel, not only does MnS form instead of Ti sulfide, but most of the Ti precipitates as FeTiP. It has been reported that increasing the amount of Mn suppresses the formation of TiC [141] because Mn decreases carbon activity in the ferrite; however, the

formation of MnS could also limit the formation of TiS and $Ti_4C_2S_2$ directly. For example, according to the work of Yoshinaga et al. [137], it is unlikely that MnS forms in steel A.

Tsunoyama et al. [57] studied three Ti-IF steels (0.0086% S, 0.033% Ti), (0.0032% S, 0.028% Ti) and (0.0008% S, 0.023% Ti) with a constant Ti_{eff}/C atomic ratio of about 1.7. After cold rolling and annealing at 850 °C, the last two steels had considerable carbon in solution and this was attributed to the very low S contents. Their results confirm our conclusion here that the Ti^*_s/S (atomic ratio) is much more important than Ti^*_c/C itself (atomic ratio), in removing C from solution. For example, although the Ti and S levels of steel B were about 1.5 times those of steel A, they displayed the same static and dynamic strain aging behaviors, mostly because they had the same values of Ti^*_s/S. On the other hand, steels B and C had the same Ti and C levels, but the Ti^*_s/S ratio of steel C was 2.5 times that of steel B. This resulted in significant amounts of solute carbon in steel C.

Note also that the solubility product for an MC carbide is, strictly speaking, only applicable in the absence of other alloying elements. In the *presence* of such elements, the solubility product for TiC, for example, would have to be modified when other carbide formers, and other non-precipitating species, are present [63].

5.8.2. Stabilization by Control of Cooling Rate

According to the results obtained here, it is apparent that even after cooling in still air, the amount of carbon left in solution is enough to produce DSA. However, furnace cooling allows sufficient time for the C to come out of

solution and satisfy the equilibrium condition of decreasing carbon solubility with decreasing temperature.

These results are in good agreement with past work on low C grades when Ti was used to prevent strain aging. In order to tie up the C and N with Ti, Glen [83] reheated all hot-rolled specimens to 950 °C, then cooled them in still air. Even with air cooling, he reported that significant amounts of carbon remained in solution. A minimum in ductility and a maximum in flow stress after tensile testing at elevated temperatures were attributed to these solute C atoms. Ochiai et al. [75, 104] concluded that, during the ordinary rolling of wire rod, the minimum amount of Ti needed to suppress strain aging was over 3 times as much as the stoichiometric amount of Ti required to combine with the C. By slowing the cooling rate during processing, the amounts of Ti required were reduced significantly. Fukuda and Shimizu [96] reported that the mechanical properties of Ti IF steels were improved when the Ti level was 10 to 20 times the C content.

As regards furnace cooling, Bleck et al [59] suggested that coiling at high temperatures along with high Ti/(C + N) ratios resulted in the stabilization of IF steels. To make sure that the total amounts of C, N, O, and S were tied up by the Ti, Leslie and Sober [87, 88] and Leslie et al. [90] added at least 2 1/2 times as much Ti as required to scavenge all these interstitials. In addition, they cooled their steels in a furnace to promote completion of the desired reactions between Ti and C, N, S, and O. With this technique, the amount of C or N remaining in solid solution was still about 0.5 ppm. Hayes and Griffis [77] added Ti to a steel for the first time in 1934 to obtain a non-strain aging steel. They suggested that a "stabilizing" heat treatment was necessary to reduce the

aging tendency of their low-carbon steel. In their view, the proper processing treatment consisted of choosing the correct temperature, holding for the proper length of time, and cooling at a very slow rate.

Although the Ti^*_{σ}/C ratio was more than unity in all the present IF steels, there was still enough carbon in solution to produce DSA. This implies that the rate at which nucleation sites appear (or their density) is the controlling factor in removing carbon from solution, rather than the rate at which precipitation occurs on these nuclei. When the carbon content is low, all the carbon is in solution at a particular reheating or annealing temperature. It is then necessary to have some pre-existing carbides or other particles present to act as nuclei on subsequent cooling. Even during cooling, when the temperature drops below the solution temperature, precipitation is difficult because of the absence of a sufficient quantity of nucleation sites. At lower temperatures, when the rate of diffusion is the controlling factor, the diffusivity is decreased. This leads to significant carbon remaining in solution, as the carbon atoms cannot come together to form clusters. In light of this, it is not surprising that the amount of carbon in solution can be higher in grades with lower total carbon contents.

The average distance X through which a carbon atom can diffuse in time t is given by:

$$X^2 = Dt \qquad (5.19)$$

At low temperatures, the value of D is so small that C atoms cannot diffuse over significant distances during the cooling cycle. Many therefore cannot find nucleation sites on which to precipitate.

A weighted average diffusion coefficient, D, of 10^{-8} cm^2/s has been suggested [166] as necessary for the C diffusivity during the cooling time from high temperatures. For example, in the case of water quenching from 1200 °C, the effective cooling time, t, is about 3 s. The diffusion distance is therefore about 1.7 μm, which means that a spherical region of radius 1.7 μm can be depleted of carbon during quenching from 1200 °C. This can happen provided the C atoms find nucleation sites in their vicinities; otherwise they remain in solution. This radius increases to 20 and 155 μm for still air and furnace cooling from 1200 °C, respectively. Katoh et al [61] reported that they obtained an AI of 30 MPa when they overaged an Al-killed steel; in this case, the mean distance for C diffusion was about 2 μm.

With reference to the present results, it is evident that, only during furnace cooling was the diffusion path, 155 μm, for the C atoms longer than the distance to the nucleation sites at which precipitation occurred.

5.9. Bake Hardening

5.9.1. Effect of Prestrain and Temperature

As was illustrated in Fig. 4.23, three different behaviors are observed when the SBH method is employed. At low prestrains, the amount of bake hardening increases with the prestrain until it reaches a maximum. When the prestrain is further increased, the bake hardening decreases because the carbon/dislocation ratio decreases. In the third stage, the bake hardening increases slightly or approaches a plateau. Some workers [51] have shown that the increase in the third stage begins at about 4% prestrain. By contrast, others [47] have observed no significant increase after a 5% prestrain and report that the third stage corresponds to a plateau. This may arise because no

significant increase in dislocation density occurs after a 5% prestrain [242]. The present results correspond mostly to the latter case, in which no pronounced increase is observed after 4% prestraining.

The situation is a little different in the case of baking at 100 and 250 °C. At 100 °C, the bake hardening increased continuously with the prestrain. At this relatively low temperature, maximum pinning corresponded to higher prestrains or longer aging times. Elsen and Hougardy [240] reported similar results at the same solute carbon level, 5 ppm. They observed that, in samples prestrained to 1, 2 and 5%, the increase in yield strength and therefore the bake hardening at low temperatures depended on the time. To produce a 40 MPa increase in yield stress after a prestrain of 2%, they had to increase the aging time (30 min) by factor of 20 when the temperature was decreased from 180 °C to 150 °C. Kurosawa et al. [241] also reported that, for 1 and 2% prestraining, the bake hardening increased continuously with both aging temperature and time. After 2% prestraining, the plateau in the bake hardening value was not reached even after 1000 min of aging at 150 °C [242].

Similar behaviour was observed for the yield stress, which reached a plateau after baking at 200 °C (except for the case of 2% prestraining), Fig. 4.25. As discussed below, it appears that, after holding at about 200 °C, the mechanism of aging starts to change and overaging begins. For this reason, the yield point approaches a plateau at this temperature, Fig. 4.25. Furthermore, overaging becomes more pronounced at around or above 250 °C, leading to a drop in yield point. (In the case of DSBH, the yield point values are to some extent variable due to the complexity of this process. In general, behaviors similar to those produced by the SBH technique are observed, Fig. 4.28.)

With regard to the DBH process, the maximum in bake hardenability was observed at about 200 °C, with the highest level for 2% prestraining at this temperature, Fig. 4.20. This is in agreement with the findings of Li and Leslie [22, 39]. On studying the effects of DSA on the subsequent mechanical properties of low carbon steels, they reported that the maximum strength was obtained after about 5% prestraining at 200 °C.

In the case of the DSBH method, two different behaviors were observed, Fig. 4.26. For prestraining at 100 and 150 °C, the results resemble those mentioned above for the SBH technique. In this case, since the aging temperature (170 °C) is above the prestraining temperatures (100 and 150 °C), the previous structure produced by DSA is modified. In the second situation, when the aging temperature (170 °C) is below the prestraining temperatures (200 and 250 °C), it appears that the relatively high temperature of straining leads to overaging, caused by coalescence of the precipitates, as will be discussed in more detail below.

By means of TEM investigations, Stephenson and Cohen [181] confirmed the Cottrell and Leak theory [243] and the work of Wilson [182] regarding the solution and reprecipitation of carbides. They found that precipitates underwent coalescence when the aging temperature was raised above 200 °C and continued to coarsen up to 425 °C. Above this temperature, little difference was observed. This phenomenon, overaging, was reported to be responsible for decreasing the yield point after aging. Later, Wilson and Russell [244, 245] reported that the same phenomenon, overaging, occurred, even at 150 °C.

Simanovic et al. [246] found that the increase in yield stress decreased with increasing prestrain. The above decrease was attributed to a decrease in particle size and therefore in the stress required to cut through the precipitate. (The latter is proportional to the square root of the particle size.) Bailey et al. [49] reported similar results. They observed a maximum in yield stress at about 225 to 250 °C. At higher temperatures, up to 550 °C, the decrease was also attributed to the occurrence of recovery and recrystallization.

Some workers [161] have concluded that the decrease in bake hardenability, after reaching a maximum, is due to growth of the carbide particles (overaging) precipitated at the dislocations and/or redissolution of the Cottrell atmospheres formed in the first step.

On studying the bake hardenability of Ti and Nb added ultra low carbon steels, Irie et al. [55] found that the aging indices decreased when the steels were held near 300 °C. This was attributed to the formation of iron carbide.

5.9.2. Industrial Applications of the DBH and DSBH Methods

The most important factors that are required for successful press forming are:

a) low yield strength or no sharp yield drop during press forming

b) almost no Luders strain during press forming

c) high work hardening rate during forming

d) high yield strength in the finished part

e) high bake hardening values

To prevent surface defects in press forming, a low yield strength and high work hardening rate are recommended [6, 141, 160, 247]. Figure 5.5 shows that, compared to steel B, steel A has a low yield strength and a higher hardening rate. This enables it to provide better quality after press forming. In addition, almost zero yield point elongation during forming and a high yield strength in the finished part are required [125].

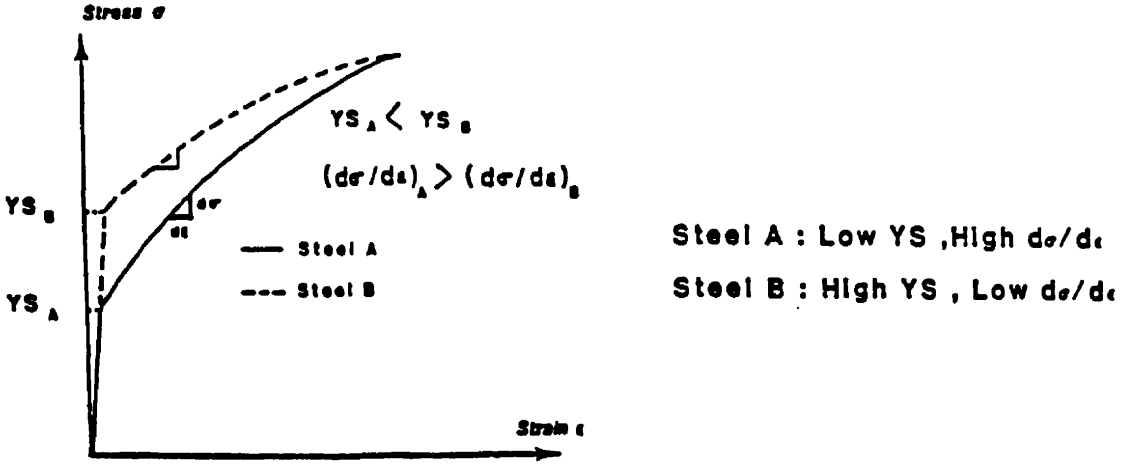

Fig. 5.5. Comparison between work hardening behaviors of two steels.

In the present work, the increase in yield point produced by baking is important so that a minimum yield strength of 210 [45] or 240-255 MPa [125] in the finished parts can be reached. Note that such values could also be reached with the aid of solid solution strengthening or the use of much higher cooling rates to raise the C solute levels, but not in the case of conventional IF steels with only about 4 ppm of solute C. For example, in the case of a Ti-Nb IF steel with 0.055% P and 0.023% Si, the aim was to reach 190 MPa in yield strength. This value was increased to 289 MPa when the alloying element levels were raised to 0.07% P, 0.6% Si, and 1.07% Mn. The yield strength for a conventional Ti-Nb IF steel, after cooling at 20 °C/s from 900 °C, is 175 MPa

[248]. In the case of the present DBH method, the yield strength produced by 2% prestraining at 200 °C is about 200 MPa.

With reference to the DBH and DSBH methods, all the requirements listed above can be satisfied by these techniques. Because they do not produce any yield point elongation, they do not require any temper rolling prior to forming.

DBH and DSBH both produce low yield strengths, which are desirable for press forming. Lou and Northwood [25, 249, 250] introduced a new criterion for the work hardening rate, namely the difference between the UTS and the yield stress. This parameter takes higher values when the prestrain is applied at high temperatures, as in the DBH and DSBH methods. High work hardening rates are associated with good quality during forming [160, 245].

In terms of warm forming, Sugimoto and Kobayashi [251] invented an apparatus used exactly for this purpose (i.e. the warm deformation of pressed automotive structural parts). A sketch is shown in Fig. 5.6. Their aim was to study the effect of forming temperatures, up to 400 °C, on the mechanical properties caused by the presence of retained austenite. The operation resembles a tensile testing machine with equipment available to control the forming speed. A graphite suspension type of lubricant was used. However, only cups of moderate size were formed.

When comparing the DBH and DSBH techniques, there is one more advantage to be listed for the DBH method; this is the elimination of one step, namely conventional bake hardening (2% prestrain). On the other hand, if it were possible to paint before forming, then again a one-step process could be used. Clearly, this is a point that requires further investigation.

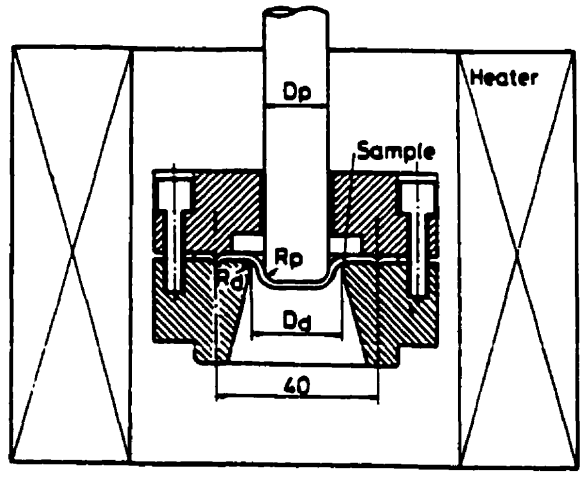

Fig. 5.6. An apparatus for warm press forming.

In terms of industrial applications, the energy needed for each tonne of sheet steel to be heated up to, for example, 200 °C is:

$$Q = m \times c \times \Delta T \qquad (5.20)$$

$$Q = 1000 \text{ kg} \times 460 \text{ J/kg °C} \times 175 \text{ °C} = 80{,}500{,}000 \text{ J} = 80.5 \times 10^6 \text{ J}$$

Considering the cost of energy for 1 kWh:

1 kWh = $ 0.0474

the price of the energy consumed is: $1.06/tonne

By comparison, the saving in alloying costs can be significant. For example, to make 1000 kg of steel with 0.03% Nb, each 100 ppm of Nb (i.e. 0.01% Nb) costs about $4 (a total of $12 for 0.03% Nb). Thus, strengthening

by DSA at a relatively low cost could become an economic alternative to the addition of alloying elements. Similar remarks apply to the cost of adding Mn, P or Si.

5.10. Continuous Annealing Techniques

According to the results of the continuous annealing simulation, when the annealing temperature is increased from 650 to 850 °C, the aging index values converge and decrease down to about 0 MPa.

Since the required high annealing temperature and rapid cooling rate are not economic, the above method constitutes a new approach to the production of bake hardenable steels. The technique simply involves producing a supersaturated C structure, then annealing it at relatively low temperatures, for example 700 °C, followed by cooling at different rates. This provides different amounts of solute C in order to produce different amounts of bake hardening. In the mechanism introduced here, precipitation is the controlling factor instead of dissolution during continuous annealing at high temperatures. The advantage in this case is therefore that the *lower* the annealing temperature, the higher the bake hardening value.

In the case of Ti-IF steels, the time for full recrystallization, for example at 700 °C, has been reported to be about 100 s [252], 105 s [136] or 120 s [253]. At 650 and 750 °C, Wilshynsky et al. [136] found this amount to be 1300 s and 50 s, respectively. They also concluded that this time was reduced significantly in the case of an unstabilized IF steel, i.e. to about 100 s at 620 °C. At the same temperatures, this time is considerably shorter in the case of low carbon or aluminum killed steels [136, 253].

To study the precipitation behavior of a series of Ti IF steels, Okamoto and Mizui [131] carried out TEM investigations on their materials after employing different annealing temperatures. It was found that, in low Mn steels, when the temperature reached 600 °C, the TiS precipitates changed to $Ti_4C_2S_2$. This process stopped at higher temperatures when the P content was high (0.08%), because FeTiP formed instead. Nevertheless, when the P and Mn levels were low, the formation of $Ti_4C_2S_2$ continued to high temperatures, e.g. 800 °C. In the latter case, holding at 800 °C for 3 min resulted solely in the formation of $Ti_4C_2S_2$.

According to the above results and considering the low Mn and P levels in the present IF steels as well as the non-equilibrium structures produced after cooling in still air, it is likely that the formation of $Ti_4C_2S_2$ was responsible for lowering the solute C during the continuous annealing treatments carried out at temperatures from 650 to 850 °C.

Van Snick et al. [51] found that when supersaturated carbon was present in Ti-Nb IF steels after hot rolling, the precipitation of carbides occurred during annealing instead of their dissolution. This finding again confirms the conclusion described above. On studying the aging behaviour of a quenched Ti IF steel, Satoh et al. [2] reported that the AI values decreased with increasing annealing temperature. This value diminished from about 38 MPa at 600 °C to 0 MPa at 800 °C. Such a decrease in aging index was attributed to TiC precipitation that started from about 700 °C. Note that, although the Ti/C (atomic ratio) was 5.4, they reported that 5 ppm of solute C was present after heat treatment and before the aging index tests. Gupta et al. [143] studied the effect of continuous annealing temperature in Ti, Nb, and Ti-Nb IF steels.

They found that Ti and Ti-Nb IF steels were insensitive to annealing temperatures from 760 to 870 °C and attributed this to the absence of solute C. A similar result was reported by Goodman et al. [254].

Irie et al. [55] studied the bake hardenability of Ti- and Nb- added ultra low carbon steels. They found, for example, that when the Ti/C (atomic ratio) was more than unity (1.1), the aging index decreased from about 12 MPa at 600 °C to 0 MPa at 750 °C. This was attributed to the precipitation of titanium carbide at the higher holding temperature. On the other hand, when the soaking temperature was increased from 800 °C to 1000 °C, the aging index increased from 0 MPa to about 60 MPa. This happened even when the Ti/C (atomic ratio) was 4.6. The cooling rate was reported to be 70 °C/s. Dilewijns et al. [248] reported similar results when they studied the bake hardenability of a Ti-Nb IF steel. Their BH values were 0 MPa after cooling at 20 °C/s from annealing temperatures of 740 and 780 °C. Fonstein and Girina [211] attributed the decrease in solute carbon, when cooling from between 650 and 800 °C, to the redistribution of solute carbon into special carbides in their Ti and Ti-Nb IF steels (even with Ti/C or Nb/C ratios less than unity); however, they did not address the nature of the special carbides.

CHAPTER 6

Conclusions

6.1. Effect of Cooling Rate

- Significant amounts of C can remain in solution at room temperature, even in interstitial free steels. This amount depends directly on the cooling rate, even in the presence of an excess of Ti, $Ti_{exc}>0$, for all the present IF steels.

- Among the six cooling rates employed, only furnace cooling (0.05 °C/s) made sufficient time available for the carbon to diffuse to nucleation sites where it precipitated out. Even still-air cooling (3 °C/s) led to a material that was supersaturated with carbon. This means that even this very slow cooling rate is still too rapid to allow the full precipitation of C in IF steels.

- The amount of carbon in solution in IF steels can be higher than in conventional low carbon steels because of the scarcity of nucleation sites.

6.2. Effect of Chemical Composition

Although the $(Ti^*_C)/C$ ratios in all three Ti IF steels were greater than unity, they exhibited significant static and dynamic strain aging, the extent of which depended on chemical composition and cooling rate. It seems that, under ordinary rolling conditions, Ti_{exc} must be considerably greater than zero to prevent aging phenomena from taking place.

- Steels with the same Ti^*_s/S ratios displayed the same aging behaviors, even though they had different Ti and S (wt%) levels. The higher the Ti^*_s/S ratio, the greater the potential for aging.

- Even the Ti-Nb IF steel with a $(Ti^*_c+Nb)/C$ ratio above unity exhibited pronounced aging behaviour. When the $(Ti^*_c+Nb)/C$ ratio was the same as that of Ti^*_c/C in the Ti IF steels, the Ti-Nb IF steel showed the same aging behaviour as the Ti IF steels.

6.3. Static Strain Aging Behaviour

- According to the present aging index tests, significant static strain aging can take place in IF steels when stabilization is incomplete. This phenomenon manifested itself by the return of a sharp yield point and the Luders strain.

- The measured aging indices increase with cooling rate and austenite reheat temperature as the above changes in these experimental parameters lead to the presence of more carbon in solution.

- For a fixed cooling rate and reheat temperature, the higher the Ti*s/S ratio, the greater the aging index value.

- Only IF steels with aging indices below 10 MPa (and therefore with solute C levels below 1 ppm) can be considered as non-aging steels.

6.4. Dynamic Strain Aging Behaviour

Tensile tests were carried out on heat treated samples of Ti and Ti-Nb IF steels from room temperature to 450 °C and at four strain rates from 10^{-4} to 10^{-1} s^{-1}. The characteristics observed led to the following conclusions.

- When the strain rate is increased from 10^{-4} to 10^{-1} s^{-1}, the temperatures at which serrated flow appears shift from 100 to about 220 °C, while the temperature associated with the disappearance of serrations increases from 300 to about 425 °C. This can be attributed to the occurrence of dynamic strain aging, a phenomenon associated with the presence of interstitials in a supposedly "interstitial-free" steel.

- The flow stress and UTS display maxima in the dynamic strain aging range. When the strain rate is increased, these maxima shift to higher temperatures. For example, for the UTS, it shifts from about 230 °C for 10^{-4} s^{-1} to about 340 °C for 10^{-1} s^{-1}.

- At all strain rates, the fracture strains display minima at intermediate temperatures. When the strain rate is increased, not only do the positions of these minima shift to higher temperatures but their values also increase. This indicates that the presence of carbon in solution is strongly deleterious to the formability and ductility of IF steels by promoting the occurrence of dynamic strain aging, which leads in turn to negative rate sensitivities.

- It appears that DSA can take place during warm rolling, which leads to higher flow stresses and higher energy consumptions. Also, if it occurs

during flattening, it can be deleterious to the mechanical properties of the sheet.

- Even 1.5 ppm of solute C (specimens of steel A cooled from 900 °C in still air) can produce significant DSA behaviour.

- The activation energy for the *appearance* of serrations is about 82 kJ/mole, which is in good agreement with the activation energy for the diffusion of carbon in α-iron. That for the *disappearance* of the serrations is 132 kJ/mole. The latter corresponds to the sum of the diffusion activation energy and the binding energy of interstitial solutes at dislocations.

6.5 Bake Hardening

Two new methods for bake hardening, *dynamic* bake hardening (DBH) and *dynamic*-static bake hardening (DSBH) were introduced here. They have the following characteristics:

- DSBH and DBH led to more bake hardening than does SBH (the conventional method). For example, in the case of a 2% prestrain at 100 °C, the amounts produced by the DSBH and DBH methods are about 15 and 8 times the SBH value, respectively. The minimum amount of bake hardening is about 3 MPa (2% prestrain at 100 °C with the SBH method) and the maximum value is about 55 MPa (4% prestrain at 150 °C with the DSBH method). Generally speaking, the lowest bake hardening values were obtained in the case of SBH. Conversely, the highest amounts were observed in the case of the DSBH method when the temperature of

dynamic aging (100 or 150 °C) is lower than that of subsequent static aging (170 °C). In the other cases, the DBH method exhibited the higher values.

- There is no Luders strain during prestraining in the cases of the DBH and DSBH methods nor is there a sharp yield point or yield drop.

- The yield stress during prestraining by the DBH and DSBH procedures is about 45 MPa less than that associated with the SBH technique.

- The work hardening rate during prestraining is much higher in the DBH and DSBH methods than in the SBH process. This is because there is much more pronounced work hardening during dynamic strain aging than when straining is carried out at room temperature. As a result, the yield strength after prestraining is much higher in the DBH and DSBH methods.

- With increasing prestrain, the yield/tensile strength ratio increases until it attains a value of almost unity in some cases of the DBH technique.

- Although a sharp yield point and the Luders strain are rarely observed after employing the DBH procedure, they are more significant after application of both the SBH and DSBH processes.

- A bake hardening value of about 55 MPa (4% prestrain at 150 °C with the DSBH method) is obtained with the aid of only 4 ppm solute C in the case of the Ti IF steel.

- The yield strengths produced by all three methods reach a plateau after about 200 °C. It appears that overaging takes place above this temperature and is responsible for a drop in yield stress.

6.6. Coiling and Continuous Annealing Techniques

- When the cooling rate from the coiling temperature (650 °C) is increased from 0.01 to 0.03 °C/s, the amount of solute C is increased fourfold. This can represent differences in solute C levels between the coil ends and the middle.

- According to the results of the continuous annealing simulation, when the annealing temperature is increased from 650 to 850 °C, the aging index values decrease and converge to about 0 MPa, whatever the cooling rate or chemical composition. These conclusions were confirmed by the internal friction measurements.

- A new approach for the production of a bake hardenable steel involves reheating of a supersaturated material to different soaking (annealing) temperatures followed by cooling at various rates. This yields different solute C levels suitable for bake hardening. The controlling factor in this approach is precipitation instead of the dissolution of particles. The advantage that follows from this method is that the lower the annealing temperature, the higher the solute C level and therefore the aging index value.

6.7. Calibration Between Solute C and Aging Index

- Based on the results of the internal friction tests, a calibration was established between the solute C and aging index values that can readily lead to prediction of the aging behaviour of IF steels.

Statement of Originality and Contribution to Knowledge

In this work, the characteristics of dynamic strain aging (DSA) were determined for the first time in four interstitial free (IF) steels. For this purpose, a wide range of reheat temperatures (in the austenite as well as the ferrite ranges) were employed, together with various cooling rates and different chemical compositions. The critical cooling rates at which IF steels are fully stabilized were determined, as well as the chemical compositions that are most likely to prevent aging phenomena from being observed.

A model was developed and proposed based on the present results to predict the occurrence of DSA at the temperatures and strain rates involved in the processing of IF steels, e.g. ferrite rolling and flattening.

To the best of our knowledge, this is first time that DSA has been studied in the ferrite region using a torsion machine.

A link between dynamic strain aging and bake hardenability was also determined. This link is important when the rising cost of alloying elements and the demand for high strength steels make it imperative to evaluate all possible strengthening mechanisms that do not depend on additional alloying. This is the most significant use of solute C in IF steels. The results can be used to assess whether a steel that displays the ability to undergo considerable hardening by means of dynamic strain aging also has appreciable bake hardenability.

Two new techniques based on the above link were introduced for the process of *dynamic* bake hardening. These methods produced much higher bake hardening values, up to 55 MPa, with lower solute C levels (only about 4 ppm), even though the Ti*/C ratio was greater than unity. These methods have the following advantages compared to conventional bake hardening:

a) they involve low yield strengths or the absence of yield drops prior to press forming
b) they largely eliminate the Luders strain before press forming
c) they increase the work hardening rate during forming
d) they lead to high yield strengths in finished parts
e) they produce higher bake hardening values.

A new approach was proposed to produce bake hardenable steels using lower annealing temperatures. This is of interest when the use of high annealing temperatures is impractical and is especially relevant when the Ti*/C ratio is greater than unity. A problem with conventional continuous annealing is that the annealing temperature increases with the Ti*/C ratio. The new technique introduced here is based on precipitation at lower annealing temperatures in a supersaturated material, instead of the dissolution of particles at high soaking temperatures.

Finally, a calibration was established between the aging index and the amount of solute carbon applicable to the case of IF steels. Since this calibration can readily predict the aging behaviour of these steels, it can be of considerable interest to steelmakers.

References

1. H. Takechi: in Proc. of the Symp. on Developments in the Annealing of Sheet Steel, TMS, Cincinnati, 1992, pp. 3-23.
2. S. Satoh, M. Morita, T. Katoh and O. Hashimoto: in Proc. of the Symp. on Developments in the Annealing of Sheet Steels, TMS, Cincinnati, 1992, pp. 177-188.
3. K. Ushioda, O. Akisue, K. Koyama and T. Hayashida: in Proc. of the Symp. On Developments in the Annealing of Sheet Steels, TMS, Cincinnati, 1992, pp. 261-285.
4. I.G. Ritchie and Z.L. Pan: in Proc. of the Symp. on IF Steel Sheet: Processing, Fabrication and Properties, CIM, Ottawa, 1991, pp. 39-53.
5. J.D. Baird: Iron and Steel, 1963, vols. 5, 7, 8, and 10, pp. 186-192, 326-334, 368-374, and 450-457.
6. H. Takechi: in Proc. of the Symp. on Hot- and Cold-Rolled Sheet Steel, TMS, Cincinnati, 1987, pp. 117-138
7. L. Meyer, W. Bleck, and W. Muschenborn: in Proc. Inter. Forum Phys. Metall. of IF Steels, ISIJ, Tokyo, 1994, pp. 203-222.
8. J.D. Baird: Met. Rev., 1971, vol. 16, pp. 1-18.
9. W.C. Leslie: The Physical Metallurgy of Steel, McGraw-Hill, New York, 1983.
10. A. S. Keh, Y. Nakada, and W.C. Leslie: in Dislocation Dynamics, ed. by W.A. Owen and M.J. Roberts, McGraw-Hill, New York, 1968, pp. 381-408.
11. A.V.D. Buekel and U.F. Kocks: Acta Metall., 1982, vol. 30, pp. 1027-1034.
12. B. Ule, J.V. Gvardjancic and M.L. Sarazin: Canad. Metall. Quart., 1996, vol. 35, pp. 159-168.
13. S.M. Pickard and F. Guiu: Acta Metall., 1988, vol. 36, pp. 1417-1427.
14. V.T.L. Buono, B.M. Gonzalez and M.S. Andrade: Scripta Mater., 1998, vol. 38, pp. 185-190.

15. A. Wolfenden, S.V. Raj and S.K.R. Kondlapudi: J. Mater. Res., 1994, vol. 9, pp. 1166-1173.
16. E.A. Little and D.R. Harries: Metal Science Journal, 1970, vol. 4, pp. 195-200.
17. T.C. Lindley and C.E. Richards: Metal Science Journal, 1970, vol. 4, pp. 81-84.
18. J.M. Brzeski, J.E. Hack, R. Darolia and R.D. Field: Mater. Sci. Eng., 1993, vol. A170, pp. 11-18.
19. L.P. Kubin and Y. Estrin: Acta Metall. et Mater., 1992, vol. 40, pp. 1037-1044.
20. Metals Handbook, 8th Ed., vol. 7, 1972, ASM, Metals Park, Ohio.
21. P. Venugopal, S. Venugopal and V. Seetharaman: J. of Materials Processing Technology, 1990, vol. 21, pp. 91-100.
22. C.C. Li and W.C. Leslie: Metall. Trans. A, 1978, vol. 9A, pp. 1765-1775.
23. D.C. Collinson, P.D. Hodgson and B.A. Parker: in Proc. of the Symp. on Modelling of Metal Rolling Processes, IOM, London, 1993, pp. 283-195.
24. B.H. Lee and I.S. Kim: J. of Nuclear Materials, 1995, vol. 226, pp. 216-225.
25. S. Lou and D.O. Northwood: Canadian Metallurgical Quarterly, 1994, vol. 33, pp. 243-249.
26. D. Wagner, C. Prioul and D. Francois: J. of Alloys and Comp., 1994, vol. 211/212, pp. 132-135.
27. K.T. Hong and S.W. Nam: Acta Metall., 1989, vol. 37, pp. 31-34.
28. P. Rodrigues: Bull Mater. Sci., 1984, vol. 6, pp. 653-658.
29. P.G. McCormick: Acta Metall., 1988, vol. 36, pp. 3061-3067.
30. P.G. McCormick and Y. Estrin: in Modeling the Deformation of Crystalline Solids, Ed. T.C. Lowe, A.D. Rollett, P.S. Follansbee and G.S. Daehn, TMS-AIME, Warrendale PA, 1991, pp. 293-308.
31. Y. Brechet and Y. Estrin: Acta Metall. et Mater., 1995, vol. 43, pp. 955-963.

32. K. Mitsunobu and K. Ushioda: Scan. J. Metallurgy, 1984, vol 13, pp. 276-282.

33. B.J. Brindley: Acta Metall., 1970, vol. 18, pp. 325-329.

34. G. Schoeck: Acta Metall., 1984, vol. 32, pp. 1229-1234.

35. A. Karimi Taheri, T.M. Maccagno and J.J. Jonas: ISIJ Int., 1995, vol. 35, pp. 1532-1540.

36. D. Blanc and J.L. Strudel: in the Proc. of 7th Int. Conf. on the Strength of Metals and Alloys, Montreal, Canada, 1985, pp. 349-354.

37. R. McCallum, S. Yue and J.J. Jonas: Wire J. Int., 1994, vol. 27, pp. 102-107.

38. L.P. Kubin, K. Chihab and Y. Estrin: in Patterns, Defects and Microstructures in Nonequilibrium Systems, NATO ASI Series, 1986, pp. 220-236.

39. C.C. Li, A. Yaker and W.C. Leslie: in the Proc. of 4th Int. Conf. on the Strength of Metals and Alloys, vol. 2, Nancy, France, 1976, pp. 731-735.

40. W.C. Leslie and A.S. Keh: in Mechanical Working of Steel II, ed. by T.G. Bradbury, 1964, New York, Gordon and Breach, pp. 337-377.

41. S.R. Lynes and I.P. O'Reilly: in the Proc. of the Symp. on High-Strength Sheet Steels for the Automotive Industry, AIME, Baltimore, MD, 1994, pp. 79-88.

42. W.C. Jeong: Metall. Mater. Trans. A, 1998, vol. 29, pp. 463-467..

43. J-O Sperle and K. Olsson: in Proc. of the Symp. on High-Strength Sheet Steels for the Automotive Industry, AIME, Baltimore, MD, 1994, pp. 65-78.

44. A. Itami, K. Ushioda, N. Kimura, H. Asano, Y. Kimura and K. Koyama: Nippon Steel Tech. Report, No. 64, 1995, pp. 26-32.

45. F. Rana, R. Skolly and I. Gupta: in Proc. of the Symp. on High-Strength Sheet Steels for the Automotive Industry, AIME, Baltimore, MD, 1994, pp. 89-102.

46. Y. Tokunaga and H. Kato: in Proc. of the Symp. on Metallurgy of Vacuum- Degassed Steel Products, TMS, Pennsylvania, 1989, pp. 91-108.

47. J.M. Rubianes and P. Zimmer: in Proc. of the Symp. on High-Strength Sheet Steels for the Automotive Industry, AIME, Baltimore, MD, 1994, pp. 111-117.

48. C-S Lee and B.K. Zuidema: in Proc. of the Symp. on High-Strength Sheet Steels for the Automotive Industry, AIME, Baltimore, MD, 1994, pp. 103-110.

49. F.D. Bailey, R.P. Foley, and D.K. Matlock: in Proc. of the Symp. on High-Strength Sheet Steels for the Automotive Industry, AIME, Baltimore, MD, 1994, pp. 119-133.

50. W. Bleck, R. Bode, O. Maid and L. Meyer: in Proc. of the Symp. on High-Strength Sheet Steels for the Automotive Industry, AIME, Baltimore , MD, 1994, pp. 141-148.

51. A. Van Snick, D. Vanderschueren, S. Vandeputte and J. Dilewijns: in the Proc. of 39th MWSP Conference, Indianapolis, USA, 1997, pp. 225-232.

52. S. Satoh, S. Okada, T. Kato, O. Hashimoto, T. Hanazawa and H. Tsunekawa: Kawasaki Steel Tech. Report, No. 27, 1992, pp. 31-38.

53. M.P. Autio: in Proc. of the Symp. on Hot- and Cold-Rolled Sheet Steel, TMS, Cincinnati, 1987, pp. 197-219.

54. K. Sakata, S. Satoh, T. Kato, and O. Hashimoto: in Proc. Inter. Forum Phys. Metall. of IF Steels, ISIJ, Tokyo, 1994, pp. 279-288.

55. T. Irie, S. Satoh, A. Yasuda, and O. Hashimoto: in Proc. of the Symp. on Metallurgy of Continuous-Annealed Sheet Steel, TMS-AIME, Dallas, 1982, pp. 155-171.

56. T. Hayashida, M. Oda, T. Yamada, Y. Matsukawa and J. Tanaka: in Proc. of the Symp. on High-Strength Sheet Steels for the Automotive Industry, Iron and Steel Society, Baltimore 1994, pp. 135-139.

57. K. Tsunoyama, K. Sakata, T. Obara, S. Satoh, K. Hashiguchi, and T. Irie: in Proc. of the Symp. on Hot- and Cold-Rolled Sheet Steel, TMS, Cincinnati, 1987, pp. 155-164.

58. I. Gupta and D. Bhattacharya. in Proc. of the Symp. on Metallurgy of Vacuum-Degassed Steel Products, TMS, Indianapolis, 1989, pp. 43-72.

59. W. Bleck, R. Bode, and F. Hahn: in Proc. of the Symp. on Metallurgy of Vacuum-Degassed Steel Products, TMS, Indianapolis, 1989, pp. 73-90.

60. S. Ono, O. Nozoe, T. Shimomura, and K. Matsudo: in Proc. of the Symp. on Metallurgy of Continuous Annealed Sheet Steel, TMS-AIME, Dallas, 1982, pp. 99-115.

61. H. Katoh, H. Takechi, N. Takahashi, and M. Abe: in Proc. of the Symp. on Technology of Continuously Annealed Cold-rolled Sheet Steel, TMS-AIME, Detroit, 1984, pp. 37-58.

62. G. Krauss, D.O. Wilshynsky, and D.K. Matlock: in the Proc. of International Conference on IF Steel Sheet, Ottawa, Canada, 1991, pp. 1-14.

63. M. Hasebe: in Proc. Inter. Forum Phys. Metall. of IF Steels, ISIJ, Tokyo, 1994, pp. 37-43.

64. N. Takahashi, M. Abe, O. Akisue and H. Katoh: in Proc. of the Symp. on Metallurgy of Continuous Annealed Sheet Steel, TMS-AIME, Dallas, 1982, pp. 51-81.

65. K. Tsunoyama, S. Satoh, Y. Yamazaki, and H. Abe: in Proc. of the Symp. on Metallurgy of Vacuum-Degassed Steel Products, TMS, Indianapolis, 1989, pp. 127-141.

66. Z. Lei and A. Jones: in the Proc. of International Conference on Phys. Metall. of IF Steels, ISIJ, Tokyo, 1994, pp. 161-164.

67. A. Najafi-Zadeh, J.J. Jonas and S. Yue: Metall. Trans. A, 1992, vol. 23A, pp. 2607-2617.

68. P.R. Cetlin, S. Yue, J.J. Jonas and T.M. Maccagno: Metall. Trans. A, 1993, vol. 24A, pp. 1543-1553.

69. G. Tither, C.I. Garcia, M. Hua, and A.J. Deardo: in Proc. Inter. Forum Phys. Metall. of IF Steels, ISIJ, Tokyo, 1994, pp. 293-322.

70. D. Alaoua, S. Lartigue, A. Larere and L. Priester: Materials Science and Eng., 1994, vol. A189, pp. 155-163.

71. K. Ushioda, N. Yoshinaga, K. Koyama, and O. Akisue: in Proc. Inter. Forum Phys. Metall. of IF Steels, ISIJ, Tokyo, 1994, pp. 227-244.

72. M. Prikryl, Y.P. Lin and S.V. Subramanian: Scripta Metall. et. Mate., 1990, vol. 24, pp. 375-380.

73. J.L. Ruiz-Aparicio, C.I. Garcia and A.J. Deardo: in Proc. of Inter. Symp. on Low Carbon Steels for the 90's, TMS, Pittsburgh, USA, 1993, pp. 419-426.

74. S.V. Subramanian, M. Prikryl, A. Ulabhaje and K. Balasubramanian: in the Proc. of International Conference on IF Steel Sheet, Ottawa, Canada, 1991, pp. 15-38.

75. I. Ochiai, H. Ohba, and A. Kawana: in Proc. of Annual Convention of the Wire Association International, Guildford, 1994, pp. 72-82.

76. E.R. Morgan and D.J. Knight: Mechanical Working of Steel II, Metallurgical Society Conferences, Chicago, 1964, vol. 26, pp. 379-400.

77. A. Hayes and R.O. Griffis: Metals and Alloys, 1934, vol. 5, pp. 110-112.

78. C.A. Edwards, D.L. Phillips, and H.N. Jones: J. Iron and Steel Inst., 1940, vol. 142, pp. 199-236.

79. G.F. Comstock: Proc. Am. Soc. Testing Materials, 1943, vol. 43, pp. 521-546.

80. K. Dies: Sheet Metal Ind., 1943, vol. 18, pp. 1907-1909, 2079-2086.

81. G.F. Comstock: Titanium in Iron and Steel, John Wiley and Sons, Inc., New York, 1955.

82. R.P. Steijn and R.M. Brick: Trans. ASM, 1954, vol. 46, pp. 1406-1448.

83. J. Glen: J. Iron and Steel Inst., 1957, vol. 186, pp. 21-48.

84. E.R. Morgan and J.C. Shyne: Trans AIME, 1957, vol. 209, pp. 65- 69.

85. M. Castagna, A. Ferro, F.S. Rossi, J. Sebille, and G. Szabo-Miszenti: Mem. Sci. Rev. Met., 1966, vol. 63, pp. 555-561.

86. G.A. Beresnev, V.I. Sarrak, and R.I. Entin: Soviet Physics-Doklady, 1966, vol. 11, pp. 252-254.

87. W.C. Leslie and R.J. Sober: Trans. ASM, 1967, vol. 60, pp. 99-111.

88. W.C. Leslie and R.J. Sober: Trans. ASM, 1967, vol. 60, pp. 459-484.

89. H.R. Rosinger, W.J. Bratina, and G.B. Craig: Trans. TMS-AIME, 1969, vol. 245, pp. 2097- 2098.

90. W.C. Leslie, R.J. Sober, S.G. Babcock, and S.J. Green: Trans. ASM, 1969, vol. 62, pp. 690-710.

91. H.D. Solomon, C.J. McMahon, and W.C. Leslie: Trans. ASM, 1969, vol. 62, pp. 886-890.

92. J.R. Rellick and C.J. McMahon: Metall. Trans., 1970, vol. 1, pp. 929-937.

93. W.C. Leslie: Metall. Trans., 1972, vol. 3, pp. 5-26.

94. L.J. Cuddy and W.C. Leslie: Acta Metall., 1972, vol. 20, pp. 1157-1167.

95. J.A. Elias and R.E. Hook: in Proc. 13th MWSP Conf., ISS-AIME, 1971, pp. 348-368.

96. N. Fukuda and M. Shimizu: Journal of Japan Society for Technology of Plasticity, 1972, vol. 13, pp. 841-850.

97. N. Fukuda and M. Shimizu: Trans. ISIJ, 1977, vol. 17, pp. 339-348.

98. R.E. Hook, A.J. Heckler and J.A. Elias: Metall. Trans. A, 1975, vol. 6A, pp. 1683-1692.

99. C. Weidig, M. Espindola, B. Gonzalez, P. Rodrigues and M. Andrade: Wire Journal International, 1995, vol. 28, pp. 82-85.

100. A. Karimi Taheri, T.M. Maccagno and J.J. Jonas: Materials Science and Tech., 1995, vol. 11, pp. 1139-1146.

101. A. Karimi Taheri, T.M. Maccagno and J.J. Jonas: Metall. and Materials Trans. A, 1995, vol. 26A, pp.1183-1193.

102. I.C. McIvor: Iron and Steel Making, 1989, vol. 16, pp. 55-62.

103. F. Boratto, C. Weidig, P. Rodrigues and B.M. Gonzalez: Wire Journal International, 1993, vol. 26, pp. 86-89.

104. I. Ochiai, H. Ohba, and A. Kawana: Wire Journal International, 1994, vol. 27 pp. 74-83.

105. I.G. Ritchie and C. Osborne: Steel Wire Research, 1989, vol. 5b, pp. 291-295.

106. Z. L. Pan, I.G. Ritchie and N. Bailey: Mechanics and Mechanisms of Material Damping, ASTM STP 1169, ASTM, Philadelphia, 1992, pp. 535-547.

107. L. B. Magalas: J. de Physique, 1996, vol. 6, pp. 163-172.

108. H. Katoh, K. Koyama, K. Komiya, M. Usuda and C. Fujii: Trans. ISIJ, 1985, vol. 25, p. 196.

109. Y. Wen, Q. Su and M. Wutting: in the Proc. of 39th MWSP Conference, 1997, Indianapolis, USA, pp. 271-280.

110. S. Satoh and T. Kato: ISIJ Int., 1992, vol. 32, pp. 764-770.

111. S.K. Chang and J.H. Kwak: ISIJ Int., 1997, vol. 37, pp. 74-79.

112. S. Satoh, T. Obara and K. Tsunoyama: Trans. ISIJ, 1986, vol. 16, pp. 737-744.

113. Y.S. Hwang, H.C. Chen and T.S. Chou: in Proc. of the Symp. on High-Strength Sheet Steels for the Automotive Industry, Iron and Steel Society, Baltimore 1994, pp. 187-193.

114. J.H. Kwak and S.K. Chang: in Proc. of the Symp. on Developments in the Annealing of Sheet Steel, pp. 411-424.

115. A.J. Boucek and J.F. Butler: in Proc. of the Symp. on Hot- and Cold-Rolled Sheet Steel, TMS, Cincinnati, 1987, pp. 177-195.

116. ASTM Standard E 8M, in Annual Book of ASTM Standards, Amer. Soc. Testing Mat., Philadelphia, 1990, vol. 01.02., pp. 598-612.

117. S.L. Semiatin, G.D. Lahoti and J.J Jonas: Mechanical Testing, ASM Metals Handbook, 9th Ed., ASM, Metals Park, Ohio, 1985, p. 154-184.

118. A.S. Keh and W.C. Leslie: in Materials Science Research, ed. by H.H Stadelmaier and W.W. Austin, 1963, New York, Plenum Press, pp. 208-250.

119. X. Yang, D. Vanderschueren, J. Dilewijns, C. Standaert and Y. Houbaert: ISIJ Int., 1996, vol. 36, pp. 1286-1294.

120. S. Akamatsu, N. Hasebe, T. Senuma, Y. Matsumura and O. Akisue: ISIJ Int., 1994, vol. 34, pp. 9-16.

121. F.H. Samuel, S. Yue and J.J. Jonas: in Proc. of the Symp. on Metallurgy of Vacuum-Degassed Steel Products, TMS, Pennsylvania, 1989, pp. 395-413.

122. J. Chipman: Metall. Trans., 1972, vol. 3, pp. 55-64, Metals Handbook, 8th Ed., vol. 8, ASM, Metals Park, Ohio, 1973.

123. C.A. Wert: Trans. AIME, 1950, vol. 188, pp. 1242-1244.

124. J.D. Fast: in Interaction of Metals and Gases, Academic Press, New York, 1965.

125. R.P. Foley, M.E. Fine and S.K. Bhat: in Proc. of the 39th MWSP Conference, 1997, Indianapolis, USA, pp. 653-666.

126. N.D. Ryan and H.J. McQueen: in Proc. of 7th Int. Conf. on the Strength of Metals and Alloys, Montreal, Canada, 1985, pp. 935-940.

127. S. Yue and J.J. Jonas: Mater. Forum, 1990, vol. 14, pp. 245-252.

128. A. Najafi-Zadeh, S. Yue and J.J. Jonas: ISIJ Int., 1992, vol. 32, pp. 213-221.

129. C. Ouchi, T. Sampei and I. Kozasu: Trans. ISIJ, 1982, vol. 22, p. 214.

130. T. Maki: in the Proc. Inter. Forum Phys. Metall. of IF Steels, ISIJ, Tokyo, 1994, pp. 183-197.

131. A. Okamoto and N. Mizui: in Proc. of the Symp. on Metallurgy of Vacuum-Degassed Steel Products, TMS, Pennsylvania, 1989, pp. 161-180.

132. F. Moussy, M. Munier, and C. Brun: in Proc. of the Symp. on Hot- and Cold-Rolled Sheet Steel, TMS, Cincinnati, 1987, pp. 25-39.

133. Ph. Paulus and M. Economopoulus: in Proc. of the Symp. on Hot- and Cold-Rolled Sheet Steel, TMS, Cincinnati, 1987, pp. 95-111.

134. N. Prum, U. Meers, H. Mathy, P. Messien, and V. Leroy: in Proc. of the Symp. on Hot- and Cold-Rolled Sheet Steel, TMS, Cincinnati, 1987, pp. 3-23.

135. D.O. Wilshynsky, D.K. Matlock and G. Krauss: in Proc. of the Symp. on Metallurgy of Vacuum-Degassed Steel Products, TMS, Pennsylvania, 1989, pp. 247-261.

136. D.O. Wilshynsky-Dresler, D.K. Matlock and G. Krauss: in Proc. Inter. Forum Phys. Metall. of IF Steels, ISIJ, Tokyo, 1994, pp. 13-31.

137. N. Yoshinaga, K. Ushioda, S. Akamatsu and O. Akisue: ISIJ Int., 1994, vol. 34, pp. 24-32.

138. Z. Yao: in Proc. of the Symp. on High-Strength Sheet Steels for the Automotive Industry, Iron and Steel Society, Baltimore 1994, pp. 37-43.

139. R. Pradhan: in Proc. of the Symp. on Technology of Continuously Annealed Cold-rolled Sheet Steel, TMS-AIME, Detroit, 1984, pp. 297-317.

140. S. Hashimoto, T. Kashima, N. Nakajima and M. Miyahara: in Proc. of the Symp. on Metallurgy of Vacuum-Degassed Steel Products, TMS, Pennsylvania, 1989, pp. 357-370.

141. C. Brun, P. Patou and P. Parniere: in Proc. of the Symp. on Metallurgy of Continuous Annealed Sheet Steel, TMS-AIME, Dallas, 1982, pp. 173-197.

142. K.I. Nilsson and N. Mizui: in Proc. of the Symp. on Metallurgy of Vacuum-Degassed Steel Products, TMS, Pennsylvania, 1989, pp. 143-160.

143. I. Gupta, T. Parayil and L.T. Shiang: in Proc. of the Symp. on Hot- and Cold-Rolled Sheet Steel, TMS, Cincinnati, 1987, pp. 139-153.

144. S. Osaka, N. Tanaka, K. Matsudo, Y. Fukuoka and H. Ishioka: Iron and Steel Eng., 1980, vol. 57, pp. 67-72.

145. E.A. Cook and R. Mieloo: in Proc. of Symp. on Developments in the Annealing of Sheet Steels, TMS, Cincinnati, 1992, pp. 143-147.

146. J.D. Baird and C.R. Mackenzie: J. Iron and Steel Inst., 1964, vol. 202, pp. 427-436.

147. B.J. Brindley and J.T. Barnby: Acta Metall., 1968, vol. 16, pp. 41-44.

148. Y. Bergstrom and W. Roberts: Acta Metall., 1973, vol. 21, pp. 741-745.

149. J.D. Baird: The Inhomogeneity of Plastic Deformation, ASM, Metals Park, Ohio, 1973, pp. 191-222.

150. S.C. Tjong and S.M. Zhu: Metall. And Mate. Trans. A, 1997, vol. 28A, pp. 1347-1355.

151. D. Wagner, J.C. Moreno and C. Prioul: J. Physique, 1996, vol. C8, pp. 159-162.

152. J.D. Baird and A. Jamieson: J. Iron and Steel Inst., 1966, vol. 204, pp. 793-803.

153. Y. Bergstrom and W. Roberts: Acta Metall., 1971, vol. 19, pp. 815-823.

154. C.G. Brun and J.L. Pansera: in Proc. of the Symp. on Metallurgy of Vacuum-Degassed Steel Products, TMS, Indianapolis, 1989, pp. 229-246.

155. M.L. Weaver, R.D. Noebe, J.J. Lewandowski, B.F. Oliver and M.J. Kaufman: Intermetallics, 1996, vol. 4, pp. 533-542.

156. D.Q. Bai, S. Yue, T.M. Maccagno and J.J. Jonas: Metall. Trans, 1998, vol. 29A, pp. 1383-1394.

157. S.V. Subramanian and J. Gao: in Proc. Inter. Forum Phys. Metall. of IF Steels, ISIJ, Tokyo, 1994, pp. 53-66.

158. P. Messien and V. Leroy: Steel Research, 1989, vol. 60, pp. 320-328.

159. K.G. Chin, H.J. Kang and S.K. Chang: in Proc. of Symp. on Developments in the Annealing of Sheet Steels, TMS, Cincinnati, 1992, pp. 305-319.

160. A. Lankila and A. Ranta-Eskola: in Proc. of Symp. on Developments in the Annealing of Sheet Steels, TMS, Cincinnati, 1992, pp. 151-158.

161. E. Kozeschink and B. Buchmayr: Steel Research, 1997, vol. 68, pp. 224-230.

162. G. Lagerberg and B.S. Lement: Trans. ASM, 1958, vol. 50, pp. 141-162.

163. P. Stark, B.L. Averbach, and M. Cohen: Acta Metall., 1958, vol. 6, pp.149-155.

164. J.F. Butler: Trans. AIME, 1962, vol. 224, pp. 89-96.

165. D.T. Gawne: Mater. Sci. Tech., 1985, vol.1, pp. 583-592.

166. P. N. Richards and K.V. Barratt: Trans. ASM, 1965, vol. 58, pp. 601-610.

167. H. Saitoh and K. Ushioda: ISIJ Int., 1989, vol. 29, pp. 960-965.

168. K. Ushioda, N. Yoshinaga, H. Saitoh and O. Akisue: Defect and Diffusion Forum, 1993, vol. 95/98, pp. 375-380.

169. H. Saitoh and K. Ushioda: Materials Trans. JIM, 1993, vol. 34, pp. 13-19.

170. M Kitamura, I. Tsukatani, and T. Inoue: ISIJ International, 1994, vol. 34, No. 1, pp. 115-122.

171. S.K. Putatunda, R. Krohn, A. Sengupta, I. Singh, and R.G. Davies: In the Proc. of International Conference on Low Carbon Steels for 90's, TMS, 1993, Pittsburgh, USA, pp. 453-464.

172. B.J. Brindley and J.T. Barnby: Acta Metall., 1966, vol. 14, pp. 1765-1780.

173. P. Dadras: Trans. JIM, 1978, vol. 19, pp. 230-232.

174. J.W. Kim and I.S. Kim: Nuclear Eng. and Design, 1997, vol. 174, pp. 59-67.

175. K.B.S. Rao, M.G. Castelli and J.R. Ellis: Scripta Metall. et Mater., 1995, vol. 33, pp. 1005-1012.

176. L. Shi and D.O. Northwood: Acta. Metall. Mater., 1995, vol. 43, pp. 453-460.

177. A.H. Cottrell: in Relation of Properties to Microstructure, ASM, 1954, pp. 131-162.

178. A.H. Cottrell: Phil. Mag., 1953, vol. 44, pp. 829-832.

179. B.B. Hundy: J. Iron and steel Inst., 1954, vol. 178, pp. 34-38.

180. W.S. Owen and M.J. Roberts: in Dislocation Dynamics, ed. by A.R. Rosenfield, McGraw Hill, New York, 1968, pp 357-379.

181. E.T. Stephenson and M. Cohen, Trans. ASM, 1961, vol. 54, pp. 72-83.

182. D.V. Wilson: Acta. Metall., 1957, vol. 5, pp. 293-302.

183. J.E. Pavlick: Trans. ASM, 1967, vol. 60, pp. 194-197.

184. A. Okamoto, Y. Hayashi, M. Takashi, and S. Sugisawa: in SAE Technical Paper Series, SAE 820018, 1982, pp. 21-27.

185. O. Hashimoto, S. Satoh, T. Irie and N. Ohashi: in Proc. of the Symp. on Advances in the Physical Metallurgy and Applications of Steels, Liverpol, 1981, pp. 21-24.

186. H. Katoh, K. Koyama and K. Kawasaki: in Proc. of the Symp. on Technology of Continuously Annealed Cold-Rolled Sheet Steel, TMS-AIME, Detroit, 1984, pp. 79-94.

187. K. Tsunoyama, T. Obara, S. Satoh, H. Abe, O. Shibasaki and N. Useugi: Kawasaki Steel Tech. Report, No. 24, 1991, pp. 84-90.

188. J.S. Blakemore and E.O. Hall: J. Iron and Steel Inst., 1966, pp. 817-820.

189. S. Kinoshita, P.J. Wray, and G.T. Horne: Trans. TMS-AIME, 1965, vol. 223, pp. 1903-1905.

190. R.W. Honeycombe: Steel: Microstructures and Properties, Edward Arnold Ltd., London, 1995.

191. A.W. Sleeswyk: Acta Metall., 1960, vol. 8, pp. 130-132.

192. P.G. McCormick: Acta Metall., 1973, vol. 21, pp. 873-878.

193. P.G. McCormick: Scripta Metall., 1973, vol. 7, pp. 945-948.

194. T. Mura, I. Tamura, and J.O. Brittain: Journal of Applied Physics, 1961, vol. 32, pp. 92-96.

195. A.H. Cottrell and A.T. Churchman: J. Iron and Steel Inst., 1949, vol. 162, pp. 271-276.

196. T. Kawasaki, H. Izumi and Y. Sawaki: Trans. ASM, 1967, vol. 60, pp. 707-711.

197. P.G. Forrest and L.M. Hopkins: In the Relation Between the Structure and Mechanical Properties of Metals, London, 1963, p. 438.

198. P. G. Forrest: Proc. Roy. Soc. A, 1957, vol. 242, pp. 223-227.

199. M. J. Roberts and W.S. Owen: Metall. Trans., 1970, vol. 1, pp. 3203-3213.

200. W.R. Clough, L.A. Jackman, and Y.G. Andreev: J. Basic Eng., 1968, vol. 90D, pp. 13-20.

201. K. Kamber, D. Keefer, and C.A. Wert: Acta. Metall., 1961, vol. 9, pp. 403-414.

202. K.G. Samuel, S.L. Mannan and P. Rodriguez: Acta. Metall., 1988, vol. 36, pp. 2323-2327.

203. G. Thomas, D. Schmatz, and W. Gerberich: in Proc. of the Symp. on High-Strength Materials, Berkeley, 1964, pp. 251-307.

204. Smithells Metals Reference Book, ed. by E.A. Brandes and G.B. Brook, Butterworths-Heinemann Ltd., Oxford, 1992.

205. R.F. Vyhnal and S.V. Radcliffe: Acta. Metall., 1972, vol. 20, pp. 435-445.

206. B. Mintz and D.V. Wilson: Acta. Metall., 1965, vol. 13, pp. 947-956.

207. C.F. Jenkins and G.V. Smith: Trans. Metall. Soc. AIME., 1969, vol. 245, pp. 2149-2156.

208. E.A. Little and D.R. Harries: ASTM Special Tech. Publ., 1969, vol. 457, pp. 215-240.

209. T. Gladman and F.B. Pickering: J. Iron and Steel Inst., 1965, vol. 203, pp. 1212-1217.

210. Y.S. Hwang and H.C. Chen: in Proc. of Inter. Symp. on Low Carbon Steels for the 90's, TMS, Pittsburgh, USA, 1993, pp. 475-480.

211. N.M. Fonstein and O.A. Girina: in Proc. Inter. Forum Phys. Metall. of IF Steels, ISIJ, Tokyo, 1994, pp. 33-36.

212. P. Messien, J.C. Herman, V. Leroy, and A. Benoit: in Proc. of Symp. on Developments in the Annealing of Sheet Steels, TMS, Cincinnati, 1992, pp. 287-303.

213. J. Friedel: Dislocations, Pergamon Press, New York, 1967.

214. M.R. Barnett, J.J. Jonas, and P.D. Hodgson: Iron and Steelmaker, 1996, vol. 23, pp. 39-45.

215. M.R. Barnett and J.J. Jonas: ISIJ Int., 1997, vol. 37, pp. 697-705.

216. A. Nadai and M.J. Manjoine: J. Appl. Mech., 1941, vol. 63, pp. 77-91A.

217. M.J. Manjoine: Trans. ASME, 1944, vol. 66, pp. 211-218A.

218. A.W. Sleeswyk: Acta. Metall., 1958, vol. 6, pp. 598-603.

219. P.G. McCormick: Acta. Metall., 1972, vol. 20, pp. 351-354.

220. H. Takechi: in the Proc. of Symp. on the Metallurgy and Appli. of Modern IF Steel Grades, CBMM/NPC Gmbh, Dusseldorf, Germany, 1990, pp. 1-13.

221. T. Yamada, M. Oda and O. Akisue: ISIJ Int., 1995, vol. 35, pp. 1422-1429.

222. P.N. Richards and K.V. Barratt: Trans. ASM, 1965, vol. 48, pp. 611-617.

223. L.P. Kubin, K. Chihab, and Y. Estrin: Acta Metall., 1988, vol. 36, pp. 2707-2718.

224. L.P. Kubin and Y. Estrin: Acta Metall., 1985, vol. 33, pp. 397-407.

225. P. Penning: Acta. Metall., 1972, vol. 20, pp. 1169-1175.

226. Y. Estrin and P.G. McCormick: Acta Metall., 1991, vol. 39, pp. 2977-2983.

227. M. Abe, Y. Kokabu, N. Arai, and S. Hayami: Journal of the Japan Inst. Metals, 1981, vol. 45, pp. 942-947.

228. S.V. Subramanian, M. Prikryl, B.D. Gaulin, D.D. Clifford, S. Benincasa and I. O'Reilly: ISIJ Int., 1994, vol. 34, pp. 61-69.

229. M. Hua, C.I. Garcia and A.J. DeArdo: Scripta Metall. et Mater., 1993, vol. 28, pp. 973-978.

230. W.J. Liu, S. Yue and J.J. Jonas: Metall. Trans. A, 1989, vol. 20A, pp. 1907-1925.

231. S.V. Subramanian and M. Prikryl: in Proc. of Symp. on Developments in the Annealing of Sheet Steels, TMS, Cincinnati, 1992, pp. 219-245.

232. W.J. Liu and J.J. Jonas: Metall. Trans. A, 1989, vol. 20A, pp. 1361-1374.

233. W.J. Liu and J.J. Jonas: ISIJ Int., 1994, vol. 34, pp. 761-763.

234. M. Hua, C.I. Garcia and A.J. DeArdo: in the Proc. of International Conference on Low Carbon Steels for 90's, TMS, 1993, Pittsburgh, USA, pp. 445-451.

235. S. Hinotani, J. Endo, T. Takayama, N. Mizui and Y. Inokuma: ISIJ Int., 1994, vol. 34, pp. 17-23.

236. D.T. Llewellyn: Ironmaking and Steelmaking, 1993, vol. 20, pp. 25-41.

237. A.W. Cramb and M. Byrne: in Proc. of the Symp. on Metallurgy of Vacuum-Degassed Steel Products, TMS, Indianapolis, 1989, pp. 3-27.

238. J. Shi, X. Wang, Z. Ru, J. Lu, B. Kong and C. Wang: in the Proc. of Int. Conf. on Advanced Automobile Materials, The Chinese Soc. for Metals, Beijing, China, Nov. 1997, pp. 215-220.

239. D. McLean: Mechanical Properties of Metals, J. Wiley & Sons, New York, 1962.

240. P. Elsen and H.P. Hougardy: Steel Research, 1993, vol. 64, pp. 431-436.

241. M. Kurosawa, S. Satoh, T. Obara and K. Tsunoyama: Kawasaki Steel Tech. Report, No. 18, 1988, pp. 61-65.

242. J.M. Rubianes and P. Zimmer: Revue de Metallurgie, 1996, vol. 93, pp. 99-101.

243. A. H. Cottrell and G.M. Leak: J. of Iron and Steel Inst., 1952, vol. 172, pp. 301-306.

244. D.V. Wilson and B. Russell: Acta Metall., 1960, vol. 8, pp. 36-45.

245. D.V. Wilson and B. Russell: Acta Metall., 1960, vol. 8, pp. 468-479.

246. Z. Simanovic, U.J. Brand, M. Ichikawa and S.V. Subramanian: in the Proc. of Int. Conf. on Thermech. Proc. of Steels and other Metals, THERMEC '97, Wollongong, Australia, TMS, 1997, pp. 419-425.

247. F. Bugnard, D. Rault and M. Entringer: in Proc. of the Symp. on Hot- and Cold-Rolled Sheet Steel, TMS, Cincinnati, 1987, pp. 165-176.

248. J. Dilewijns, D. Vanderschueren, M. Baetens, K. Mols and S. Claessens: in the Proc. of Int. Conf. on Thermech. Proc. of Steels and other Metals, THERMEC '97, Wollongong, Australia, TMS, 1997, pp. 467-473.

249. S. Lou and D.O. Northwood: Can. Metall. Quar., 1992, vol. 131, pp. 225-229.

250. S. Lou and D.O. Northwood: J. of Mater. Eng. and Perf., 1994, vol. 3, pp. 344-349.

251. K. Sugimoto and M. Kobayashi: in Proc. of the Symp. on High-Strength Sheet Steels for the Automotive Industry, Iron and Steel Society, Baltimore 1994, pp. 255-265.

252. A. Pichler, M. Mayr, G. Hribernig, H. Presslinger and P. Stiaszny: in Proc. Inter. Forum Phys. Metall. of IF Steels, ISIJ, Tokyo, 1994, pp. 249-268.

253. M.R. Barnett, J.J. Jonas and P. D. Hodgson: in Proc. of the 37th MWSP Conf., 1995, Hamilton, USA, pp. 971-978.

254. S.R. Goodman, P.R. Mould and J.C. Siple: in Proc. of the Symp. on Technology of Continuously Annealed Cold-Rolled Sheet Steel, TMS-AIME, Detroit, 1984, pp. 167-183.